



UNIVERSITA' DEGLI STUDI DI PADOVA

Centro Interdipartimentale di Studi e Attività Spaziali (CISAS)

**SCUOLA DI DOTTORATO DI RICERCA IN SCIENZE TECNOLOGIE E
MISURE SPAZIALI (XX Ciclo)**

Sede Amministrativa: Università degli Studi di Padova

**Indirizzo: Astronautica e Scienze da Satellite
Curriculum: Ottica e Strumentazione Spaziale**

Tesi

(nell'Ambito MIUR: Tecnologie Innovative per la Tutela dell'Ambiente)

DEVELOPMENT OF SENSORS FOR ULTRAVIOLET RADIATION MONITORING

**SVILUPPO DI SENSORI PER IL MONITORAGGIO DELLA RADIAZIONE
ULTRAVIOLETTA**

Dottorando: Garoli Denis

Supervisore: Prof. Piergiorgio Nicolosi (Università degli Studi di Padova)

Co-Supervisore: Dr.ssa Maria Guglielmina Pelizzo (CNR – INFN - Italia)

Coordinatore dell'Indirizzo: Prof. Pierluigi Bernacca (Università degli Studi di Padova)

Direttore della Scuola: Prof. Pierluigi Bernacca

31 Dicembre 2007

Contents

Contents.....	II
List of table.....	IV
List of figure.....	V
Abbreviation and Symbol List.....	IX
Riassunto.....	XI
Summary.....	XXI
1. UV radiation: theoretical principles and measurements techniques.....	1
1.1. Introduction.....	1
1.2. Interaction of UV with Matter.....	2
1.3. Cellular and Molecular Studies.....	3
1.4. Animal Studies.....	3
1.5. Health Effects on Humans.....	4
1.5.1. Skin.....	4
1.5.2. Immune System.....	5
1.5.3. Eye.....	5
1.6. Environment.....	5
1.7. Biological Weighting Factors and Spectrally Weighted Quantities.....	6
1.7.1. Some important action spectrum.....	6
1.8. Measurement Techniques.....	7
1.8.1. Detectors.....	8
1.8.2. Radiometers.....	9
1.8.3. Spectroradiometers.....	9
1.8.4. Calibration.....	10
2. Optical technology for biologically effective UV measurements.....	13
2.1. Design of optical elements.....	14
2.1.1. Interferential filters.....	14
2.1.1.1. Erythema - Interferential filters.....	15
2.1.1.2. DNA Damage - Interferential filters.....	16
2.1.1.3. Vitamin D3 Production - Interferential filters.....	17
2.1.1.4. Eye Damage - Interferential filters.....	17
2.1.1.5. Plant Damage - Interferential filters.....	18
2.1.1.6. The case of water disinfection - Interferential filters.....	19
2.1.1.7. Cone Angle Response of the Interferential filters.....	20
3. Characterization of optical elements.....	23
3.1. input optic: diffusive element characterization.....	24
3.1.1. Lambert's Cosine Law.....	25
3.1.2. Lambertian Surface.....	25
3.1.3. Diffuser characterization.....	26
3.2. Laboratory activities: thin films deposition and characterization.....	27
3.2.1. Thin Films deposition at Luxel and LUXOR.....	28
3.2.2. Optical constants derivation.....	29
3.2.2.1. Ellipsometric measurements at Luxel.....	29
3.2.2.2. Optical constants derivation at LUXOR.....	34
3.2.3. Spectral Transmittance.....	37
3.2.4. Stability tests.....	40
3.2.4.1. Thermal stability tests.....	40
3.2.4.2. Photostability tests.....	42
3.3. Laboratory activities: UV detector characterization and calibration.....	43
3.3.1. Relative Spectral Response Measurements.....	44
3.3.1.1. Facility.....	44
3.3.1.2. Methodology.....	44
3.3.1.3. Band-pass error.....	46
3.3.1.4. Percentage error.....	46

3.3.2. Absolute spectral response measurements.....	47
3.3.2.1. Facility.....	47
3.3.2.2. Methodology.....	47
3.3.2.3. Lamp stability.....	49
3.3.2.4. Beam uniformity.....	49
3.3.2.5. Si photodiode active area uniformity.....	50
3.3.2.6. Percentage error.....	50
4. UV Source and Photoprotection.....	53
4.1. Factors affecting solar UV levels.....	53
4.1.1. Ozone depletion effects.....	54
4.2. Trends in UV.....	54
4.3. UV monitoring.....	55
4.4. UV Artificial Sources.....	56
4.4.1. Incandescent sources.....	56
4.4.2. Gaseous discharge sources.....	56
4.4.2.1. Low pressure discharge lamps - Germicidal lamps.....	57
4.4.2.2. Fluorescent lamps.....	57
4.4.2.3. High pressure discharge lamps.....	57
4.4.2.4. Xenon, compact and linear arcs.....	57
4.4.3. Arc welding.....	58
4.4.4. Sunbeds.....	59
4.5. Protective measures - Photoprotection.....	60
4.5.1. Education.....	60
4.5.2. Protection Factors.....	60
4.5.3. Clothing.....	60
4.5.4. Eye Protection.....	62
4.5.5. Sunscreens.....	63
5. Instruments realization and application.....	67
5.1. Prototype realization.....	68
5.1.2. Calibration.....	69
5.1.3. Cosine response.....	69
5.2. Characterizing the performances of the radiometers.....	69
5.2.1. Calibration uncertainty u_{cal}	70
5.2.2. Short wavelength range response characteristic u	70
5.2.3. Long wavelength range response characteristic r	71
5.2.4. Directional response characteristic f_2	72
5.2.5. Linearity characteristic f_3	72
5.2.6. Display unit characteristic f_4	73
5.2.7. Fatigue characteristic f_5	74
5.2.8. Temperature dependence characteristic f_6	75
5.2.9. Modulated radiation characteristic f_7	76
5.2.10. Polarization response characteristic f_8	77
5.2.11. Spatial response characteristic f_9	78
5.2.12. Range change characteristic f_{11}	79
5.3. Application in artificial source monitoring.....	79
5.4. Application in extraterrestrial environments.....	82
5.4.1. Activity Description.....	83
5.5. Astronautical applications.....	84
5.5.1. Bone Loss in Space Flight.....	85
5.5.2. The role of Vitamin D.....	86
5.5.3. Proposed experimental study and procedure.....	86
6. Conclusions.....	89
References.....	91
Attached WBS.....	97

List of Tables

Table 4.1. Effective Irradiance measurements on different sunbed models.....	59
Table 4.2. UVB transmission properties of common fabrics.....	61
Table 5.1. Effective Irradiance computed with EAC and prototypes response curves.....	81

List of Figures

Figure 1.1. Ultraviolet spectral regions. Conventional subdivision based on biological effects.....	2
Figure 1.2. Some important action spectrum overlapped with a clear sky UV solar irradiance.....	7
Figure 2.1. Erythema Action Spectrum Radiometer. Filter response curves and radiometer response for the ZrO_2/SiO_2 and ZrO_2/MgF_2 design respectively.....	16
Figure 2.2. Erythema (Only UVA spectral region) Action Spectrum Radiometer. Filter response curves and radiometer response for the ZrO_2/SiO_2 and ZrO_2/MgF_2 design respectively.....	16
Figure 2.3. DNA Damage Action Spectrum Radiometer. Filter response curves and radiometer response for the ZrO_2/SiO_2 and ZrO_2/MgF_2 design respectively.....	17
Figure 2.4. Vitamin D3 Production Action Spectrum Radiometer. Filter response curves and radiometer response for the ZrO_2/SiO_2 and ZrO_2/MgF_2 design respectively.....	17
Figure 2.5. Conjunctivitis Action Spectrum Radiometer. Filter response curves and radiometer response for the ZrO_2/SiO_2 and ZrO_2/MgF_2 design respectively.....	18
Figure 2.6. Keratite Action Spectrum Radiometer. Filter response curves and radiometer response for the ZrO_2/SiO_2 and ZrO_2/MgF_2 design respectively.....	18
Figure 2.7. Higher Plant Damage Action Spectrum Radiometer. Filter response curves and radiometer response for the ZrO_2/SiO_2 and ZrO_2/MgF_2 design respectively.....	19
Figure 2.8. Bacillus Subtilis Action Spectrum Radiometer. Filter response curves and radiometer response for the ZrO_2/SiO_2 and ZrO_2/MgF_2 design respectively.....	19
Figure 2.9. Filter cone angle acceptance for Vitamin D3 and DNA Damage ZrO_2/MgF_2 filters design respectively.....	20
Figure 2.10. Mechanical mounting of the head of the radiometer. Baffle design for the cone-angle limitation.....	21
Figure 3.1. Typical radiometer layout.....	23
Figure 3.2. Suntube monitoring.....	24
Figure 3.3. Schematic Representation of the Cosine Law.....	25
Figure 3.4. Schematic Representation of a Lambertian Surface.....	25
Figure 3.5. Transmittance measurements on diffusive elements.....	26
Figure 3.6. Deviation from the cosine law. Error (%) and absolute deviation from theoretical values.....	27
Figure 3.7. Electron Beam Deposition Facility at LUXOR.....	28
Figure 3.8. Cary Varian 5000 UV/Vis/NIR Spectrophotometric Equipment at LUXOR.....	28

Figure 3.9. Profilometer at Department of Physics - University of Padova.....	29
Figure 3.10. VUV-VASE profilometer (J.A. Woollam Co., Inc.).....	30
Figure 3.11. Optical constants of SiO ₂ prepared at Luxel.....	30
Figure 3.12. Optical constants of ZrO ₂ prepared at Luxel.....	30
Figure 3.13. Optical constants of MgF ₂ prepared at Luxel.....	31
Figure 3.14. Example of the analytical software results.....	31
Figure 3.15. Schematic representation of light – film – substrate interaction.....	32
Figure 3.16. Principle of ellipsometric measurements.....	32
Figure 3.17. Example of fitting procedure on experimental ellipsometric data. SiO ₂ Sample.....	33
Figure 3.18. Transmittance measurements and best-fit simulation of ZrO ₂ and MgF ₂ thin films.....	35
Figure 3.19. Profilometric measurements on ZrO ₂ and MgF ₂ thin films prepared at LUXOR. Comparison with thickness estimated from the best-fit procedure.....	36
Figure 3.20. Optical Constants comparison of ZrO ₂ thin film prepared with different process.....	36
Figure 3.21. Optical Constants comparison of MgF ₂ thin film prepared with different process.....	36
Figure 3.22. Optical layout of the Varian Cary 5000 Spectrophotometer at LUXOR.....	37
Figure 3.23. Experimental set-up for the spectral transmittance measurements.....	37
Figure 3.24. Transmittance measurements on Erythema filters – Structure comprising ZrO ₂ /MgF ₂ . Comparison between Target curve and different deposition runs.....	38
Figure 3.25. Transmittance measurements on Erythema filters – Structure comprising ZrO ₂ /MgF ₂ . Transmittance performances reproducibility between the different samples.....	38
Figure 3.26. Transmittance measurements on Conjunctivities filters – Structure comprising ZrO ₂ /SiO ₂ . Comparison between Target curve and different deposition runs.....	39
Figure 3.27. Transmittance measurements on Conjunctivities filters – Structure comprising ZrO ₂ /SiO ₂ . Transmittance performances reproducibility between the different samples.....	39
Figure 3.28. Temperature of Exposure for the multilayer structures tested.....	41
Figure 3.29. Thermal Stability Tests on ZrO ₂ /MgF ₂ multilayer structures.....	41
Figure 3.30. Thermal Stability Tests on ZrO ₂ /SiO ₂ multilayer structures.....	41
Figure 3.31. ZrO ₂ /MgF ₂ Photostability Tests – 10 Days of Exposure (1h/day – 200SED/Day).....	42

Figure 3.32. ZrO ₂ /SiO ₂ Photostability – Tests on 1st Run Deposition Films – 10 Days of Exposure (1h/day – 200SED/Day).....	43
Figure 3.33. ZrO ₂ /SiO ₂ Photostability – Tests on 2 nd Run Deposition Films – 10 Days of Exposure (1h/day – 200SED/Day).....	43
Figure 3.34. Bentham spectroradiometer at Deltaohm s.r.l.....	44
Figure 3.35. Relative spectral response curves for the different photodiodes.....	45
Figure 3.36 Relative spectral response curve for a SiC photodiode obtained from measurements with two different lamp sources.....	45
Figure 3.37. Percentage errors associated to the SiC, GaN and AlGaIn- type B photodiodes.....	46
Figure 3.38. Optronic Laboratories spectroradiometer at Deltaohm.....	47
Figure 3.39. Set-up for the absolute spectral response measurements.....	48
Figure 3.40 Absolute spectral response curves for the different photodiodes.....	48
Figure 3.41. Stability of the XENON lamp over time.....	49
Figure 3.42. Photocurrent (pA) measurements to verify beam uniformity over a 3×3 mm ² area.....	49
Fig.3.43. Si calibrated photodiode measurement (nA) to verify uniformity of response over an active area of 6×6 mm ²	50
Figure 4.1. Irradiance spectrum of Lot-Oriel 300W Solar Simulator at LUXOR. Comparison with the standard solar emission on earth.....	58
Figure 4.2. Irradiance measurements of a Xenon Source (Solar Simulator) performed with different radiometers and under different wavebands. The transmittance curves of the bandpass filters used for the measurements are also reported.....	58
Figure 4.3. Irradiance (effective) values of sunbeds – Values correspondent to Measurements 1, 23 and 24.....	59
Figure 4.4. Example of Fabrics transmittance measured at LUXOR. Comparison between different materials.....	62
Figure 4.5. Example of Eyeglass transmittance measured at LUXOR. Comparison between high quality and low cost materials.....	62
Figure 4.6. Laboratory for sunscreens tests.....	64
Figure 4.7. a) In vivo microscopic image of skin (50x Optical Zoom). b)Microscopic image of Transpore 3M (20x Optical Zoom). c) Microscopic image of hydrated Vitro Skin (20x Optical Zoom).....	64
Figure 4.8. Transmission spectra of three different commercial products, applied on Transpore, with similar SPF.....	65
Figure 4.9. Photostability of two different commercial products.....	65
Figure 5.1. LUXOR Broad-band Radiometers.....	67

VIII

Figure 5.2. Senserit® Radiometer. Image and Attended Performance..... 68

Figure 5.3. Senserit® Prototypes performance..... 68

Figure 5.4. Example of Irradiance values of commercial sunbeds..... 80

Figure 5.5. Vitamin D synthesis like radiometer..... 87

Abbreviation and symbol list

The following subsections list the abbreviations, symbols and mathematical notations used. The numbers refer to the page where the abbreviation or symbol are explained and defined.

Abbreviations and symbol

UV	UltraViolet	from p.1
UVC	UltraViolet C from 100 to 280 nanometers	from p.1
UVB	UltraViolet B from 280 to 315 nanometers	from p.1
UVA	UltraViolet A from 315 to 400 nanometers	from p.1
SCC	squamous cell carcinomas	from p.4
PSC	posterior subcapsular cataracts	from p.5
H	radiant exposure	from p.6
E	irradiance	from p.6
E_{λ}	spectral irradiance	from p.6
H_{λ}	spectral radiant exposure	from p.6
Q	Radiant Energy	from p.6
W	Radiant Energy Density	from p.6
Φ	Radiant Flux	from p.6
M	Radiant Exitance	from p.6
I	Radiant Intensity	from p.6
L	Radiance	from p.6
CIE	Commission Internationale de l'Eclairage	from p.6
S_{λ}	action spectrum.	from p.6
IEC	International Electrotechnical Commission	from p.7
Si	silicon	from p.8
GaAsP	Gallium-arsenide-phosphide	from p.8
GaP	gallium-phosphide	from p.8
NEP	noise-equivalent-power	from p.8
EUV	Extreme UltraViolet	from p.14
Vis	Visible Light	from p.14
NIR	Near InfraRed	from p.14
APC	antigen-presenting cells	from p.15
ZrO ₂	Zirconium dioxide or Zirconia	from p.16
SiO ₂	Silicon dioxide or Silica	from p.16
MgF ₂	Magnesium fluoride	from p.16
CPDs	cyclobutane–pyrimidine dimers	from p.16
25(OH)D	25 hydroxyvitamin D	from p.17
1,25(OH)2D3	1,25-dihydroxyvitamin D3	from p.17
PTFE	Teflon	from p.26
BaSO ₄	Barium sulphate	from p.26
PLD	Pulse Laser Deposition	from p.28
VUV	Vacuum Ultra Violet	from p.29
$n(\lambda)$	real part of the refractive index	from p.30
$k(\lambda)$	immaginary part of the refractive index	from p.30
SensErit®	Sensor Erythema	from p.37
SED	Standard Erythemal Dose	from p.42

SiC	Silicon Carbide	from p.43
GaN	Gallium Nitride	from p.43
AlGaN	Aluminium gallium nitride	from p.44
S/N	Signal to Noise Ratio	from p.46
NO _x	oxides of nitrogen	from p.54
WMO	World Meteorological Organization	from p.54
GAW	Global Atmosphere Watch	from p.55
HID	high intensity discharge	from p.57
SPF	Sun Protection Factor	from p.60
ED	effective dose	from p.60
PF	protection factor	from p.60
UPF	Ultraviolet Protection Factor	from p.61
EPF	eye protection factor	from p.62
IRPA	International Radiation Protection Association	from p.62
INIRC	International Non-Ionizing Radiation Committee	from p.62
PABA	Para-aminobenzoic acid	from p.63
NPL	National Physics Laboratory	from p.69
EAC	Erythema Action Curve	from p.80
IVA	Intravehicular activity	from p.86
EVA	Extravehicular activity	from p.86
BGP	Osteocalcin bone gla protein	from p.88
BAP	Bone alkaline phosphatase	from p.88
PICP	carboxyl-terminal propeptide of human type 1 procollagen	from p.88
Pyr	pyridinoline	from p.88
CTX	type I collagen C-telopeptide (Crosslaps(TM))	from p.88
D-Pyr	deoxypyridinoline	from p.88
PTH	parathyroid hormone	from p.88
GH	somatotropin	from p.88
IGF-1	somatomedin	from p.88

Riassunto

Introduzione

L'ozono stratosferico è noto per essere il più importante fattore atmosferico coinvolto nell'assorbimento della radiazione UV. Vi sono, tuttavia, altri effetti che influenzano il trasferimento di energia da parte della radiazione UV al suolo: nubi, aerosol, ozono troposferico ed altri inquinanti gassosi. I rapporti tra i vari fenomeni che si svolgono in atmosfera sono complessi e non ben conosciuti. Pertanto, il monitoraggio dei livelli di UV al suolo è necessario per esplorare cambiamenti atmosferici e conseguenti effetti sulla biosfera e sulla vita.

In questo secolo, inoltre, l'uomo viaggerà nello spazio e in tale ambiente gli effetti della radiazione UV sulla salute e sui materiali non sono ancora completamente compresi.

Uno strumento in grado di misurare uno o più irradimenti efficaci da irradiazione UV solare deve avere una sensibilità decrescente con la lunghezza d'onda deve essere stabile alla temperatura e garantire riposte riproducibili nel lungo termine. Inoltre la risposta del sensore deve essere in accordo con la legge del coseno. Queste sono solo alcune condizioni importanti per la progettazione di un buon sensore, ma come ottenere una particolare risposta spettrale che possa ricostruire una efficacia biologica?

Questo lavoro riguarda lo sviluppo di sensori innovativi per misurazioni biologiche efficace UV e le loro possibili applicazioni nel campo della ricerca sulla terra e nello spazio.

Tecnologie ottiche per la misura dell'irradimento efficace biologico della radiazione UV

Ci sono due possibili opzioni per la misura dell'irradimento UV efficace: utilizzare uno strumento a scansione rappresentato da un spettroradiometro, o scegliere uno strumento a banda larga chiamato radiometro.

Attualmente in commercio sono disponibili pochi strumenti a scansione in grado di lavorare per un lungo periodo all'aperto e di garantire risultati a basso errore a causa del lungo tempo di scansione e la durata limitata di componenti meccaniche. Ciò limita gravemente la precisione delle misurazioni biologiche e solleva la questione se il controllo biologico non può essere realizzato da strumenti più semplici. Questi sono rappresentati dai radiometri a banda larga. Fondamentalmente ci sono due categorie di strumenti di questa famiglia: il radiometro basato sul fosforo Robertson - Berger e lo strumento basato su filtri interferenziali. Entrambi hanno risposta rapida e sono relativamente poco costosi. Essi possono misurare uno o un gruppo selezionato di spettro d'azione o una serie di bande strette.

Molto utile per alcune applicazioni, i filtri interferenziali non sono ancora utilizzati nel monitoraggio a lungo termine delle radiazioni UV a causa della loro scarsa stabilità nel lungo termine. I numerosi sforzi compiuti per migliorare le loro prestazioni porta ad una loro più ampia applicazione.

La possibilità di ottenere praticamente qualsiasi risposta spettrale in trasmissione o in riflessione rende i filtri interferenziali la scelta migliore per questo tipo di applicazioni e

permette di sviluppare nuovi strumenti per la misurazione dell'irradiazione efficace solare.

Filtri interferenziali

Negli ultimi anni l'interesse per lo sviluppo di rivestimenti ottici ad alte prestazioni in riflessione / trasmissione in diverse regioni spettrali come EUV, raggi UV, Vis, NIR è cresciuto notevolmente. Utilizzando la tecnologia del film sottile multistrato è possibile ottenere praticamente ogni curva di risposta.

Accoppiando filtri innovativi con particolare fotodiodi UV di sufficiente area attiva, è possibile ricostruire diversi spettri di azione. Di seguito sono riportati alcuni esempi di possibili soluzioni innovative per la misurazione degli spettri d'azione.

La curva di risposta nominale del filtro interferenziale, $T_{filter}(\lambda)$ (a cui ci riferiremo come "the target curve") è ricavata, in accordo con l'equazione (1) tra il rapporto tra la curva d'azione ed il prodotto tra la curva di risposta del fotodiodi, R_{ph} e la curva di trasmissione spettrale dell'elemento diffusore T_{diff} :

$$\frac{Action_Spectrum}{R_{ph}(\lambda) \cdot T_{diff}(\lambda)} = T_{filter}(\lambda) \quad (1)$$

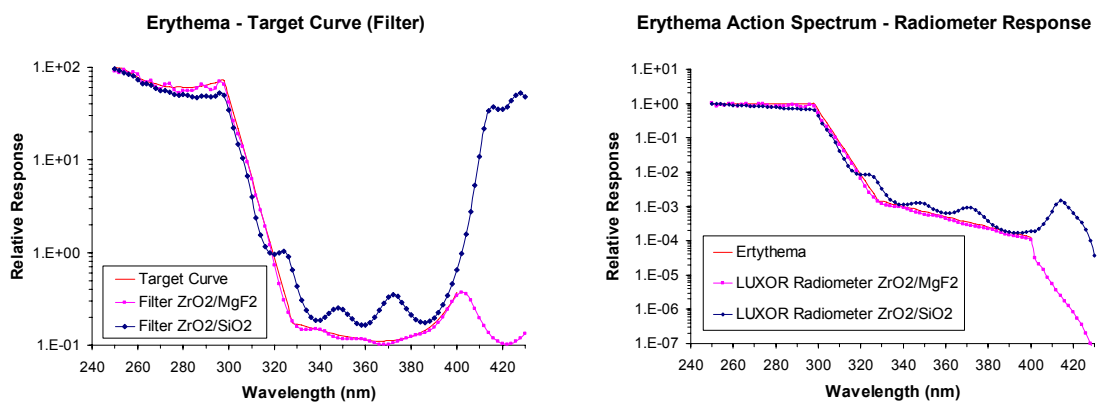


Figura 1. Radiometro con curva di risposta equivalente alla curva d'azione dell'Erythema. Curve di risposta dei filtri e curva di risposta del sensore rispettivamente per i disegni con ZrO_2/SiO_2 e ZrO_2/MgF_2 .

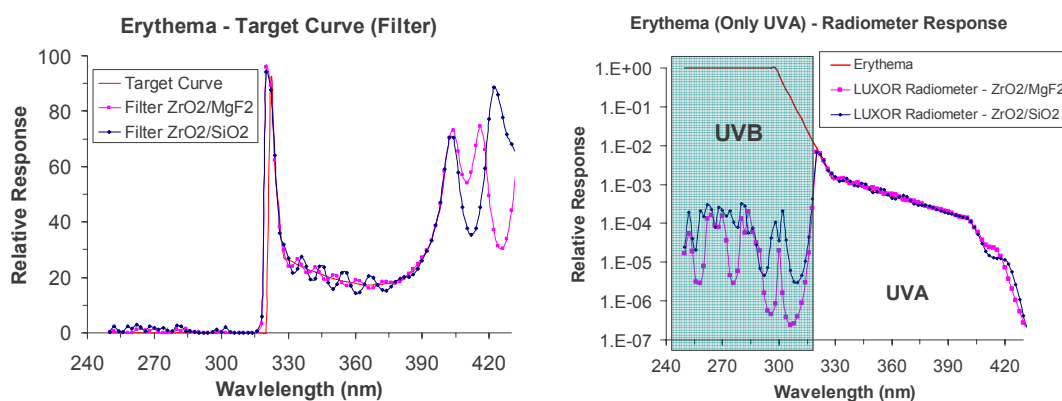


Figura 2. Radiometro con curva di risposta equivalente alla curva d'azione (Solo porzione UVA) dell'Erythema. Curve di risposta dei filtri e curva di risposta del sensore rispettivamente per I disegni con ZrO_2/SiO_2 e ZrO_2/MgF_2 .

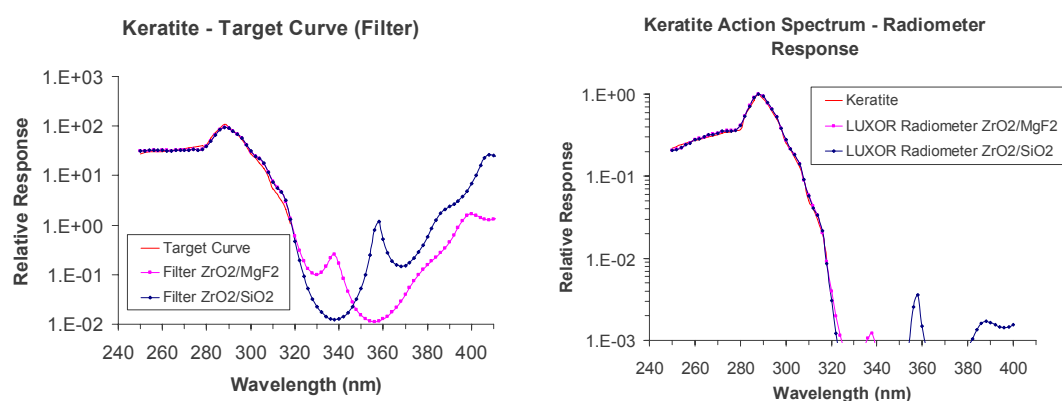


Figura 3. Radiometro con curva di risposta equivalente alla curva d'azione della Keratite. Curve di risposta dei filtri e curva di risposta del sensore rispettivamente per I disegni con ZrO_2/SiO_2 e ZrO_2/MgF_2 .

Caratterizzazione degli elementi ottici

Nelle applicazioni radiometriche la perfetta conoscenza di ogni componente della strumentazione è essenziale. Per esempio, in un tipico strumento come quello schematizzato in figura 4, è importante conoscere il comportamento dell'elemento UV diffusore in termini di proprietà diffusive e curva di trasmissione, inoltre nella progettazione di un particolare filtro interferenziale la conoscenza dei dettagli della crescita del film e delle costanti ottiche dei materiali coinvolti è essenziale.

Uno studio dettagliato dei materiali coinvolti nella progettazione del filtro è una parte fondamentale della caratterizzazione procedure. Una volta ottenuto il filtro depositato la sua stabilità nel lungo periodo e la stabilità termica dovrebbero essere parametri analizzati e, naturalmente, la sua curva di risposta spettrale di trasmissione / riflessione deve essere misurata con alta precisione. Infine, la parte principale di un radiometro è il sensore. La scelta di questa componente determina il rendimento finale dello strumento, per questo motivo, la caratterizzazione e la calibrazione di possibili rilevatori UV sono una parte fondamentale del lavoro di progettazione

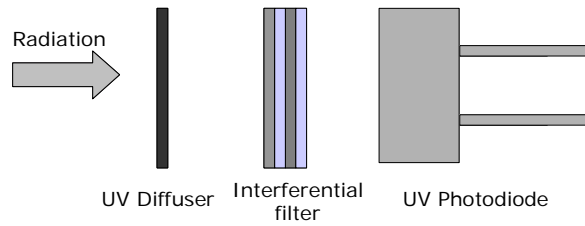


Figura 4. Tipico layout del radiometro

Elemento Diffusore

Nell'attività del mio dottorato, di diversi materiali diffusori sono stati caratterizzati:

- * Quartz preparato in laboratorio: spessore 1,9 mm e Quartz Suprasil spessore di 2 millimetri;
- * Teflon AF1600 da DUPONT;
- * Zenith SG 3201, spessore 0,1 millimetri, (ORIEL);
- * Diversi campioni di Teflon preparati in laboratorio, spessore 0,3, 0,5 e 1 mm.

Due tipi di misurazioni sono state effettuate: la misura della trasmissione spettrale del campione (in modo da recuperare $R_{diff}(\lambda)$) e misure di analisi delle proprietà diffusive (in base alla legge Coseno). I risultati sono riportati sulla trasmissione nelle figure 5 e 6.

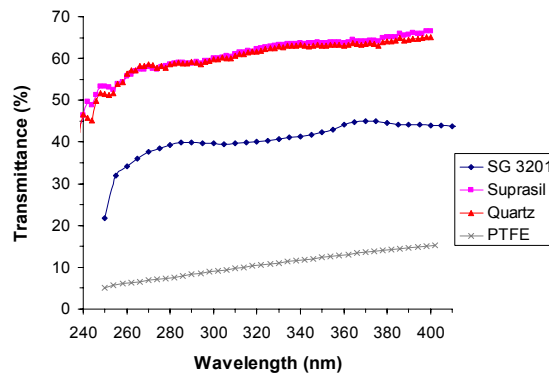


Figura 5. Misure di trasmissione su materiali diffusori UV.

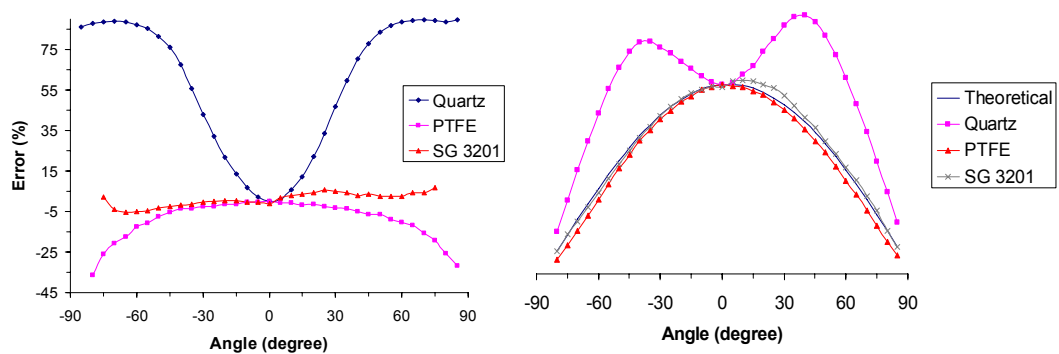


Figura 6. Deviazione rispetto alle legge del coseno. Errore (%) e assoluto rispetto ai valori ideali.

Deposizione e caratterizzazione di film sottili

L'elemento veramente innovativo dei nostri radiometri è rappresentato dai interferenziali filtri multistrati. Attualmente abbiamo una collaborazione attiva con Luxel Corp (US) e fino ad ora i filtri sono stati prodotti e acquistati presso questa azienda. All'interno di questa collaborazione sono state effettuate alcune misure profilometriche degli indici di rifrazione dei materiali coinvolti. Grazie a queste misure è stato possibile ottimizzare la progettazione dei filtri.

Sui campioni realizzati sono state eseguite numerose prove: misure di trasmissione spettrale, misure di stabilità termica e sul lungo periodo.

Campioni di test sono stati sviluppati da Luxel Corporation Inc e su questi si è svolto un lungo lavoro preliminare sulla caratterizzazione dei materiale in modo da recuperare le costanti ottiche di SiO_2 , ZrO_2 e MgF_2 , materiali coinvolti nel design dei filtri. Le prestazioni del filtri $\text{ZrO}_2/\text{MgF}_2$ e $\text{ZrO}_2/\text{SiO}_2$ preparati da Luxel sono riportate come esempio nelle figure 9 e 10, rispettivamente, per i filtri per la curva dell'eritema e per la curva d'azione della congiuntivite.

Parallelamente alle attività svolte in collaborazione con Luxel, sono state eseguite delle deposizioni di film sottili di ZrO_2 e MgF_2 presso il nostro laboratorio Luxor utilizzando un facility di deposizione a cannone elettronico (e-beam evaporation). Anche in questo caso si è eseguito un lavoro preliminare sulla caratterizzazione dei materiali al fine di valutare le costanti ottiche dei materiali. Diversi metodi di analisi sono stati seguiti per misurare l'indice di rifrazione attraverso misure di trasmittanza / riflettanza. Il risultato di queste analisi è riportato nelle figure 7 e 8.

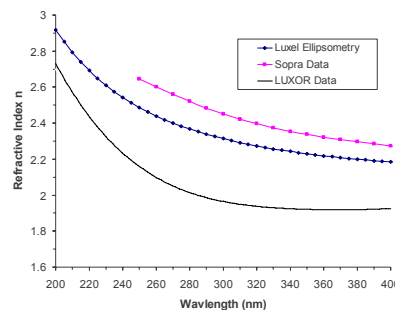


Figura 7. Confronto delle costanti ottiche di film di ZrO_2 preparati con differenti processi.

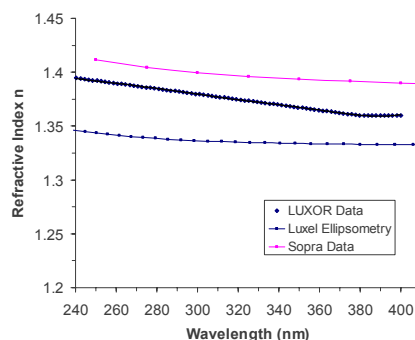


Figura 8. Confronto delle costanti ottiche di film di MgF_2 preparati con differenti processi.

La misure di trasmissione di alcuni filtri interferenziali sono riportate di seguito. Le differenze tra la curva target e le curve misurate sono derivanti dalla ottimizzazione del processo di deposizione ancora sotto indagine.

Le misurazioni sono state effettuate presso Delta Ohm utilizzando il doppio monocromatore Bentham. I dati sono completamente in accordo con i risultati ottenuti indipendentemente da Luxel. Analoghi risultati sono stati ottenuti nel nostro laboratorio utilizzando uno spettrofotometro Varian Cary 5000.

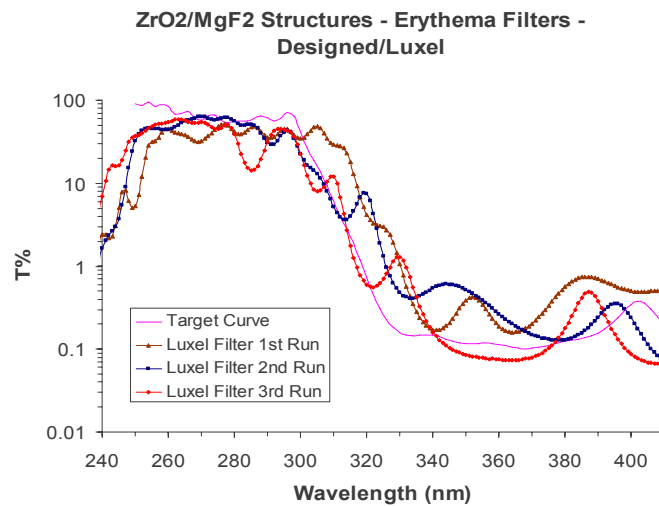


Figura 9. Confronto delle curve di trasmissione di diversi filtri per il sensore Erythema like – Struttura basata su ZrO₂/MgF₂. Confronto tra curva Target e differenti prototipi.

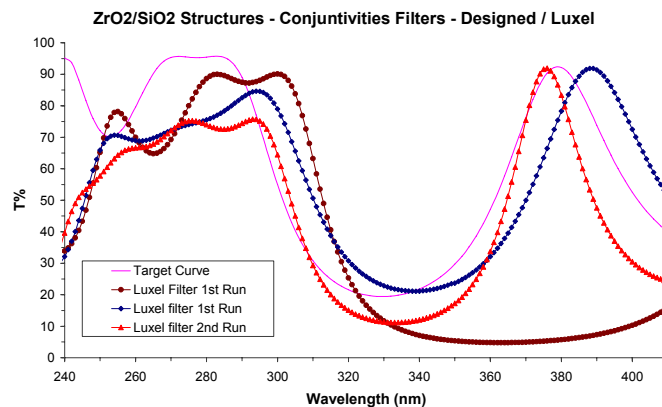


Figura 10. Confronto delle curve di trasmissione di diversi filtri per il sensore Conjunctivities like – Struttura basata su ZrO₂/SiO₂. Confronto tra curva Target e differenti prototipi.

Caratterizzazione e calibrazione di rivelatori per l'UV

Come abbiamo visto i radiometri UV a banda larga e gli spettroradiometri sono gli strumenti utilizzati per determinare rispettivamente l'irradianza totale e irradianza spettrale (cioè irradianza in funzione della lunghezza d'onda). Per la specifica

applicazione di questi strumenti, la scelta del sensore più appropriato è fondamentale. Alcuni radiometri, per esempio, sono stati progettati in modo da avere una risposta spettrale che ricostruisce un particolare spettro di azione (cioè l'efficacia relativa della radiazione UV nella produzione di una determinata risposta biologica). Come descritto sopra, questo può essere realizzato accoppiando un filtro con una corretta trasmissione spettrale ad un sensore con una specifica curva di risposta spettrale

Nell'ambito del mio dottorato sono stati caratterizzati numerosi fotodiodi UV commerciali. I campioni analizzati sono:

- Fotodiodi SiC di area attiva di 0.22 mm^2 (sei campioni)
- Fotodiodi p-i-n GaN di area attiva 0.5 mm^2 (due campioni)
- 3 differenti fotodiodi AlGaN Schottky, area attiva di 0.5 mm^2 :
 - A: picco di risposta a 250 nm (2 campioni)
 - B: picco di risposta a 300 nm (2 campioni)
 - C: picco di risposta a 300 nm, costruito con finestra UV (2 campioni).

Le curve di risposta spettrale relativa e assoluta sono state ricavate attraverso le formule 2 e 3, dove R_λ è la risposta spettrale e R'_λ la risposta spettrale del campione di riferimento. I_λ e I'_λ rappresentano le fotocorrenti misurate rispettivamente con il campione in esame e con quello di riferimento. Infine, A_{ap} e A_{ph} rappresentano rispettivamente l'area attiva illuminata e quella totale del fotodiodi:

$$R_\lambda = \frac{I_\lambda}{I'_\lambda} R'_\lambda \quad (2)$$

$$R_{\lambda=280nm}^A = \frac{A_{ap}}{A_{ph}} \frac{I_{\lambda=280nm}}{I'_{\lambda=280nm}} R'_{\lambda=280nm}, \quad (3)$$

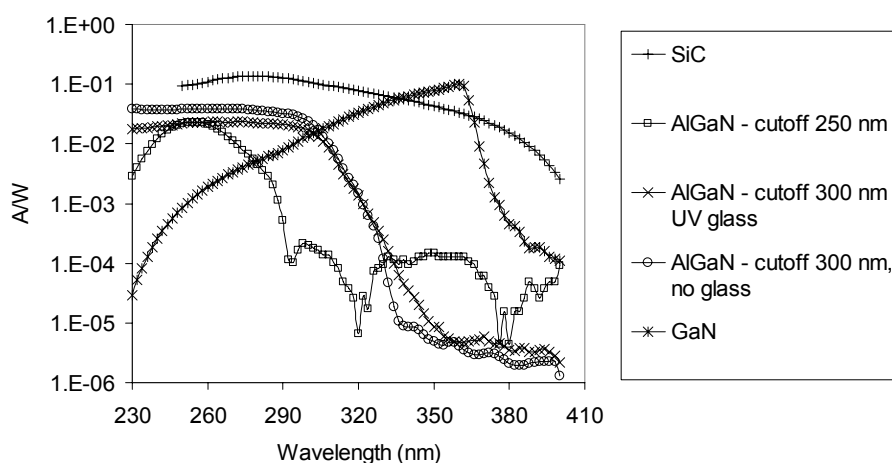


Figura 11. Curve di risposta spettrale assoluta per diversi fotodiodi.

Realizzazione ed applicazione dello strumento

Diversi prototipi di questo tipo di strumentazione sono stati sviluppati. Sensori con curva di risposta equivalente alla curva di azione dell'eritema e brevettati, inoltre questo strumento ha vinto il premio "Veneto Innovazione 2005" per la collaborazione tra università e industria. Altri sensori con particolari curve di risposta sono stati progettati, come la vitamina D, danno al DNA, Eye cataratta, ecc

Tutti questi strumenti possono essere utilizzati in numerose applicazioni sulla terra e nello spazio.

Un'immagine di un tipico radiometro sviluppato presso i laboratori LUXOR è illustrata in figura 12. Dettagli di possibili applicazioni di questa tecnologia sono presentati nella prossima sezione.



Figura 12. Immagine di un prototipo.

Applicazione nel monitoraggio delle sorgenti artificiali

L'esposizione prolungata ai raggi UV artificiali può provocare ustioni, invecchiamento della pelle, melanoma e altri tipi di cancro. Nella legge europea EN60335 - 2 - 27 la tossicità di macchine che emettono radiazioni UV per uso domestico è regolamentata e vi sono stabiliti dei limiti superiori di esposizione efficace. Come altre sorgenti artificiali, le unità abbronzanti devono essere controllate e certificate secondo la legge. Vi è la necessità di sviluppare una chiara procedura di misurazione per verificare sorgenti per solarium. Inoltre è necessario sviluppare strumenti portatili per la misura dell'irradiazione efficace per la verifica in loco. Il nostro radiometro Senserit® è stato inizialmente sviluppato e brevettato proprio con lo scopo di monitorare sorgenti per l'abbronzatura artificiale. In figura 13 sono illustrati alcuni spettri tipici di questo tipo di sorgenti. In tabella 1 sono riportati gli errori max sulla misura dell'irradiazione efficace ottenuti con Senserit su sorgenti UV per l'abbronzatura.

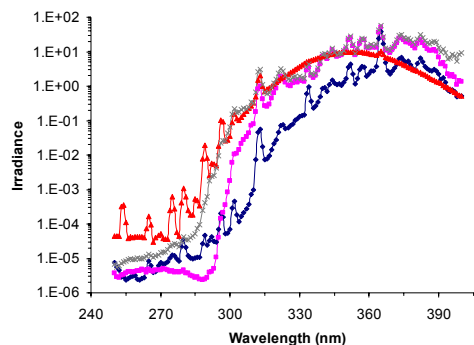


Figura 13. Esempio di irradiazione di lampade solari commerciali.

Errore % sulla misura dell'irradiazione efficace	1st Prototipo	2nd Prototipo	3rd Prototipo
	23.202	7.912	-32.650

Tabella 1. Errore % max sulla misura dell'irradiazione efficace. I tre valori sono riferiti ai primi 3 prototipi realizzati.

Applicazioni nell'astronautica

La ben nota forte dipendenza della sintesi di vitamina D da esposizione a radiazione UVB porta a considerare possibili problemi connessi ad una permanenza in ambienti privi di luce UV come ad esempio la stazione spaziale ISS o una futuristica stazione lunare permanente. La luce naturale UVB solare è normalmente assente all'interno di un ambiente come la stazione spaziale. E' necessario, pertanto, studiare la radiazione UV all'interno della stazione che potrebbe derivare da diverse sorgenti artificiali, nonché da occasionali irradamenti solare UV dietro uno degli oblò della stazione.

Questo tipo di misurazione può essere eseguita utilizzando un dosimetro UV come un Biofilm o di un radiometro con una specifica curva di risposta.

Tali strumentazioni sono state applicate finora solo sulla Terra in diversi studi in cui il monitoraggio della radiazione UV è stato effettuato in diverse zone geografiche.

L'estensione degli studi terrestri ad ambienti spaziali è possibile applicando simili strumentazioni e metodi. Usando dosimetri UV è possibile determinare l'efficacia biologica della radiazione UV presente in luoghi diversi dell'ambiente spaziale come la stazione spaziale internazionale. Tali dosimetri potrebbero essere applicati sul corpo umano per determinare la dose UV personale di un singolo cosmonauta (per i diversi effetti biologici, quali eritema, sintesi di vitamina D, Eye cataratta, danni del DNA, ecc.) Focalizzare l'esperimento sulla produzione di vitamina D e l'effetto ad essa legato di perdita di densità del tessuto osseo potrebbe dimostrare se la radiazione UV all'interno della Stazione spaziale internazionale è sufficiente per un adeguato approvvigionamento di vitamina D e se le condizioni particolari (ad esempio, l'esposizione a lampada UV) possano interagire con la formazione ossea. I dati raccolti possono essere correlati con eventuali analisi del siero dei cosmonauti in tempo reale con la possibile distinzione di diversi singoli irradamenti.

Con la misurazione della radiazione ultravioletta solare naturale che raggiunge l'interno della ISS attraverso gli oblò permetterà di valutare la pericolosità di tali radiazioni e di stabilire infine una possibile applicazione di filtri che possono modificare lo spettro di irradamento in modo da renderlo simile a quello al suolo.

Un disegno di "cabine solari" per la stazione spaziale potrebbe essere un possibile risultato dello studio

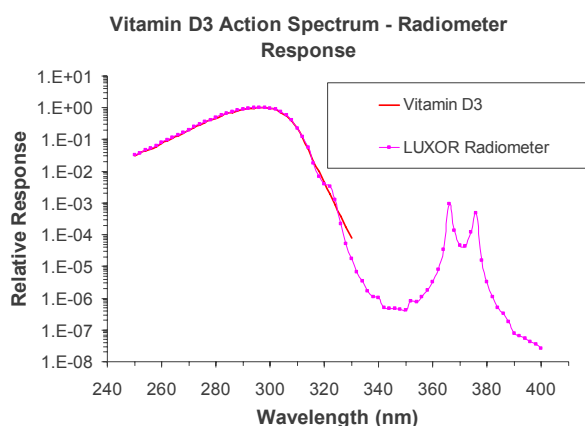


Figura 14. Radiometro per la misura della sintesi della Vitamina D

Summary

Stratospheric ozone is known to be the most important atmospheric factor determining clear sky UV radiation reaching the Earth's surface. There are, however, other effects that influence the UV radiant energy transfer: cloud cover, aerosols, tropospheric ozone, and other gaseous pollutants. The relationships between various phenomena taking place in the atmosphere are complex and not well known. Therefore, ground based UV measurements are necessary to explore atmospheric changes and resultant effects on the biosphere and on the life.

Moreover in this century the human will travel in space and in such environments the UV effects on health and on materials are not yet completely understood.

An instrument that can measure one or several effective irradiation from ultraviolet solar emission must have an increasing sensitivity with decreasing wavelength and should be temperature stabilized and long term reproducible, moreover the response of the sensor should be in agreement with the cosine law. These are only some important condition for the design of a good sensor, but how to obtain a particular spectral response that can reconstruct a biological effectiveness?

This work regards the development of innovative sensors for biological effective UV measurements and their possible applications in research field on earth and in space environments.

1. UV radiation: theoretical principles and measurements techniques

1.1. Introduction

Exposure to UV occurs from both natural and artificial sources. The sun is the principal source of exposure for most people. Solar UV undergoes significant absorption by the atmosphere. With depletion of the stratospheric ozone people and the environment will be exposed to higher intensities of UV this underscores the current need to better understand the potential health and environmental risks of UV exposure.

UV is one of the non-ionizing radiations in the electromagnetic spectrum and lies within the range of wavelengths 100 nm (which corresponds to a photon energy of approximately 12 eV) to 400 nm (figure 1.1). The short wavelength limit of the UV region is often taken as the boundary between the ionizing radiation spectrum (wavelengths < 100 nm) and the non-ionizing radiation spectrum. UV can be classified into UVA (315 - 400 nm), UVB (280 - 315 nm) and UVC (100 - 280 nm) regions, although other conventions for UVA, UVB and UVC wavelengths bands are in use.

Most artificial sources of UV, except for lasers, emit a spectral continuum of UV containing characteristic peaks, troughs and lines. These sources include various lamps used in medicine, industry, commerce, research and the home.

The fact that ultraviolet radiation affects living organisms was already known in the 19th century. The technological and scientific advances at the beginning of 20th century made it possible to measure and understand some of the biologic effects of UV. In their paper published in 1921, Hausser and Vahle [1] described the experiment that allowed the measurement of the wavelength dependency of erythema. The modern classification of UV radiation into 3 bands: UV-C, UV-B and UV-A was accepted at the Congress of the Comité Internationale de Lumière in 1932 [2]. It was based on the differences of the biologic effectiveness in those bands. Since then many studies have been performed to determine the action spectra for biological objects other than human skin. Some of these action spectra are: Erythema Action Spectrum, DNA Breaks, Polychromatic Action Spectrum for Higher Plants, Generalized plant damage,

Phytoplankton Photoinhibition. In figure 1.1 they are represented overlapped with a clear sky spectral distribution of UV solar irradiance.

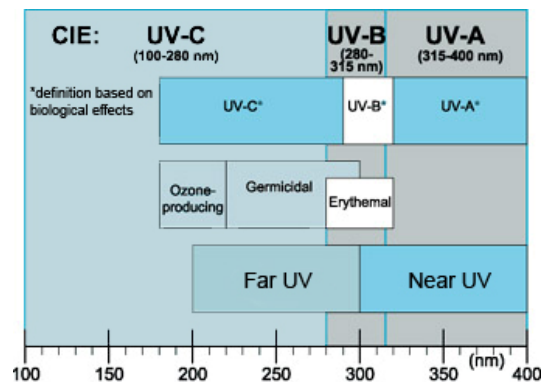


Figure 1.1. Ultraviolet spectral regions. Conventional subdivision based on biological effects.

Only the portion of the action spectrum above 290nm has any meaning for solar radiation measurements and only this spectral range was taken into consideration. Often there are many difficulties to establish a unique action spectrum for a photobiologic process (cause there may be interactions between effects at different wavelengths, repair processes may be significant during irradiation, the end point may be delayed or not well defined) and the overall uncertainty of the published action spectra varies from $\pm 17\%$ to approximately 100%.

UV-induced biological effects depend on the wavelengths of the radiation. It is necessary for a proper determination of hazard to have spectral emission data. These consist of spectral irradiance ($\text{W}/\text{m}^2\text{nm}^{-1}$) measurements or calculations of emissions from the source. The total irradiance (W/m^2) is obtained by summing over all wavelengths emitted. The biological or hazard weighted irradiance (W/m^2 effective) is determined by multiplying the spectral irradiance at each wavelength by the biological or hazard weighting factor (which quantifies the relative efficacy at each wavelength for causing the effect) and summing over all wavelengths. Such factors are obtained from action spectra.

1.2. Interaction of UV with Matter

Attenuation of UV occurs due to absorption and scattering. Reflection, refraction and diffraction are phenomena related to boundaries between media. All of these interactions may change the direction, intensity and the wavelength of UV. The quantities describing interactions of UV with matter are dependent on the wavelength. The total energy absorbed in a material is influenced by reflections from its surfaces. The attenuation coefficient describes the attenuation of UV within tissue and is the sum of the absorption and scattering coefficients. Penetration depth in a tissue is inversely proportional to the exponential attenuation coefficient.

Absorption requires transfer of radiative energy to matter. Apart from possible photomechanical effects, UV is absorbed as a result of electron transitions at the atomic and molecular level. Such molecular absorption can lead to photochemical reactions.

In most molecules the ground state or the singlet state (S_0) consists of two paired electrons. On absorption of radiant energy one of the electrons can make a transition to an excited state (S_1), provided that the incident photon energy corresponds to an existing level in the absorbing molecule. The molecule can release this absorbed energy from the excited state by:

- (a) transition directly back to the ground state, S_0 , or
- (b) transition to the generally long-lived excited triplet state, T_1 , and then discharging the remaining energy to return to S_0 .

In either case, transition back to S_0 may be radiative (a photon emitted) or non-radiative (energy dispersed by vibrational-rotational relaxation). The radiative $S_1 \rightarrow S_0$ transition is called "fluorescence" while radiative $T_1 \rightarrow S_0$ is called "phosphorescence". In addition, molecules in the S_1 or T_1 states can return to the ground state either by forming photoproducts or by transferring the energy to an acceptor molecule. The effectiveness of the photochemical process can be amplified by "photosensitizers" or impeded by "quenchers".

1.3. Cellular and Molecular Studies

To produce any change, UV must be absorbed by the biomolecule. This involves absorption of a single photon by the molecule and the production of an excited state in which one electron of the absorbing molecule is raised to a higher energy level. The primary products caused by UV exposure are generally reactive species or free radicals which form extremely quickly but which can produce effects that can last for hours, days or even years. DNA is the most critical target for damage by UVB and UVC radiations. While a considerable amount of knowledge is available concerning the interaction of UV with nucleic acids [3], controversy exists as to which lesion constitutes the most important type of pre-mutagenic damage. Cell death, chromosome changes, mutation and morphological transformations are observed after UV exposure of prokaryotic and eukaryotic cells [4]. Many different genes and several viruses (including HIV) are activated by UV exposure. The genes activated by UVB and UVC are different from those activated by UVA. Studies of DNA repair defective disorders have clearly established a link between UV induced DNA damage in skin and various types of cancer [5].

1.4. Animal Studies

Solar UV has been shown to produce cancers in domestic and food animals. In experimental animals UV causes predominantly squamous cell carcinomas (SCC). UVB is most effective at producing SCCs, although they are produced by UVA but at much higher intensities, similar to the levels needed for erythema and tanning [6]. The effectiveness of UVC is unknown except at one wavelength (254 nm). At this wavelength the effectiveness is less than UVB. Melanomas are much less common and only two animal models have been found for induction of melanoma by UV alone. An initial action spectrum determined for a type of hybrid fish indicates a peak in the UVB range but also shows a high level of effectiveness in the UVA [7]. Basal cell carcinomas are rare in animals. Exposure to suberythemal doses of UV have been shown to exacerbate a variety of infections in rodent models. UV affects infections both at the site of exposure and at distant sites. Recent work indicates that systemic infections without skin involvement may be affected. Enhanced susceptibility appears to result from T-

helper cell activity. The mechanisms associated with this suppression appear to be the same as those identified with suppression to contact and delayed type hypersensitivity responses. Suppression of these immune responses appears to be mediated by release of soluble mediators from UVB exposed skin which alters the antigen presentation by Langerhans and other cells so that they fail to activate TH 1 cells. The resulting immune suppression is antigen specific, can occur regardless of whether or not antigen is applied at the site of exposure, and is relatively long lasting. UV exposure also prevents the development of protection immunity to a variety of infections in mice and rats. Many studies in experimental animals have demonstrated that UV exposure can cause both acute and delayed effects such as cataract, photokeratitis, damage to the corneal epithelium and various retinal effects. Studies of photochemical retinal injury in aphakic monkeys have shown that the retina is six times more vulnerable to photochemical damage from UV than the visible wavelengths [8].

1.5. Health Effects on Humans

1.5.1. Skin

Acute effects on the skin consist of solar erythema, "sunburn", which, if severe enough, may result in blistering and destruction of the surface of the skin with secondary infection and systemic effects, similar to those resulting from a first or second degree heat burn. Although UVC is very efficiently absorbed by nucleic acids, the overlying dead layers of skin absorb the radiation to such a degree that there is only mild erythema and, usually, no late sequelae, even after repeated exposures. Much less is known about the biological effects of UVA. However, doses of UVA, which alone may not show any biological effect, can, in the presence of certain environmental, consumer and medicinal chemical agents, result in injury to tissues (phototoxicity, photoallergy, enhancement of photocarcinogenesis).

Chronic skin changes due to UV consist of skin cancer (both melanoma and non-melanocytic), benign abnormalities of melanocytes (freckles, melanocytic naevi and solar or senile lentigines), and a range of other chronic injuries resulting from UV exposure to keratinocytes, blood vessels and fibrous tissue, often described as "photoaging" (solar elastosis). The much increased rates of skin cancer in patients with xeroderma pigmentosum, who have a deficiency in the capacity to repair UV-induced DNA damage, suggest that direct UV damage of the DNA may be a step in the cause of these cancers [9]. This suggestion has also been supported by the observation of UV specific mutations of the p53 tumour suppressor gene in a proportion of patients with non-melanocytic skin cancer [10]. Oxidative and immune suppressant effects may also contribute to the capacity of UV to cause skin cancers. Cancer of the lip is much more common in fair than dark skin populations and is associated with outdoor work. However possible confounding with tobacco and alcohol use has not been adequately controlled in any study. The worldwide incidence of malignant melanoma has continued to increase. Strong epidemiological evidence exists that sun exposure causes cutaneous melanoma and non-melanocytic skin cancer [11]. Their incidence is less in darker than light skin groups living in the same geographical area. Risk of skin cancer decreases with increasing pigmentation. The anatomical site most seen for squamous cell carcinoma (SCC) is the head and neck, areas most exposed to the sun. Incidence of both melanoma and non-melanocytic skin cancer are increased in areas of high ambient solar UV radiation. Melanoma is strongly related to frequency of recreational

exposure to the sun and to history of sunburns. There is also suggestive evidence that exposure to sunlamps may increase the risk of melanoma [12].

1.5.2. Immune system

A number of studies suggest that UV exposures at environmental levels suppress immune responses in both rodents and man [13]. In rodents this immune suppression results in enhanced susceptibility to certain infectious diseases with skin involvement and some systemic infections. Mechanisms associated with UV-induced immunosuppression and host defense mechanisms which provide for protection against infectious agents, are similar in rodents and man. It is therefore reasonable to assume that exposure to UV may enhance the risk of infection and decrease the effectiveness of vaccines in humans.

1.5.3. Eye

The acute effects of UV on the eyes consist of the development of photokeratitis and photoconjunctivitis, which are unpleasant but usually reversible and easily prevented by appropriate eyewear. Chronic effects on the eye consist of the development of pterygium and squamous cell cancer of the conjunctiva and cataracts. A review of the studies suggests that there is sufficient evidence to link acute ocular exposure to photokeratitis but our knowledge of the effects of chronic exposure is less certain. While there is sufficient evidence that cortical and posterior subcapsular cataracts (PSC) can be caused by UVB in laboratory animals, there is limited evidence to link cortical and PSC cataracts in humans to chronic ocular exposure to UVB. Insufficient information is available to separate out the other factors contributing to cataract formation, or to state the proportion of cataracts which can be attributed to UVB exposure. There is also limited evidence to link the development of climatic droplet keratopathy and pterygium, but insufficient evidence to link uveal melanoma with UV exposure [14,15].

1.6. Environment

Increased levels of UV due to ozone layer depletion may have serious consequences for living organisms. A 10% reduction in ozone could lead to as much as a 15-20% increase in UV exposure depending on the biological process being considered. While the impact on human health, crop production, fisheries etc. is largely unknown, adverse effects of increased exposure to UVB have been reported on plant growth, photosynthesis and disease resistance. Further, the impact of increased UV levels on aquatic ecosystems (the major contributor to the earth's biomass) may be substantial. Phytoplankton, at the base of the aquatic food chain, serves as food for larvae of fish and shrimp. These in turn are consumed by fish, which subsequently provide an essential food source for many human beings and other animals. A significant reduction in phytoplankton from increased UVB exposure will directly affect the human and animal marine food source [16].

1.7. Biological Weighting Factors and Spectrally Weighted Quantities

Both radiant exposure H and irradiance E are quantities integrated over the total spectrum of interest. To describe the irradiance or radiant exposure in a very narrow spectral (wavelength) interval ($\Delta\lambda$), the quantities of *spectral irradiance* E_λ and *spectral*

radiant exposure H_λ are employed. These have the units of: Wm^{-2}nm and Jm^{-2}nm , respectively. If $E_\lambda \Delta\lambda$ is the irradiance in a narrow interval $\Delta\lambda$ around the wavelength λ , then the integrated irradiance E over the wavelength interval λ_1 to λ_2 can be written as:

$$E = \sum_{\lambda_1}^{\lambda_2} E_\lambda \Delta\lambda \quad (1.1)$$

Other spectroradiometric quantities exist with analogous definitions [17]:

- *Radiant Energy* Q (J).
- *Radiant Energy Density* $w=dQ/dV$ (J/m^3).
- *Radiant Flux* $\Phi=dQ/dt$ (J/s or Watt).
- *Radiant Exitance* $M=d\Phi/dA_{\text{orig}}$ (W/m^2).
- *Irradiance or Radiant Flux* $E=d\Phi/dA_{\text{sup}}$ (W/m^2).
- *Radiant Intensity* $I=d\Phi/d\Omega$ (W/sr).
- *Radiance* $L=dI/dA\cos\theta$ ($\text{W}/\text{sr m}^2$).

The spectroradiometric quantities are important in photobiology, and are critical in any discussion of the biological effects of UV. The biological effects of UV are strongly wavelength dependent. As a measure of these effects, "effective" or "biologically active" quantities have been introduced (CIE, 1987 [18]).

The effective irradiance E_{eff} is defined as:

$$E_{\text{eff}} = \sum E_\lambda S_\lambda \Delta\lambda \quad (1.2)$$

and similarly, the effective radiant exposure is:

$$H_{\text{eff}} = \sum H_\lambda S_\lambda \Delta\lambda \quad (1.3)$$

where S_λ is called the relative spectral effectiveness function or *action spectrum*.

The *action spectrum* gives the relative biological response of a biological element to irradiation at different wavelengths, and ideally will correspond to the absorption spectrum of critical absorbing molecules, or "chromophores".

1.7.1. Some important action spectrum

Actually there are a growing interest in applying the biological weighting factor in the measurements of the effects of UV radiation on biological matter, moreover, new ways to apply this method of dosimetry are finding place in the evaluation of UV effects on materials, such as polycarbon and other plastics components very useful in earth and even in space environments.

Probably the best known action spectrum actually is the *erythema action curve*. Based on a statistical analysis of the results of minimum erythema dose studies carried out over the past 20 years or so, and including data by Parrish *et al.* (1982) [19] on the erythemal efficacy of UVA, the CIE has promulgated a reference action curve (McKinlay

and Diffey, 1987 [20]). This function consists of three straight lines when plotted on a semi-logarithmic scale, and although individual action spectra would not have the two inflection points, the function can be readily expressed by three mathematical functions. The function has been adopted internationally by the CIE and the IEC and is being used by national organizations and authorities for the determination of the erythemal potential of an exposure to a given source of UV.

Other many important studies have been performed to determine the action spectra for biological objects other than human skin. Some of these action spectra are: DNA Breaks, Polychromatic Action Spectrum for Higher Plants, Generalized plant damage, Phytoplankton Photoinhibition [21-23]. In figure they are represented overlapped with a clear sky spectral distribution of UV solar irradiance.

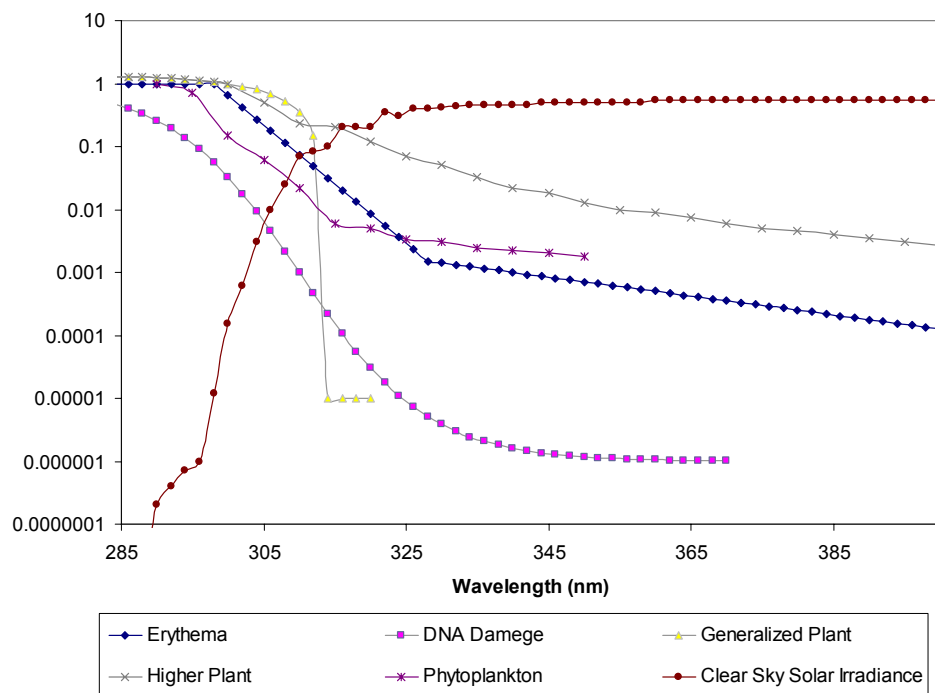


Figure 1.2. Some important action spectrum overlapped with a clear sky UV solar irradiance.

1.8. Measurement Techniques

There are three distinct types of measurement systems employed in the detection of UV:

1. radiometers,
2. spectroradiometers and
3. dosimeters.

Radiometers and spectroradiometers are direct-reading instruments that use electro-optical (physical) detectors to convert the incident radiation into an electrical signal. Radiometers measure all incident radiant power over a wide spectral range; whereas, spectroradiometers measure the radiant power distribution over a wide spectral range. Either by electronic means or by computer control, radiometers or spectroradiometers

may be modified and calibrated to operate as "dosimeters" by time-integration of the output signal from the detector.

However, by dosimeters, one usually means devices that by nature respond directly to incident dose, i.e. radiant exposure. Dosimeters may be further optically modified and calibrated to respond according to an action spectrum, thereby serving as a direct-reading instrument for dose to a particular organ.

1.8.1. Detectors

The term detector normally refers to an electro-optical device which converts an optical signal (e.g UV light) into an electronic signal which can be recorded. An important characteristic of any detector is the responsivity, defined as the quotient of the detector output (e.g amperes, A) and the radiant power incident upon the detector (e.g. watts, W). Thus units for responsivity may vary. The unit for irradiance-responsivity is often ampere-per-watt-per-square-meter (A/Wm^2). The spectral responsivity is the responsivity as a function of wavelength. The term detectivity is used to compare the detection capability (the smallest quantity of radiation that can be detected) of different types of detectors, the higher the detectivity the more sensitive the detector. Thermal detectors, such as thermopiles and pyroelectric detectors, have a much lower detectivity (less sensitive) than photodiodes, phototubes and photomultipliers.

The most common types of detectors for UV are semiconductor (junction) photodiodes, vacuum photodiodes (phototubes) and photomultipliers. Junction photodiodes are usually silicon (Si) photodiodes that may be enhanced to improve their UV responsivity and with a spectral responsivity between 190 and 1100 nm. Gallium-arsenide-phosphide (GaAsP) photodiodes have a spectral responsivity between 190 and 670 nm, and gallium-phosphide (GaP) photodiodes have a spectral responsivity between 190 and 520 nm.

Chemical detectors, such as photographic film emulsions or polymer films of polysulphone or CR-39 resins, respond to incident radiant exposure (J/m^2). Their responsivity is generally strongly wavelength dependant, and attempts are made to simulate a photobiological action spectrum directly.

The choice of an optimum detector for a specific instrument or measurement situation depends upon the requirements for ease of data collection, portability, electrical power requirements, size and accuracy. Each detector type has advantages and disadvantages. Important parameters to consider for instrument requirements are: spectral responsivity, noise-equivalent-power (NEP), linearity, time/frequency response, stability over time, environmental operating conditions, maintenance, ease of operation, the requirements upon additional electronics, and cost.

Biological detectors are also used. For example, biofilms using dried spores of *bacillus subtilis*, immobilized on transparent polyester plastic sheets. After irradiation the biofilm is incubated in a growth medium and the proteins synthesized after spore germination, stained and evaluated by photometry. The biologically effective dose is calculated using a calibration curve. The UV response of this biofilm is additive and follows the reciprocity law in the normal range of fluence rates investigated. The response is independent of temperature ($-20^{\circ}C$ to $70^{\circ}C$) and humidity. The biofilm can be stored for up to 9 months at room temperature without significant influence on the viability of spores. These detectors have been used in Antarctica and in space to measure the biological consequences of ozone variations (Quintern *et al.*, 1992 [24]).

1.8.2. Radiometers

A radiometer is a detection system that measures incident radiation. A UV radiometer usually measures irradiance in watts per square meter (W/m^2). One of the main element of a radiometer is the optical filter, it has the purpose to limit the spectral responsivity to a certain band, having a lower and upper wavelength cutoff. The band-width can vary upward from about 5 nm, but is often several tens or even hundreds of nanometers wide. Hence, radiometers are called broad-band meters as opposed to spectroradiometers. Ideally the spectral responsivity is constant within the band and zero outside, but in practice this is not possible. If the detector is sensitive to radiation outside the passband of the filter, which is normally the case, there will always be a non-zero responsivity outside the band. Signals which are produced by radiation from outside the band are called "out-of-band signals," "out-of-band leakage," or just "stray light." This limitation of radiometers can often be a serious problem, and is particularly troublesome in UV radiometers based on Si photodiode detectors, because the spectral responsivities of Si photodiodes extend to 1100 nm in the infrared. If one attempts to use such radiometers to measure small quantities of in-band radiation in the presence of large quantities of out-of-band radiation, the results will be prone to large errors. This is frequently encountered when attempting to measure the very small component of biologically active UV present in a light source spectrum.

For many purposes it is desirable to have a UV radiometer which has a spectral responsivity equal to or closely resembling a certain action spectrum. If this is achieved, the radiometer signal is directly proportional to the "effective" or "biologically active" irradiance, because the radiometer will spectrally "weight" the different wavelengths according to the action spectrum S_λ . A well known example of such a radiometer is a photometer (lux-meter or luminance-meter) which has a spectral responsiveness that closely matches the photopic (visual) response of the human eye. Radiometers are commercially available which have spectral responsivities that match, for example, the UV erythema action spectrum (McKinlay and Diffey, 1987[20]) and UV hazard action spectrum adopted by the IRPA/INIRC (1991) and ACGIH [25].

1.8.3. Spectroradiometers

A spectroradiometer is a radiometer that is capable of measuring spectral radiometric quantities directly, such as spectral irradiance or spectral radiance. The major difference between the layout of a spectroradiometer and the layout of a radiometer is the waveband selecting device which in a radiometer is usually a broadband filter, whereas in a spectroradiometer it is a monochromator or a spectrograph. Radiation entering a monochromator or a spectrograph is dispersed by a grating or a prism and only a small band of radiation is passed to the detector, the so-called bandwidth. The spectroradiometer bandwidth can be selected according to the application, but it is typically 1 - 5 nm. The waveband passed to the detector can be changed manually or automatically by rotating the grating or prism; the instrument is scanned over the spectral range of interest. This type of instrument is called a scanning spectroradiometer.

In a spectrograph, a portion of the spectrum is incident upon a linear photodiode array which can be read diode by diode. This can occur very rapidly and a spectrum displayed almost instantly. This type of spectroradiometer is therefore useful for studies where time resolution is important. Another advantage is that there are no moving parts

compared to a scanning spectroradiometer. However, spectrographs have disadvantages over scanning systems, such as spectral resolution and detectivity. Spectroradiometers are more complex to operate and maintain than radiometers; they are considerably more expensive; and there are many pitfalls for the inexperienced user. Spectroradiometers generally employ the same kind of input optics as radiometers.

In an ideal spectroradiometer, the monochromator passes a small band of wavelengths to the detector, and passes no radiation outside this band. In practice the out-of-band radiation (leakage or stray-light) that is passed to the detector is of the order of 0.1 percent of the amount of in-band radiation depending upon the quality and size of the monochromator. In certain measurement situations this may give rise to errors (just as in radiometers): the signal caused by out-of-band radiation may be of the same order of magnitude as the signal caused by in-band radiation. For example, if one attempts to measure the solar UV spectrum in the 290-310 nm region, this error occurs because the solar spectrum decreases about five orders of magnitude from 310 nm to 290 nm. To overcome this error, a double monochromator may be used. A double monochromator is essentially two identical monochromators coupled in tandem, the output of the first becomes the input of the second monochromator. The stray light of a double monochromator is typically 0.01 percent.

1.8.4. Calibration

Improper or inadequate calibration of UV radiometers, spectroradiometers and dosimeters is a serious and common source of error. It is important to maintain a good calibration record for the instruments, but only experience on instrument stability will determine how often calibration is needed. The error caused by calibration provides the minimum uncertainty that can be obtained in measurement situations. Other sources of uncertainty include geometry and spectrum of source emission, detector-source geometry (angular errors), environmental influences and time factors. Radiometers can be calibrated by using a source of known irradiance. This may either be a line source, such as a mercury lamp or a laser, or by a broadband source, such as a tungsten halogen lamp. It must be realized that the irradiance-responsivity will depend upon the source used for calibration. For example, a radiometer which has been calibrated against a line source will give erratic readings if used to measure a broadband source. In practice it is advisable to have radiometers calibrated against a source which emits a spectrum similar to those of the sources to be measured.

Complete calibration of radiometers and spectral radiometers include analysis of the cosine response of the instrument, the azimuthal response and the temperature sensitivity of the instrument. Recent work on instrument calibration and intercomparison has shown that instruments can vary greatly in these quantities even when the instruments agree on a simple spectral calibration. In the field, instruments will measure different quantities depending on the temperature and angle of incident radiation. Spectroradiometers are calibrated against standard lamps of known spectral irradiance (or radiance). Such lamps can be obtained from the standards institutes in various countries. Intercomparison of lamp calibration from institute to institute can vary by as much as eight percent in the UV region, while better agreement is common in the visible region of standard lamps. This discrepancy should be noted when comparing results based on instruments calibrated from different lamp standards.

A tungsten halogen lamp is used as the standard lamp for wavelengths between 250 and 2500 nm, whereas a deuterium lamp is used in the region between 180 and 300-

400 nm. It is good practice to operate the standard lamp only when calibrating a working-standard lamp and then use the working-standard for routine calibration of a spectroradiometer. For very accurate work it is recommended to maintain three calibrated lamps in order to find out whether a change in response/calibration, at least of a spectroradiometer, is caused by changes in the standard lamp used for calibration or by changes in the spectroradiometer. Dosimeters are calibrated in the same way as radiometers except that exposure time is an integral part of the calibration process. To obtain a reliable calibration for radiometers and dosimeters, it is advisable to calibrate them against a source which emits a spectrum similar to the one that is to be measured.

2. Optical technology for biologically effective UV measurements

There are two possible choices for the measurements of UV effective irradiance: by a scanning instrument represented by a spectroradiometer or by a broad-band instrument called radiometer.

Nowadays there are few commercially available scanning spectroradiometer that can be used for long term outdoor operation and they don't deliver error free results cause of the long time scan, the scan frequency and the limited lifetime of the mechanical components. This limits seriously the accuracy of the biological measurements and raise the question whether the biological monitoring cannot be achieved by simpler instruments. These are represented by the broad band radiometers. Basically there are two categories of instruments under this family: the phosphor based Robertson-Berger meter and interference filter based instruments. Both have fast response and are relatively inexpensive. They can measure one band shaped to a selected action spectrum or a series of narrow bands.

Very useful for some applications, interference filters are yet not used in long term monitoring of UV cause of their lack of long term stability. The many efforts made to improve their performance will lead to their extensive application.

The possibility to obtain practically any desired spectral response in transmittance/reflectance make the interference filters the best choice for this kind of application and permitted to develop new possible instruments for the measurements of the effective solar irradiance.

2.1. Design of optical elements

As said above broadband UV radiometers and spectroradiometers are the instruments used to determine the total irradiance or the spectral irradiance (i.e. irradiance as function of the wavelength) from a UV source. For any specific application of these instruments, the choice of the proper detector is fundamental. Some radiometers, for example, are designed in order to have a spectral response that matches an action spectrum which describes the relative effectiveness of UV radiation at a particular wavelength in producing a particular biological response. This can be accomplished coupling a filter with a proper spectral transmission to a detector with a specific spectral response curve.

2.1.1. Interferential filters

In recent years interest in developing optical coating with particular performances in reflectivity or transmittance in several spectral regions such as EUV, UV, Vis, NIR has grown considerably. Using the technology of multilayer thin films it's possible to obtain practically every response curve.

Coupling innovative designed interference filters with a UV photodiode of sufficient active area, we can reconstruct several action spectra. In the next sessions possible innovative solutions for the measurements of the action spectra are reported.

All the presented solutions were obtained coupling a commercial photodiode with an interference filter designed with particular materials. Moreover, the radiometer integrates a diffuser element to better agree the cosine law.

The main problem related with solar irradiance measurements on earth are made up by the low solar emission in the UV spectral region. All the wavelengths under 280/290nm are completely absorbed by the atmosphere and the total energy reaching the ground in clear sky condition is about 40W/m² at noon, while the emission from an artificial source is about ten times this value. This condition lead to choice a detector with a relatively large active area. A simple procedure show that a photodiode with an active area of 1mm² can ensure a sufficient signal for the electronical amplification.

A possible alternative solution could be separating the spectral range of work of the sensor into two or more region. This solution is particularly suitable in the case of the erythema like detector, where the spectral separation into two region corresponding to UVB (280-315nm) and UVA (315-400nm) could be interesting for particular application such as sunscreen performance monitoring.

The nominal interferential filter curves, $T_{filter}(\lambda)$ (referred to as "the target curve") were derived, according to equation (2.1) from the ratio between the nominal action curve and the product between the photodiode spectral response curve R_{ph} and the diffuser spectral transmission T_{diff} .

$$\frac{Action_Spectrum}{R_{ph}(\lambda) \cdot T_{dif}(\lambda)} = T_{filter}(\lambda) \quad (2.1)$$

The transmission target curves were obtained by setting their maximum value around 100%, which maximized the signal on the photodiode. Commercial software (TFCALC–Software Spectra Inc.) was used to optimize the design of the filter. It that can simulate the optical properties of film structures consisting of ~5,000 layers deposited on the front or on the back surface of a suitable substrate. An optical constants database, both for substrates and film materials, can be stored in the form of tables or complex refractive index dispersion formula versus wavelengths. The materials database, available free of charge for research purposes by Sopra Company (<http://www.soprasa.com/more/database.asp>), was used for first theoretical calculations; however, the optical constants used for the final design of the filter were experimentally derived. Different illuminants stored in a database as tables of spectral intensity versus wavelength can be used to evaluate the performance of the optical element. In this case, the spectral intensity distribution corresponding to the white illuminant was always adopted. The radiation incident on the film can be a collimated beam or a cone of rays with a given angular aperture, and the angle of incidence can be varied from 0° to 89.999°. In the case of a cone of rays, the computed transmission corresponds to the average value for the considered angular beam aperture. The software follows an optimization procedure to obtain a filter structure with a transmission curve that matches the “target curve” as closely as possible (in this case the $R_{\text{filter}}(\lambda)$ curve). Different material couples and numbers of layers were considered in the design. By using the optimization software tools, the thickness of each single layer was calculated to minimize the difference—set according to a merit function between the target curve and the transmission curve of the filter under design.

2.1.1.1. Erythema - Interferential filters

Long exposition to sun radiation cause burns, skin aging, erythema and even melanoma cancer. In the European regulation EN60335-2-27 [26] the toxicity of UV radiation emitting machines for domestic use is discussed and upper-limit exposition effective dose are established. As well as other artificial sources, sun tanning units should be monitored and certified according with the law. There is the necessity to develop a clear measurement procedure to verify sunbed irradiance in metrological laboratories, and to develop portable instrumentation for the irradiance verification in situ.

In order to measure the total effective irradiance of sunbed and sun lamp a new radiometer with a spectral response curve equivalent to the CIE erythema action one has been designed and realized. The sensor is hand portable, user friendly and competitive on the market. Moreover the instrument can be used for outdoor monitoring.

Sunburn is an acute UV caused damage of the skin, manifested by reddening and in some case blistering. The sunburn is a delayed erythema initially characterized by the appearance of 'sunburn cells', the depletion of antigen-presenting cells (APC), and the infiltration of the epidermis and dermis by a variety of inflammatory cells, e.g. mast cells, monocytes and lymphocytes. Subsequently the skin responds with hyperproliferation. Sensitivity to sunburn varies based on pigmentation, where lightly pigmented individuals are much more sensitive than heavily pigmented ones. Being best known from men, sun burn can be observed also on pigs.

In the next figures the response curves of the designed filters and radiometers are reported. Figure 2.2 reports the design for a filter/radiometer optimized only for the UVA

spectral region. We are not aware of the realization radiometer with this behaviour and with such performances.

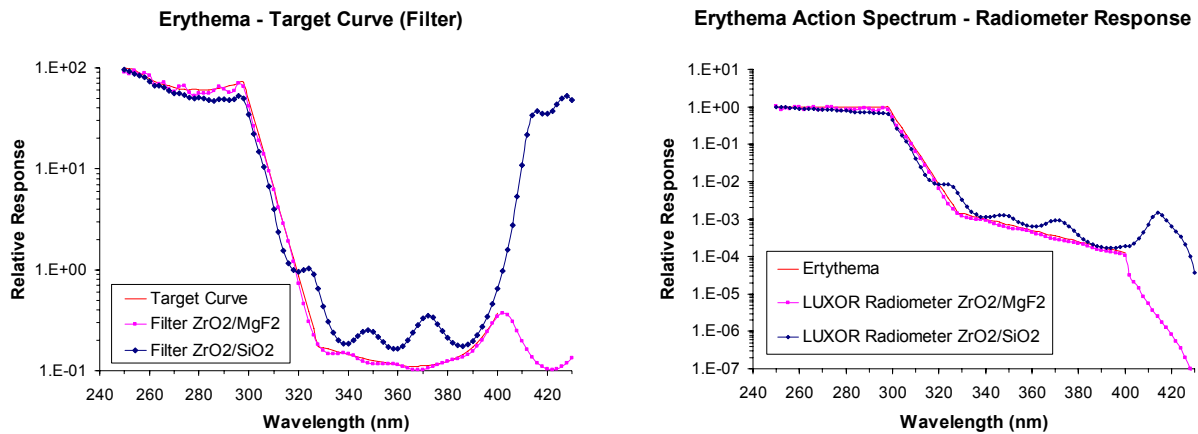


Figure 2.1. Erythema Action Spectrum Radiometer. Filter response curves and radiometer response for the ZrO_2/SiO_2 and ZrO_2/MgF_2 design respectively.

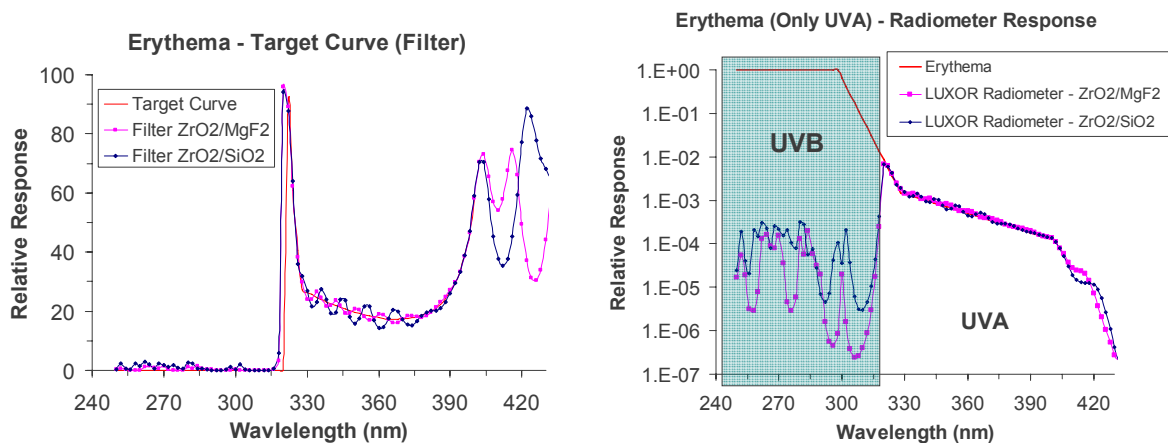


Figure 2.2. Erythema (Only UVA spectral region) Action Spectrum Radiometer. Filter response curves and radiometer response for the ZrO_2/SiO_2 and ZrO_2/MgF_2 design respectively.

2.1.1.2. DNA Damage - Interferential filters

DNA is certainly one of the key targets for UV-induced damage in a variety of organisms ranging from bacteria to humans. UV radiation induces two of the most abundant mutagenic and cytotoxic DNA lesions such as cyclobutane–pyrimidine dimers (CPDs) and 6–4 photoproducts (6–4PPs) and their Dewar valence isomers.

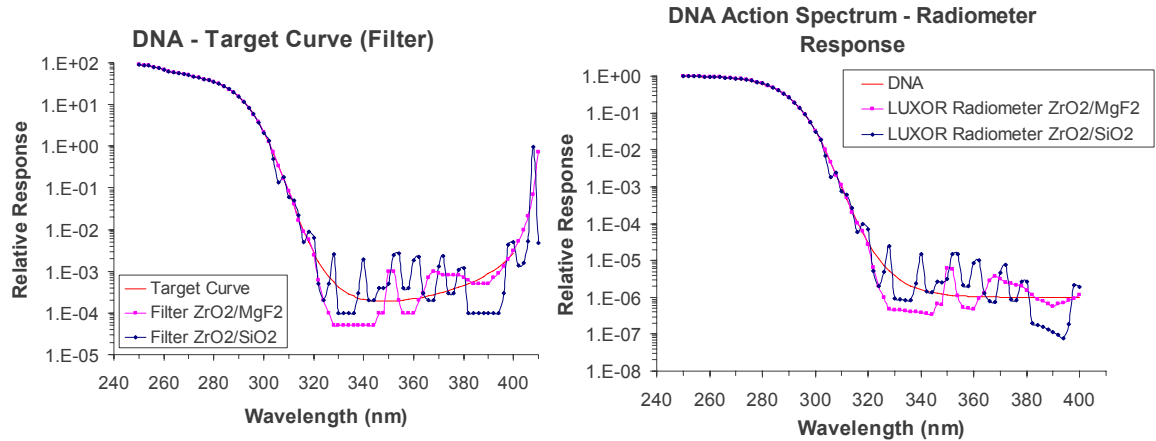


Figure 2.3. DNA Damage Action Spectrum Radiometer. Filter response curves and radiometer response for the $\text{ZrO}_2/\text{SiO}_2$ and $\text{ZrO}_2/\text{MgF}_2$ design respectively.

2.1.1.3. Vitamin D3 Production - Interferential filters

Vitamin D helps to prevent diseases as Rickets and other bone diseases; Internal cancers and Multiple sclerosis [27]

- UVB radiation (290-315 nm) converts 7-dehydrocholesterol into pre-vitamin D3
- Previtamin D3 undergoes a thermal isomerization that results in the formation of vitamin D3 (25 hydroxyvitamin D (25(OH)D)). This is converted to 1,25-dihydroxyvitamin D3 (1,25(OH)2D3) in the liver and kidney.

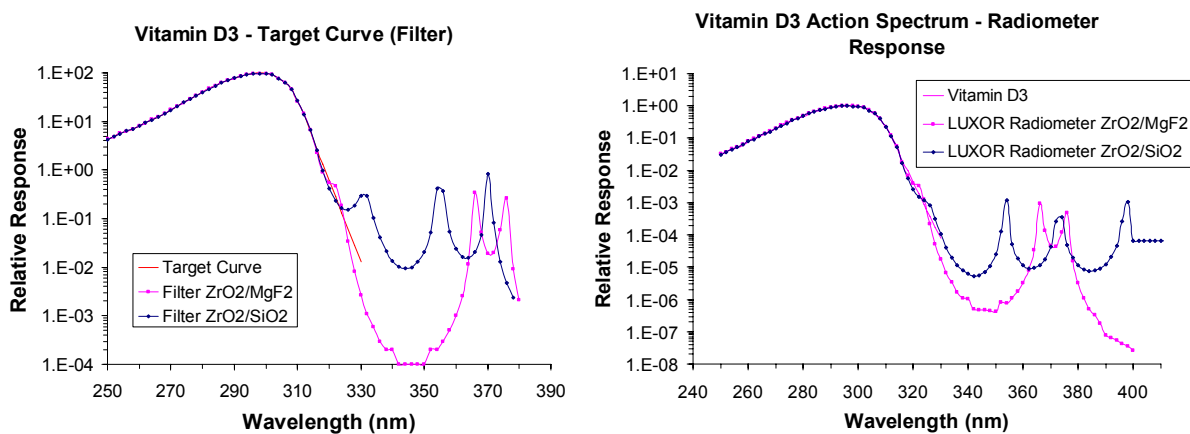


Figure 2.4. Vitamin D3 Production Action Spectrum Radiometer. Filter response curves and radiometer response for the $\text{ZrO}_2/\text{SiO}_2$ and $\text{ZrO}_2/\text{MgF}_2$ design respectively.

2.1.1.4. Eye Damage - Interferential filters

UV radiation of high intensity can damage the front-most parts of the eye in a manner of hours or even mere minutes. It can result in inflammation of the cornea (photo keratitis) and of the conjunctiva (photo conjunctivitis). The damage can be felt as a sharp pain in the eyes. Because new cornea and conjunctiva cells constantly re-grow, the damage is reversible [28].

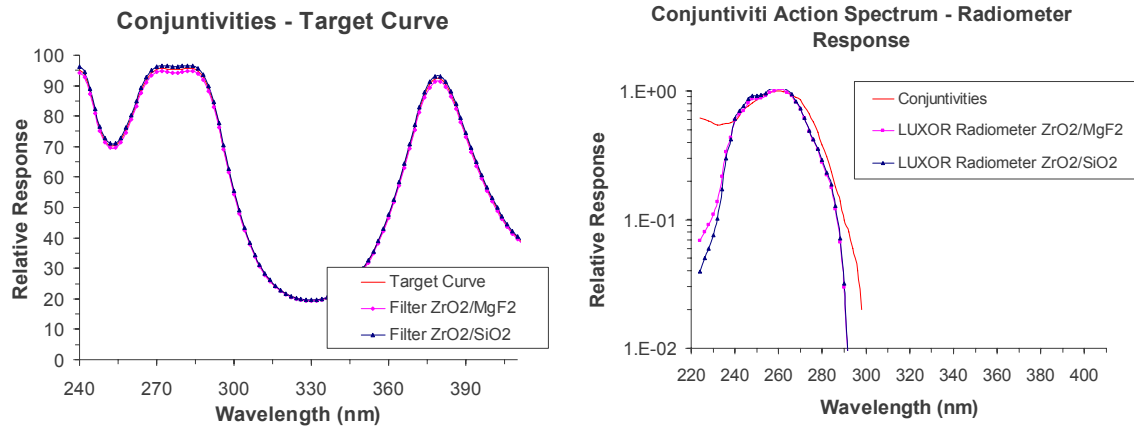


Figure 2.5. Conjunctivitis Action Spectrum Radiometer. Filter response curves and radiometer response for the ZrO₂/SiO₂ and ZrO₂/MgF₂ design respectively.

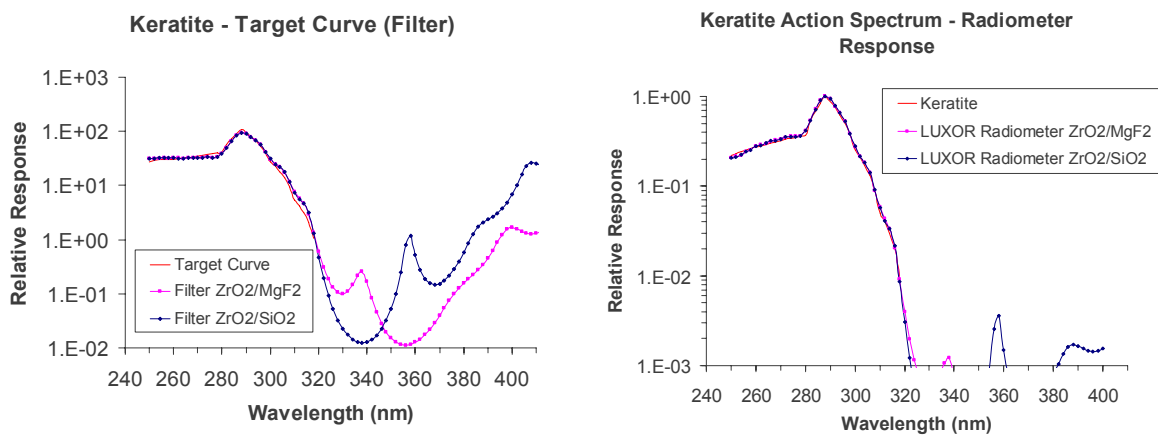


Figure 2.6. Keratite Action Spectrum Radiometer. Filter response curves and radiometer response for the ZrO₂/SiO₂ and ZrO₂/MgF₂ design respectively.

2.1.1.5. Plant Damage - Interferential filters

Photosynthetic primary production, the basis of most global food chains, is inhibited by UV radiation. Evaluating UV inhibition is therefore important for assessing the role of natural levels of UV radiation in regulating ecosystem behavior as well as the potential impact of stratospheric ozone depletion on global ecosystems. As both photosynthesis and UV fluxes are subject to diurnal variations [29-31].

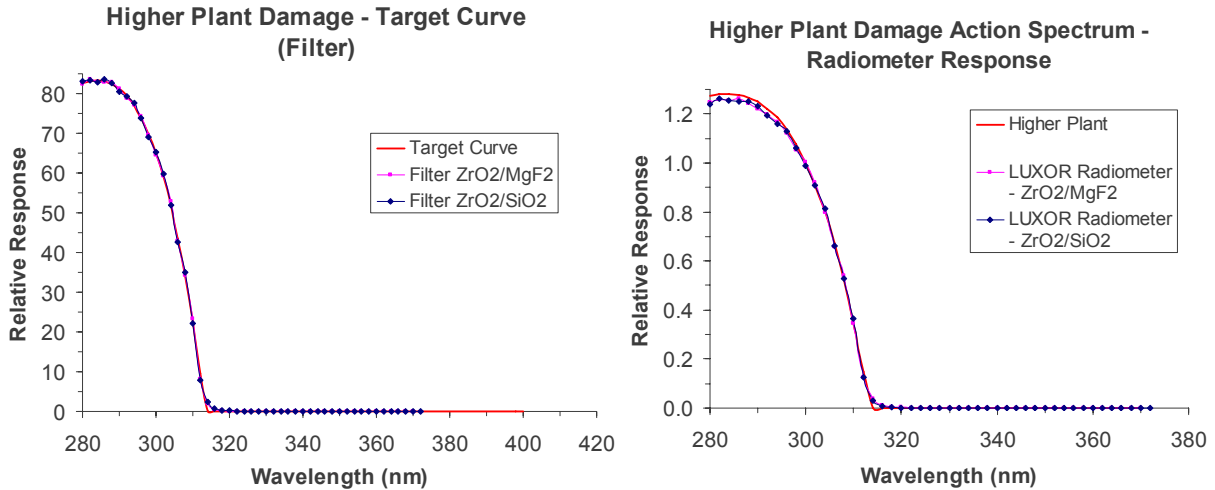


Figure 2.7. Higher Plant Damage Action Spectrum Radiometer. Filter response curves and radiometer response for the $\text{ZrO}_2/\text{SiO}_2$ and $\text{ZrO}_2/\text{MgF}_2$ design respectively.

2.1.1.6. The case of water disinfection - Interferential filters

Ultraviolet (UV) disinfection has grown in acceptance as a primary disinfection process for water since its efficacy for inactivating *Cryptosporidium* was revealed [32]. The microbicidal UV fluence under polychromatic radiation from UV lamps is typically measured using the DNA absorbance spectrum as a weighting factor for the relative wavelength effectiveness. However, this DNA-based weighting does not necessarily match the spectral sensitivity of the microorganism being tested. *Bacillus subtilis* spores are often used for UV reactor validation in Europe [33].

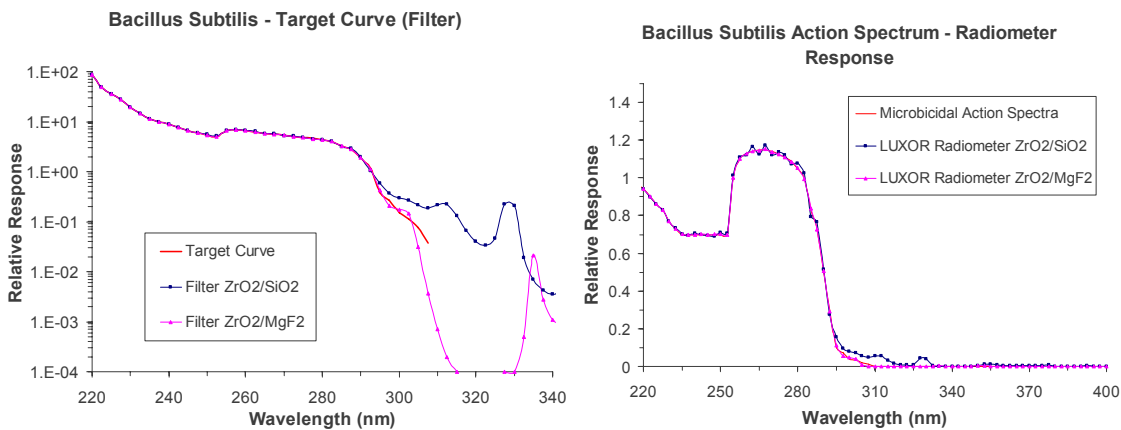


Figure 2.8. Bacillus Subtilis Action Spectrum Radiometer. Filter response curves and radiometer response for the $\text{ZrO}_2/\text{SiO}_2$ and $\text{ZrO}_2/\text{MgF}_2$ design respectively.

In all the figures above the transmission of optimized filters with a structure made of $\text{SiO}_2/\text{ZrO}_2$ is compared with the structure derived by using many alternate layers of

MgF₂ and ZrO₂. The improved matching of the target curves obtained with the new design is clear. We are not aware of the realization of an interferential filter based on this material couple made with so many layers and this improvement represent the most innovative aspect of my activities on this field. In all the cases the substrate is UV grade fused silica with a thickness of 1 mm. The spectral responses of the detector heads, derived from the product of the characteristic curves of the designed filters, the photodiode, and the diffuser, are compared with the action curves.

2.1.1.7. Cone Angle Response of the Interferential filters

It is clear from the figures that the match between the curves is very good for a collimated radiation that has an incidence angle of 0°. Since the spectral response of the interferential filter depends on the radiation incidence angle on the filter, by using the specific TFCalc tool previously described, the sensor response for different cone angles was also simulated. In the majority of cases, the match of the action curves was excellent in the case of a 40° incidence radiation cone angle; this means that the detector head design should define the field of view angular aperture of the photodiode within this value, i.e., the distance between photodiode and the entrance optics must be set accordingly. (This angle must not be mixed up with the input angle: radiation coming from the whole 180° solid angle in space impinges the diffusing entrance optics.) As illustrated in figure 2.9 in some cases the cone angle can be up to 60 degrees. In figure 2.10 a layout of the mechanical mounting of the detector head is reported showing how the baffles limit the cone angle of acceptance of the incoming radiation.

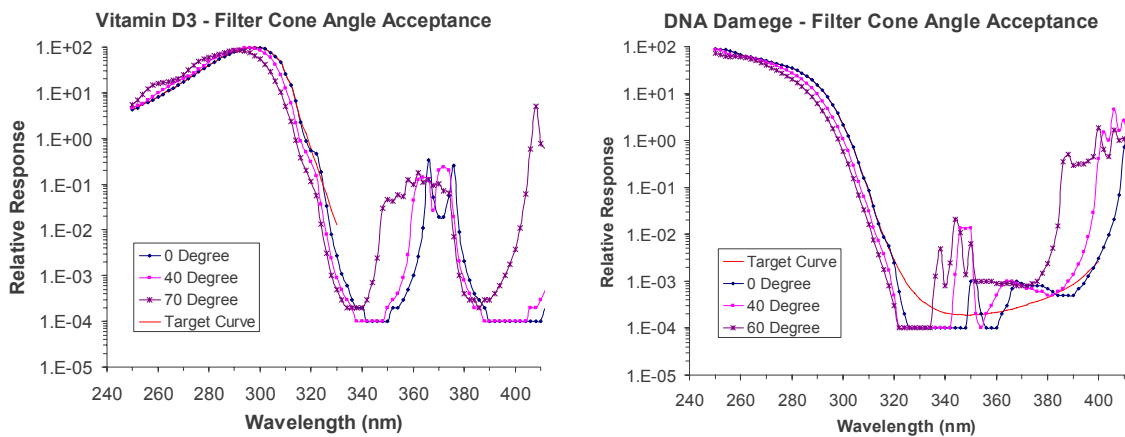


Figure 2.9. Filter cone angle acceptance for Vitamin D3 and DNA Damage ZrO₂/MgF₂ filters design respectively.

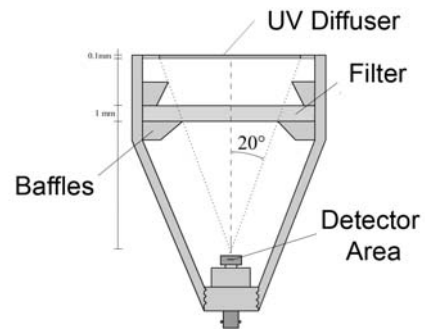


Figure 2.10. Mechanical mounting of the head of the radiometer. Baffle design for the cone-angle limitation.

3. Characterization of optical elements

In application of radiometric technology the perfect knowledge of every component of the instrumentation is essential. For example in a typical instrument layout such as in figure 3.1 it's important to know the behaviors of the UV diffuser in terms of diffusive properties and spectral transmittance, moreover in the design of a particular interferential filter the knowledge of the details of film growing and of material optical constants are essential. A multilayer structure can be prepared by several deposition techniques such as Magnetron Sputtering, Electron Beam, Laser Ablation, etc. The properties of the film obtained with different techniques can present important differences. For such reasons a detailed study of materials involved in the filter design is a fundamental part of the characterization procedures. Once obtained the deposited filter its long time and thermal stability should be analyzed and naturally its spectral transmittance/reflectance must be measured with high accuracy. Finally, the principal part of a radiometer is the detector. The right choice of this component determines the final performance of the instrument, for this reason the characterization and calibration of possible UV detector are a fundamental part of the design work.

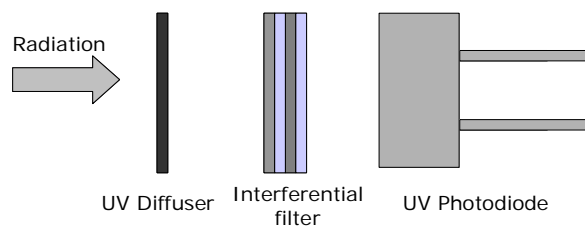


Figure 3.1. Typical radiometer layout

3.1. input optic: diffusive element characterization

Global solar irradiance measurements performed by most of the existing UV spectroradiometers suffer from the non ideal angular response of their entrance optics, which in most cases results in underestimation of the measured irradiances. The magnitude of this error, which is commonly known as cosine error, can vary from a few percent to 10% or 20%, depending on the measurement conditions and the characteristics of the system.[34-37] These systematic but variable-magnitude errors of UV measurements impose great difficulties on attempts to establish comparable data sets among instruments but may also affect the homogeneity of the measurements performed by the same instrument under variable conditions. Given that replacement of the input optics with others of better response awaits—for most of the instruments—substantial development in their design, it is essential to develop methods to reduce the magnitude of this error to lower and acceptable levels ~i.e., 1–2%. [38].

When selecting input optics for a measurement application, consider both the size of the source and the viewing angle of the intended real-world receiver. Suppose, for example, that you were measuring the erythemal (sunburn) effect of the sun on human skin. While the sun may be considered very much a point source, skylight, refracted and reflected by the atmosphere, contributes significantly to the overall amount of light reaching the earth's surface. Sunlight is a combination of a point source and a 2π steradian area source. The skin, since it is relatively flat and diffuse, is an effective cosine receiver. It absorbs radiation in proportion to the incident angle of the light. An appropriate measurement system should also have a cosine response. If you aimed the detector directly at the sun and tracked the sun's path, you would be measuring the maximum irradiance. If, however, you wanted to measure the effect on a person laying on the beach, you might want the detector to face straight up, regardless of the sun's position. Different measurement geometries necessitate specialized input optics. Radiance and luminance measurements require a narrow viewing angle ($< 4^\circ$) in order to satisfy the conditions underlying the measurement units. Power measurements, on the other hand, require a uniform response to radiation regardless of input angle to capture all light. There may also be occasions when the need for additional signal or the desire to exclude off-angle light affects the choice of input optics. A high gain lens, for example, is often used to amplify a distant point source. A detector can be calibrated to use any input optics as long as they reflect the overall goal of the measurement.



Figure 3.2. Suntube monitoring.

3.1.1. Lambert's Cosine Law

The irradiance or illuminance falling on any surface varies as the cosine of the incident angle, θ . The perceived measurement area orthogonal to the incident flux is reduced at oblique angles, causing light to spread out over a wider area than it would if perpendicular to the measurement plane. To measure the amount of light falling on human skin, you need to mimic the skin's cosine response. Since filter rings restrict off-angle light, a cosine diffuser must be used to correct the spatial responsivity. In full immersion applications like the phototherapy booth shown above (Figure 3.2), off angle light is significant, requiring accurate cosine correction optics.

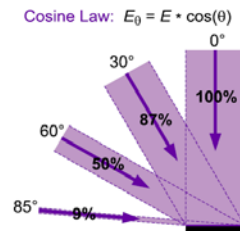


Figure 3.3. Schematic Representation of the Cosine Law

3.1.2. Lambertian Surface

A Lambertian surface provides uniform diffusion of the incident radiation such that its radiance or luminance is the same in all directions from which it can be measured. Many diffuse surfaces are, in fact, Lambertian. The human eye, with its restricted solid viewing angle, is an ideal luminance, or brightness, detector. Since, by the cosine law, a radiance detector sees twice as much surface area in the same solid angle for the 60° case, the average incremental reflection must be half the magnitude of the reflection in the 0° case. Figure 3.4 shows that a reflection from a diffuse Lambertian surface obeys the cosine law by distributing reflected energy in proportion to the cosine of the reflected angle. A Lambertian surface that has a radiance of 1.0 W/cm²sr will radiate a total of $\pi \cdot A$ watts, where A is the area of the surface, into a hemisphere of 2 π steradians. Since the radiant exitance of the surface is equal to the total power divided by the total area, the radiant exitance is π W/cm². In other words, if you were to illuminate a surface with an irradiance of 3.1416 W/cm², then you will measure a radiance on that surface of 1.00 W/cm²sr (if it is 100% reflective).

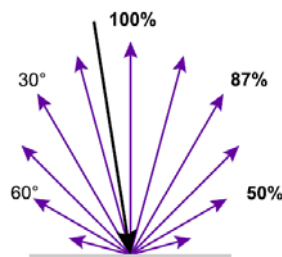


Figure 3.4. Schematic Representation of a Lambertian Surface.

3.1.3. Diffuser characterization

A bare silicon cell has a near perfect cosine response, as do all diffuse planar surfaces. As soon as you place a filter in front of the detector, however, you change the spatial responsivity of the cell by restricting off-angle light. Fused silica or optical quartz with a ground (rough) internal hemisphere makes an excellent diffuser with adequate transmission in the ultraviolet. Teflon (PTFE) is an excellent alternative for UV and visible applications, but is not an effective diffuser for infrared light. Lastly, an integrating sphere coated with BaSO₄ or PTFE powder is the ideal cosine receiver, since the planar sphere aperture defines the cosine relationship.

Within the activities of my Ph.D, different materials/samples were characterized:

- 🌀 Laboratory prepared quartz, thickness 1.9 mm and Suprasil thickness 2 mm
- 🌀 Teflon AF1600 from DUPONT
- 🌀 Zenith SG 3201, thickness 0.1 mm, from ORIEL
- 🌀 Different teflon samples prepared in laboratory, thickness 0.3, 0.5 and 1 mm

Two types of measurements were made: transmission of the sample (in order to recover $R_{diff}(\lambda)$) and analysis of diffusion properties (according to Lambert Cosine Law). The results on transmission are reported in Figure 3.5.

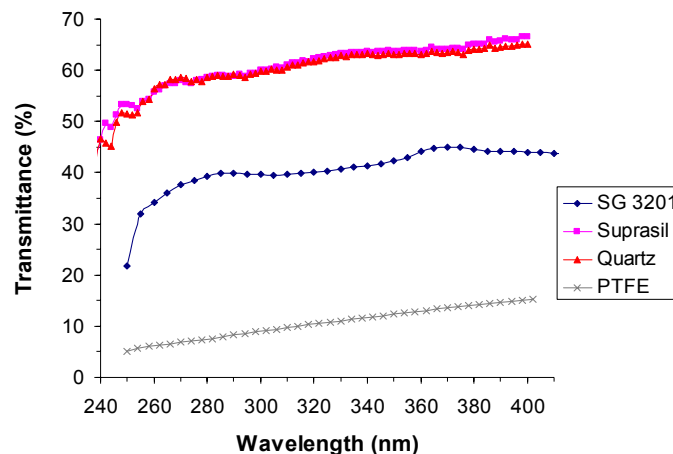


Figure 3.5. Transmittance measurements on diffusive elements

Results on diffusion properties are reported in Figure 3.6. Best diffusers are Teflon and Zenith SG 3201, which match the cosine curve really well in the whole range. Unfortunately, if Teflon thickness is around 1 mm the transmission is low (around 5-15 %), which can be a problem to detect irradiance of low power sources, unless larger area photodiodes are used to compensate for power losses (with additional cost); so, only thin sample as SG3021 have high transmission (50%), but on the other side thin elements are difficult to be mounted and supported in the instrument case.

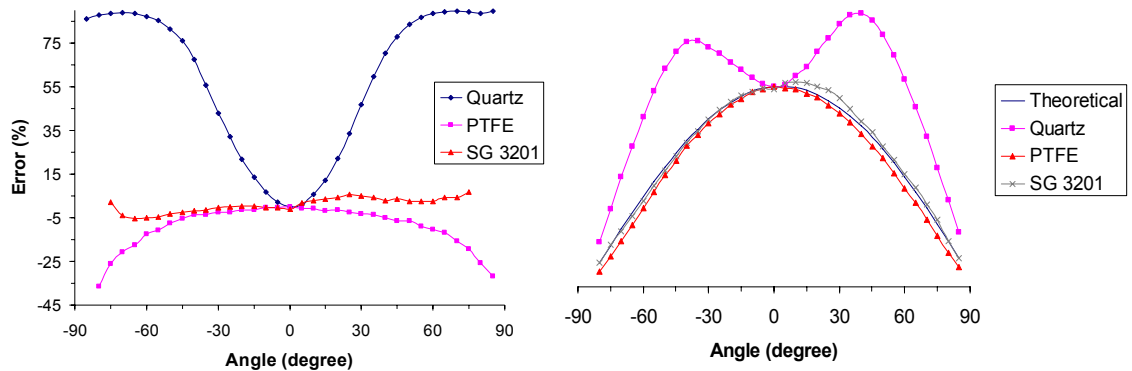


Figure 3.6. Deviation from the cosine law. Error (%) and absolute deviation from theoretical values.

3.2. Laboratory activities: thin films deposition and characterization

The behavior of a given material to an incident electromagnetic wave is related to the energy dependent complex index of refraction $n = n + ik$. Various methods are used to determine the optical constants n and k including reflectance measurements, angle-dependent electron yield, transmission measurements, interferometry, and ellipsometry. Methods for deriving optical constants from reflectance measurements at multiple incidence angles have already been applied for several thin film materials in the EUV and soft x-ray regions and this method can be applied even in the near UV spectral range without using a vacuum facility [39].

The ability to produce optimized multilayer designs, and to reliably model instrument performance depends crucially on the availability of accurate optical constants for the constituent multilayer materials.

Determination of optical constants is taken by means of reflective measurements in the whole Soft X-Ray to Visible from reflectance using the Fresnel equation and a least-square fitting procedure. [40]

As said above, the main and mainly innovative element of our radiometers is the interferential multilayer filter. At the present time we have an active collaboration with Luxel Corp. (US). Till now the produced filters were purchased from this company, within our collaboration some profilometric measurements of the index of refraction of the involved materials have been performed. Thanks to these measurements we can optimize the filters design.

On the prepared samples we performed several tests, i.e. spectral transmittance measurements, time stability and thermal stability measurements. In the next pages the results of such tests are presented.

The next step of the filters development was the homemade preparation. In our laboratories we can deposited thin films via Magnetron Sputtering (in collaboration with

LNL-INFN Legnaro), Electron Beam (Figure 3.7) and Pulse Laser Deposition (PLD) (at Luxor).

Before depositing the final multilayer structure we grown single layer films in order to measure the optical constants of the involved materials, since these will be dependent on the deposition technique.

The optical constants will be measured by using a spectrophotometer working in 180-3300nm spectral range (Figure 3.8) measuring transmittance and reflectance vs incident angle at the different wavelengths and deriving the optical constants values from a best-fit procedure. Moreover, mechanical profilometric measurements and interferometric measurements were used in order to get the thickness of the films.



Figure 3.7. Electron Beam Deposition Facility at LUXOR



Figure 3.8. Cary Varian 5000 UV/Vis/NIR Spectrophotometric Equipment at LUXOR

3.2.1. Thin Films deposition at Luxel and LUXOR

Test filter samples were developed by Luxel Corporation Inc. Preliminary work on material characterization was performed to recover the optical constants of SiO_2 , ZrO_2 and MgF_2 . Detail of the experimental measurements of the optical constants are reported in the next session. The final design of the filters were optimized by using the experimentally derived optical constant data. The performances of the $\text{ZrO}_2/\text{MgF}_2$ and $\text{ZrO}_2/\text{SiO}_2$ interferential filters prepared by Luxel are reported in the session 3.2.3 for the erythema filter design and conjunctivitis filter design respectively.

Side by side with the activities performed at Luxel, depositions of ZrO_2 and MgF_2 thin film and multilayer structures have been performed at LUXOR by using an electron beam evaporator facility. Also in this case preliminary work on material characterization has been performed in order to evaluate the optical constants of the materials. Different analytical methods have been followed to measure the refractive index from transmittance/reflectance measurements. The detail of the computation are reported in the next session.

In order to evaluate the refractive index of the materials, thin single layer films have been deposited by electron-beam evaporation of granular material (MgF_2 , purity 99.5%; ZrO_2 , 99.5%) in a high-vacuum chamber pumped with a turbo molecular pump. The base pressure before deposition was 1×10^{-6} mbar. The oxygen pressure during ZrO_2 deposition was 5.5×10^{-5} mbar. The deposition rate was monitored and controlled by a quartz oscillator and it varied from 0.5 up to 0.9 Å/sec. In every run, quartz substrates (2 mm thick, 25 mm in diameter) were mounted onto a calotte and coated while the calotte was rotating. The substrate temperature was about 90 °C for the depositions of ZrO_2 film, while MgF_2 was prepared at 250°C. The thickness of the films ranged from 230 to 550 nm. We determined the mass of the films by weighing the substrates with a comparator balance (nominal resolution, 0.1 mg) before and after deposition. The thickness of the edge between the substrate and the film generated by the window in the substrate holder was determined by the stylus method with a Tencor T10 profilometer. (figure 3.9)

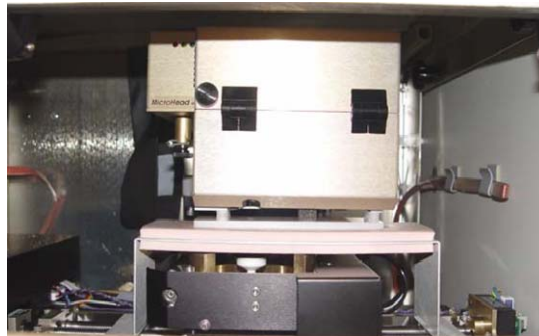


Figure 3.9. Profilometer at Department of Physics - University of Padova

3.2.2. Optical constants derivation

Different procedures were followed in order to derive the optical constants of the materials used for the realization of the interferential filters. The preliminary work performed on ZrO_2 , SiO_2 and MgF_2 at Luxel was based on ellipsometric criteria, while for ZrO_2 and MgF_2 films prepared at LUXOR mathematical best-fit methods based on transmittance/reflectance measurements was used.

3.2.2.1. Ellipsometric measurements at Luxel

Samples of ZrO_2 , MgF_2 and SiO_2 were deposited on Silicon substrates in different growth runs at Luxel. The thickness of the films were ~200nm for every materials. VUV-VASE® (J.A. Woollam Co., Inc.) was used to measure ZrO_2 , MgF_2 and SiO_2 refractive index. A picture of the instrumentation used is reported in figure 3.10.



Figure 3.10. VUV-VASE profilometer (J.A. Woollam Co., Inc.)

The film thickness and optical constants (n and k) were determined using spectroscopic ellipsometry over the wavelength range from 140 to 1700nm. The final optical constants of the films are shown in the figures below (k is in all the cases zero):

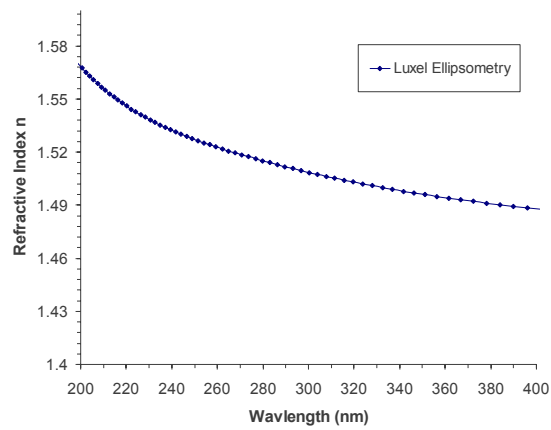


Figure 3.11. Optical constants of SiO_2 prepared at Luxel

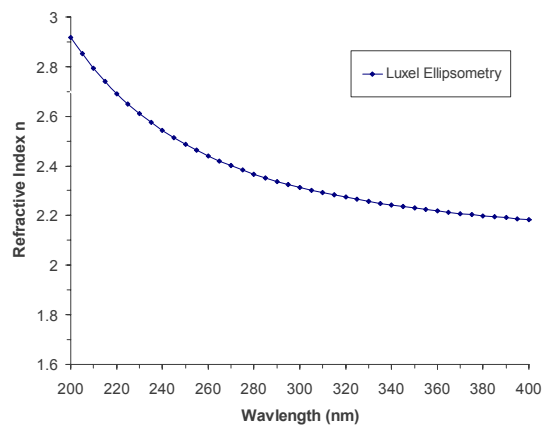


Figure 3.12. Optical constants of ZrO_2 prepared at Luxel

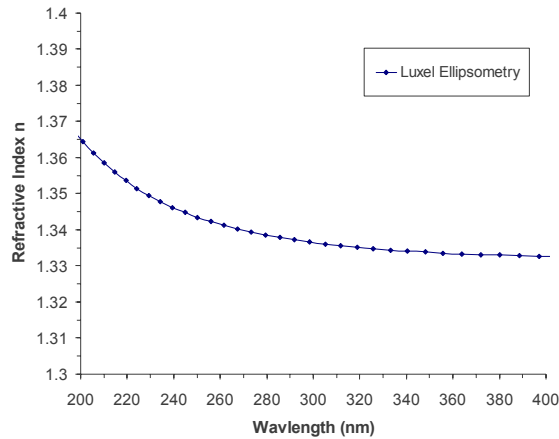


Figure 3.13. Optical constants of MgF_2 prepared at Luxel

A variable angle spectroscopic ellipsometer for the vacuum ultraviolet was used for measurements. The instrument features a wide spectral range from 140nm – 1700nm. The angle of incidence is computer controlled from 10° to 90° (25° minimum for longer wavelengths), with automated sample tilt and height adjustment. The entire optical path is enclosed inside a dry nitrogen purge to eliminate absorption from ambient water vapor and oxygen. A convenient sample load cell allows access to the stage to load samples up to 300mm in diameter. The VUV-VASE uses a rotating analyzer ellipsometer (RAE) configuration with the addition of the AutoRetarder® that changes the polarization state of light before the sample to maximize measurement accuracy. In addition, it allows advanced measurements of depolarization, Mueller-matrix elements, and generalized ellipsometry (for anisotropic materials). WVASE32 ellipsometric analysis program has been used to analyze the experimental measurements. It provides many modeling options. In addition to modeling and analyzing the ellipsometric data, WVASE32 also analyzes and simulates reflectance and transmission data (figure 3.14).

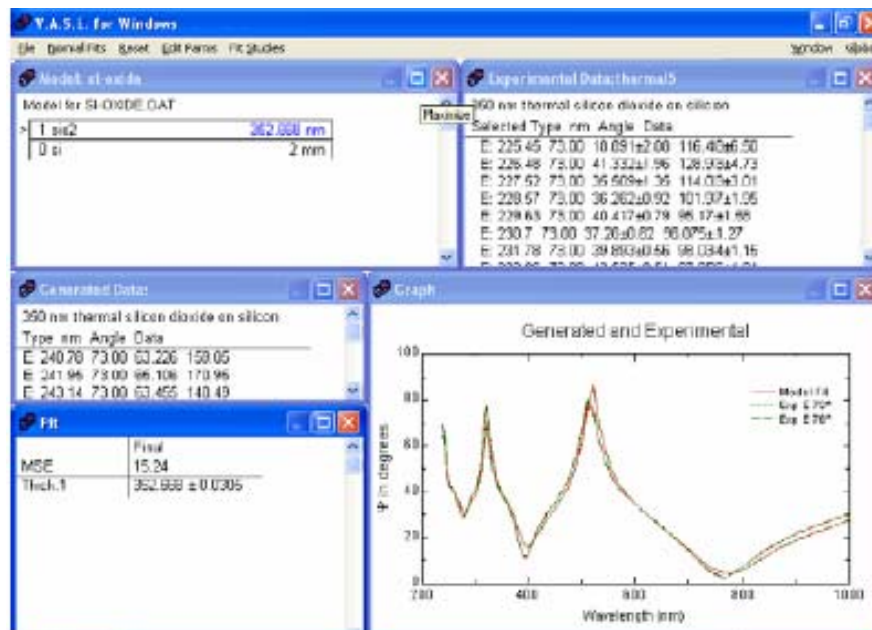


Figure 3.14. Example of the analytical software results.

Ellipsometry uses polarized light to characterize thin film and bulk materials. A change in polarization is measured after reflecting light from the surface. Thin film thickness (t) and optical constants (n, k) are derived from the measurement. Information is obtained from each layer interacting with the measurement. Light returning from the film–substrate interface interferes with the surface reflection to provide layer information (figure 3.15).

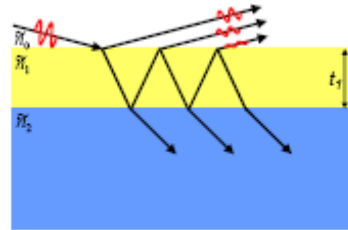
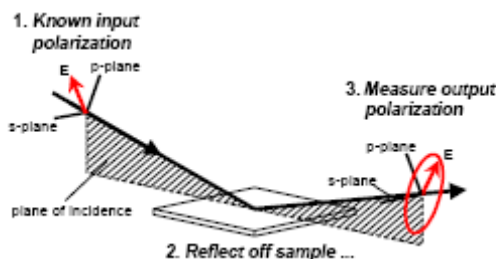


Figure 3.15. Schematic representation of light – film – substrate interaction

An ellipsometry measurement is a description of the change in polarization as polarized light is reflected from a sample surface. It is expressed as two parameters for each wavelength-angle combination: Psi (ψ) and Delta (Δ). These values can be related to the ratio of complex Fresnel reflection coefficients, R_p and R_s , for p- and s- polarized light, respectively (figure 3.16):



$$\rho = \frac{R_p}{R_s} = \tan(\psi)e^{i\Delta}$$

Figure 3.16. Principle of ellipsometric measurements.

Ellipsometry offers three main advantages over simple intensity-based reflection or transmission measurements:

1. Measurement is defined by a ratio, thus ellipsometry is not sensitive to changes in absolute intensity of measurement beam (i.e. the sample becomes the 'reference' for the measurement).
2. Phase information (from Δ) provides enhanced sensitivity to ultra-thin films, even down to sub-nm level.
3. Ellipsometry measures 2 values (Ψ and Δ) at each wavelength, doubling the information content compared to an intensity reflection or transmission measurement.

The most common ellipsometry measurement is film thickness and refractive index. However, ellipsometry can also investigate surface and interfacial roughness, degree of crystallinity, alloy and doping concentration, retardation, and more. These values are typically determined via a model-based analysis of the ellipsometry data [41-43].

Data analysis is a very important part of spectroscopic ellipsometry (SE): without data analysis SE only measures the ellipsometry parameters Psi and Delta (Ψ and Δ) versus wavelength. Data analysis is used to determine optical constants, layer thickness, and other material properties. The basic steps of this approach include:

1. SE data is measured on the sample.
2. A model describes the measured sample using layers for each material. Thickness and optical constants (n and k) describe each layer over the measured wavelength range, with estimates for any unknown properties.
3. The unknown properties of the sample are defined as model “fit” parameters. The software automatically adjusts these parameters to improve the agreement between the measured and model-generated data.
4. The results of the fit are evaluated. If results are not acceptable, the process can be repeated with a new model or different “fit” parameters until the best description is found (figure 3.17).

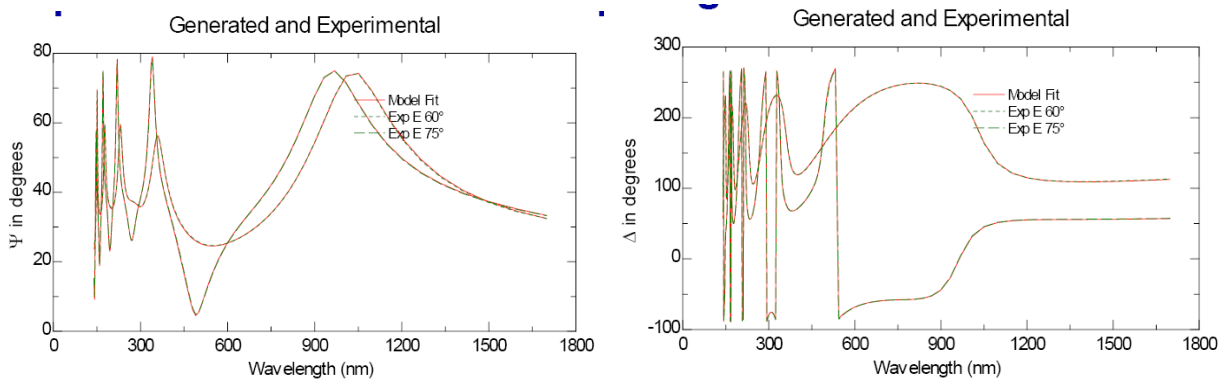


Figure 3.17. Example of fitting procedure on experimental ellipsometric data. SiO₂ Sample.

In order to better understand the procedure of ellipsometric measurements the detail of the SiO₂ optical constants derivation are reported.

As for the other materials, ellipsometric data were acquired from 140-1700nm, at 60° and 75°, near the center of the sample.

- The substrate was modelled using a Si standard layer. This because, although the optical constants for most materials are variable, crystalline substrates can have very consistent properties. Silicon is one such material (at least in the ultraviolet to near infrared wavelength region). Thus, the silicon optical constants can be modelled using “known” values from the published literature. The values typically chosen were developed by Herzinger et al.[44] This reference also provides excellent values for thermally grown SiO₂ films. There is a thin interface between the silicon substrate and the SiO₂ layer, which is also described in this reference.
- The film was modelled using an absorbing oscillator model. Two oscillators (one Lorentz and one Gaussian) were used to describe the absorption. A variety of oscillator models are available; including Drude, Lorentz, Gaussian, Harmonic, Tauc-Lorentz, Herzinger-Johs, and more [45]. While each is different, they function in a similar manner. The $\epsilon_2(\lambda)^*$ shape is described using oscillators with

centre energy, E_c , amplitude, A , and broadening, B . The $\varepsilon_1(\lambda)$ shape is linked to the $\varepsilon_2(\lambda)$ values through K-K consistency. There is also an ε_1 offset to account for absorption outside of the measured spectral range. A pole in the UV is used to offset the Kramers-Kronig transformation of the absorption and describe the index.

- A bandwidth of a few nm was also included in the model, and is appropriate for the instrument used.
- The film was determined to be 2171.08Å.

3.2.2.2. Optical constants derivation at LUXOR

The control of the optical properties and thickness t of the films play a fundamental role in the multilayer structure realization. The quality of the as-deposited material can be monitored in production lines through the *in-situ* determination of its optical constants (refractive index n and extinction coefficient k) and the thickness homogeneity. For that aim, ellipsometry is the most appropriate tool [46] due to the fact that it is not influenced by the adopted substrate. Alternatively, for the *ex-situ* analysis of samples grown on top of transparent substrates like glass, the use of optical transmittance is the most attractive method because optical transmission is a very easy, accurate and non-destructive measure. The problem of estimating the thickness and the optical constants of thin films using transmission data only represents a very ill-conditioned inverse problem with many local non-global solutions. Some useful approximate solutions have been found in cases where the transmittance displays a fringe pattern in a highly transparent spectral region [47–49]. Their applicability depends on the existence of interference fringes appearing in non-absorbing regions of the transmittance spectrum. The number of fringes, in turn, depends on the sample thickness. For ZrO_2 and MgF_2 deposited on quartz the minimum layer thickness needed for such analyses are of 200nm and 500nm respectively. Two methods allowing to solve the general problem with independence of the existence of interference fringes were recently reported.[50,51] The first method [50] defines a nonlinear programming problem, the unknowns of which are the coefficients to be estimated, with linear constraints that represent prior knowledge about the physical solution. This method was successful in retrieving the properties of computer made and of real world semiconductor films [50]. The second, [51] introduces an unconstrained formulation of the nonlinear programming model and solves the estimation problem using a method based on repeated calls to a recently introduced unconstrained minimization algorithm.[52] Numerical experiments show that the new formulation is reliable.[51] Here, I apply the unconstrained formulation to ZrO_2 and MgF_2 samples with thicknesses varying from 200 nm to 500 nm deposited by using electron beam evaporator. Figure 3.18 show the optical transmission spectra $T_{meas}(\lambda)$ of the films measured at room temperature with a Varian Cary 5000 Spectrophotometer. Note that the spectra of samples display a reasonable fringe pattern in the region of interest (200-450nm). The approximate properties of these two films can be extracted from the position and the magnitude of the maxima and the minima appearing in the interference pattern.[47–49]

* Optical constants of isotropic materials can be described using two representations. One representation is the complex index of refraction: $\tilde{n}=n+ik$, where the real part n is the index and the imaginary part, k , is the extinction coefficient. The index, n , describes phase velocity of light in a material compared to propagation in vacuum. The absorption of light is governed by the extinction coefficient, k . Alternately, the optical constants can be described using the complex dielectric constant, given as ε . The complex dielectric constant is related to the complex index of refraction by: $\varepsilon = \tilde{n}^2$

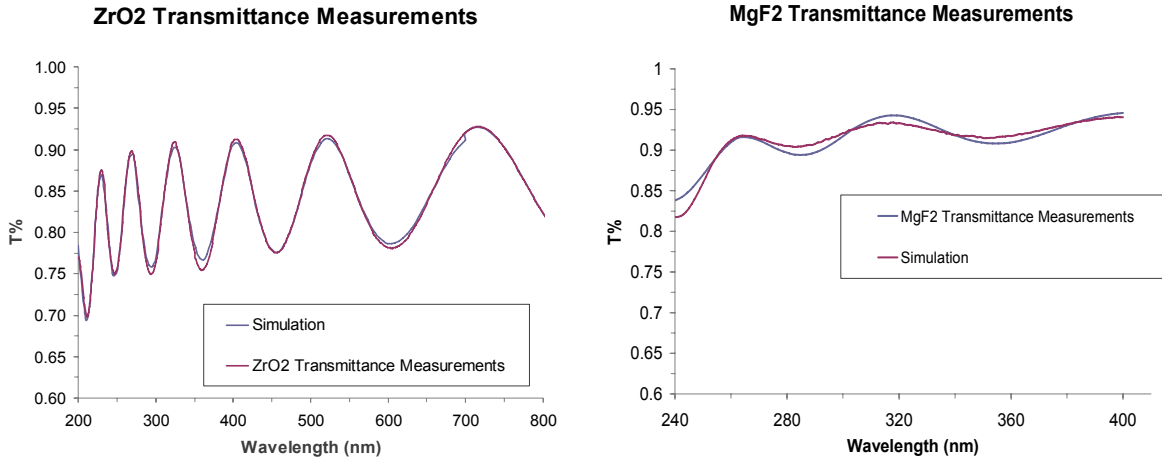


Figure 3.18. Transmittance measurements and best-fit simulation of ZrO_2 and MgF_2 thin films

A set of experimental data $[\lambda, T_{meas}(\lambda)]$ is given, and we want to estimate t , $n(\lambda)$, and $k(\lambda)$. The problem seems highly underdetermined. In fact, for known t and given λ , the following must hold [50]: $T_{meas}(\lambda) = T_{theor}(\lambda, s(\lambda), t, n(\lambda), k(\lambda))$, where T_{theor} is the calculated transmission of the film+substrate [48] and s the refractive index of the transparent substrate. This equation has two unknowns $n(\lambda)$ and $k(\lambda)$ and, in general, its set of solutions (n, k) is a curve in the two-dimensional $(n(\lambda), k(\lambda))$ space. Therefore, the set of functions (n, k) satisfying $T_{meas} = T_{theor}$ for a given t is infinite and, roughly speaking, is represented by a nonlinear manifold of dimension N in R^{2n} . The optimization process looks for a thickness that, subject to the physical input of the problem, minimizes the difference between the measured and the theoretical spectra, i. e:

$$\text{Minimize } \sum_i [T_{meas}(\lambda_i) - T_{Theor}(\lambda_i, s, t, n_i, k_i)]^2 \quad (3.1)$$

The minimization process starts sweeping a thickness range Δt_R divided into thickness steps Δt_S and proceeds decreasing Δt_R and Δt_S until the optimized thickness t_{opt} is found. As seen, the most important issue of the present method is the retrieval of the real film thickness t , since it determines the $n(\lambda)$ and $k(\lambda)$ values that minimizes the quadratic error. Fortunately, the thickness of the films can be measured by independent methods and compared with the ones obtained from the minimization process. To this aim, the film thickness was measured with a profilometer. Figure 3.19 compares the thickness obtained from the analysis of transmission data and that from the profilometer. The agreement is quite satisfactory for both the samples, specially taking into account the relative error of the mechanical measurement. Figures 3.20 and 3.21 shows the retrieved optical constants of the films in comparison with the values obtained by Luxel and data reported in literature. The differences derive from the different deposition method used.

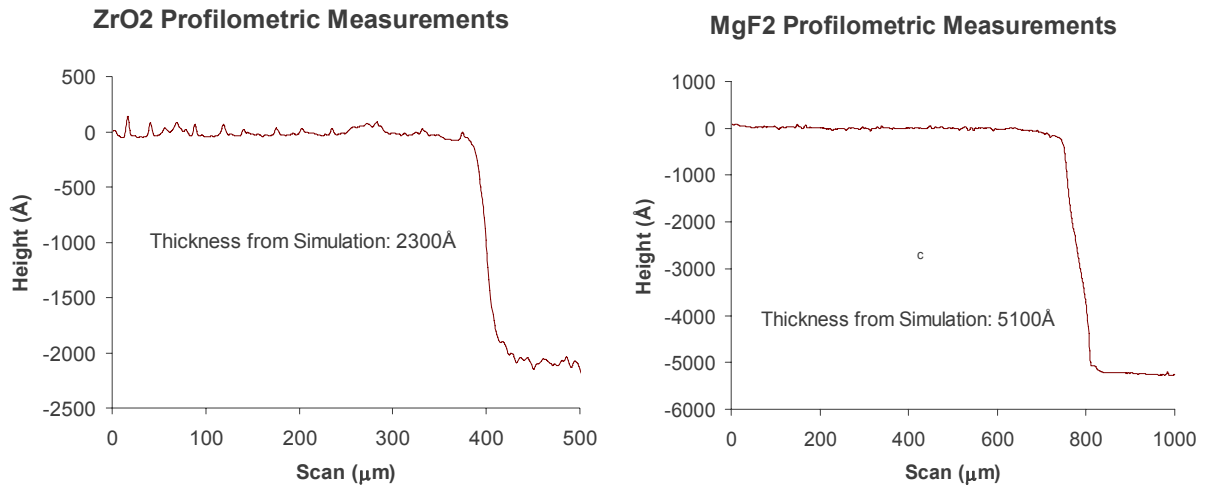


Figure 3.19. Profilometric measurements on ZrO_2 and MgF_2 thin films prepared at LUXOR. Comparison with thickness estimated from the best-fit procedure.

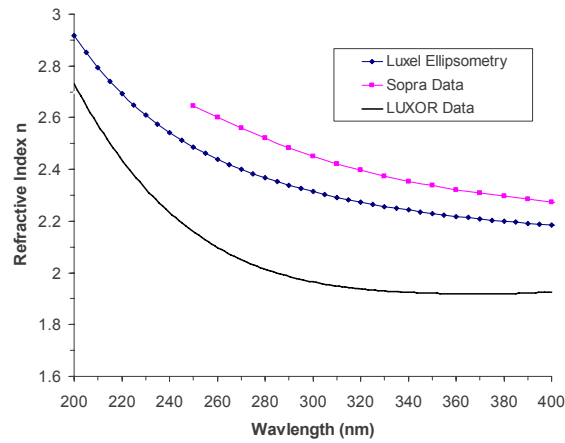


Figure 3.20. Optical Constants comparison of ZrO_2 thin film prepared with different process.

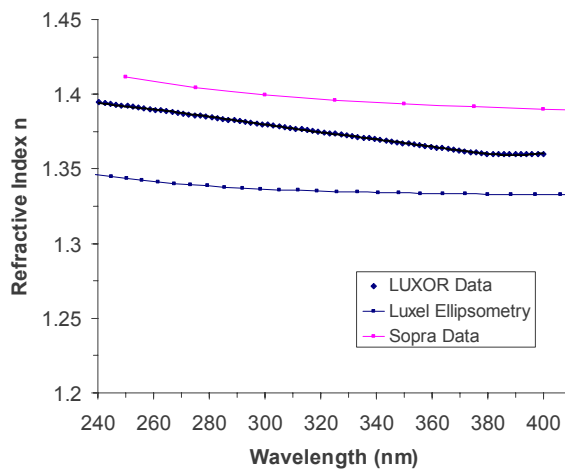


Figure 3.21. MgF_2 Optical Constants comparison of film prepared with different process.

3.2.3. Spectral Transmittance

The simple experimental configuration for the spectral transmittance measurements (transmission) preview the positioning of the source at the entrance of the monochromator and the recording of measured signal from the detector with and without the sample on the optical path. The ratio of the two measured signal with and without the sample gives the transmission (to a specific wavelength).

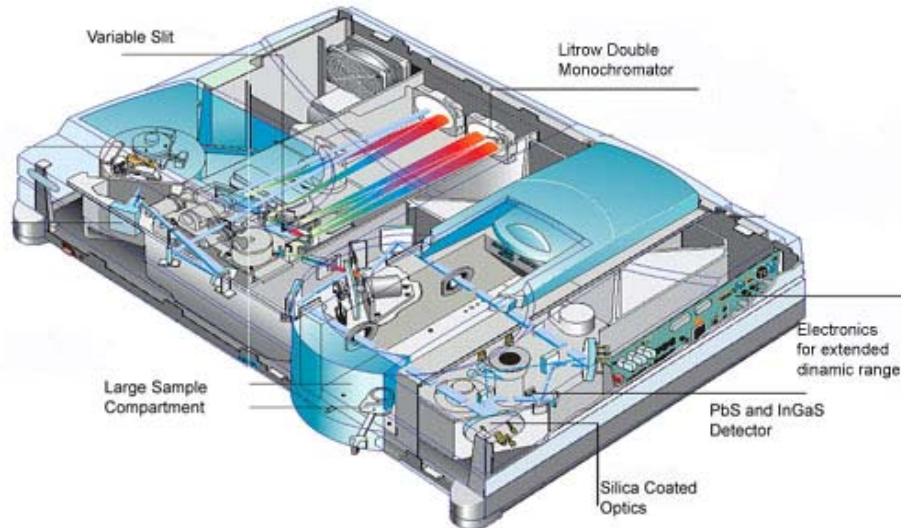


Figure 3.22. Optical layout of the Varian Cary 5000 Spectrophotometer at LUXOR

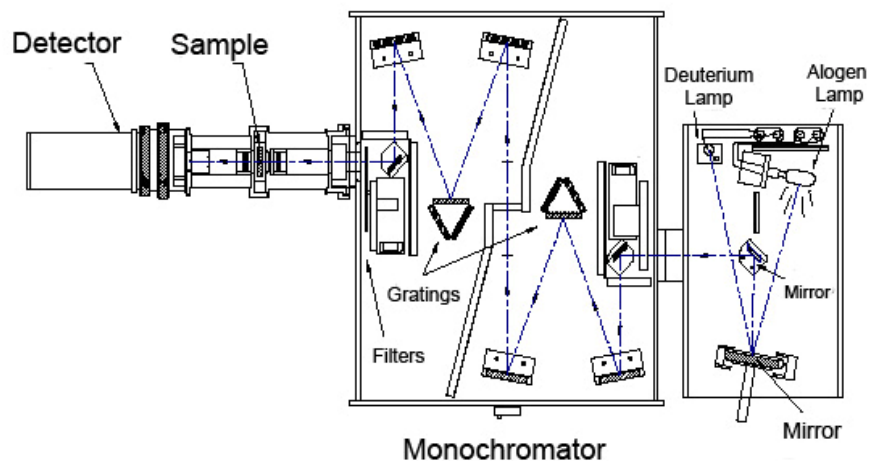


Figure 3.23. Experimental set-up for the spectral transmittance measurements

Luxel realized many different filters comprising ZrO_2 , SiO_2 and MgF_2 . ZrO_2/MgF_2 structures were prepared mainly for the project Senserit [53] of the radiometer with a response curve equivalent with the Erythema Action Spectrum. ZrO_2/SiO_2 structures were developed for the Conjunctivities Radiometer. The transmission measurements of

filters are reported in the next figures together with the target curve for comparison. The differences between the target curve and the measured ones derived from the optimization of the deposition process still under investigation.

Measurements were carried on at Delta Ohm by using the Bentham double spectral monochromator, and data are completely in agreement with the results obtained independently by Luxel. Analogue results were obtained in our laboratory by using the Varian Cary 5000 spectrophotometer (figure 3.22).

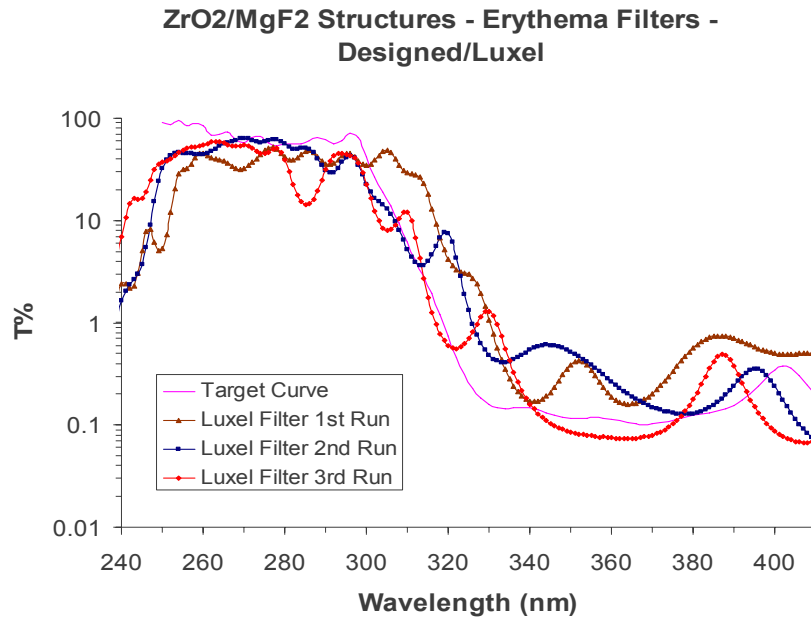


Figure 3.24. Transmittance measurements on Erythema filters – Structure comprising ZrO₂/MgF₂. Comparison between Target curve and different deposition runs.

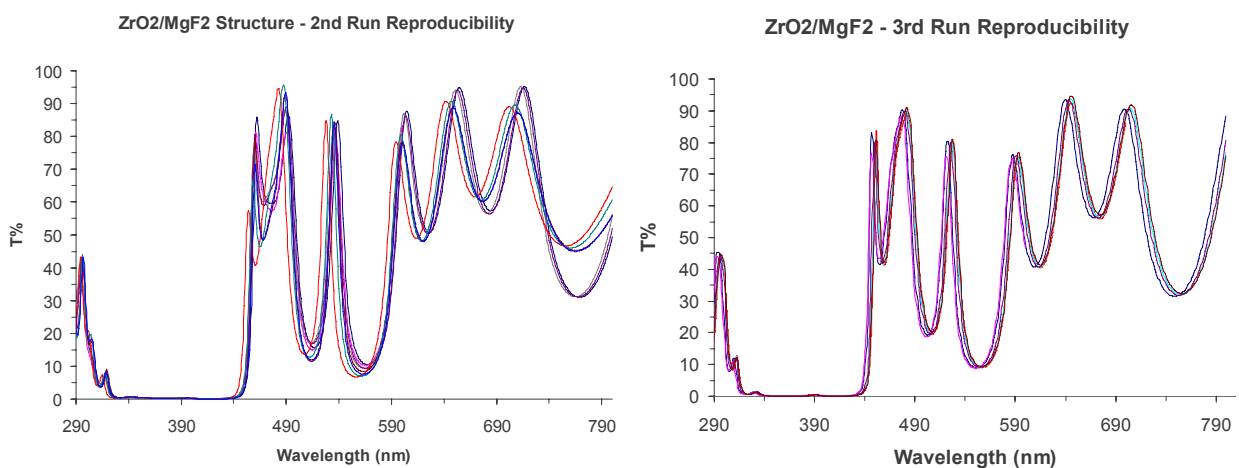


Figure 3.25. Transmittance measurements on Erythema filters – Structure comprising ZrO₂/MgF₂. Transmittance performances reproducibility between the different samples.

From the data results reported in log scale it was clear that the filter manufacturing tolerances mainly affected low transmission values, while the short wavelength edge of the filter transmission curve was quite well reproduced after the first run of deposition. We are confident that it's possible to obtain better performance with a slight improvement in the deposition procedure. Measurements were extended to the visible region to better understand the structure of the filter. Also in this case is possible to observe how the reproducibility of the transmittance performances gone better with the third run of deposition. This fact demonstrate the improvements on the deposition process. All the filters were measured just deposited and one or more years after the deposition showing the same transmission curves, which means that they were stable in a relatively long period of time without exposition to hazardous conditions. The uniformity of the filter was tested by varying the size and position of the tested area.

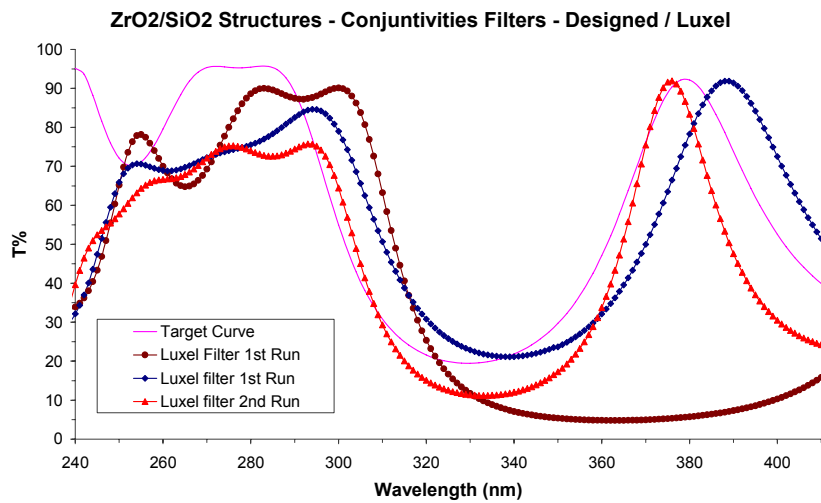


Figure 3.26. Transmittance measurements on Conjuntivities filters – Structure comprising ZrO_2/SiO_2 . Comparison between Target curve and different deposition runs.

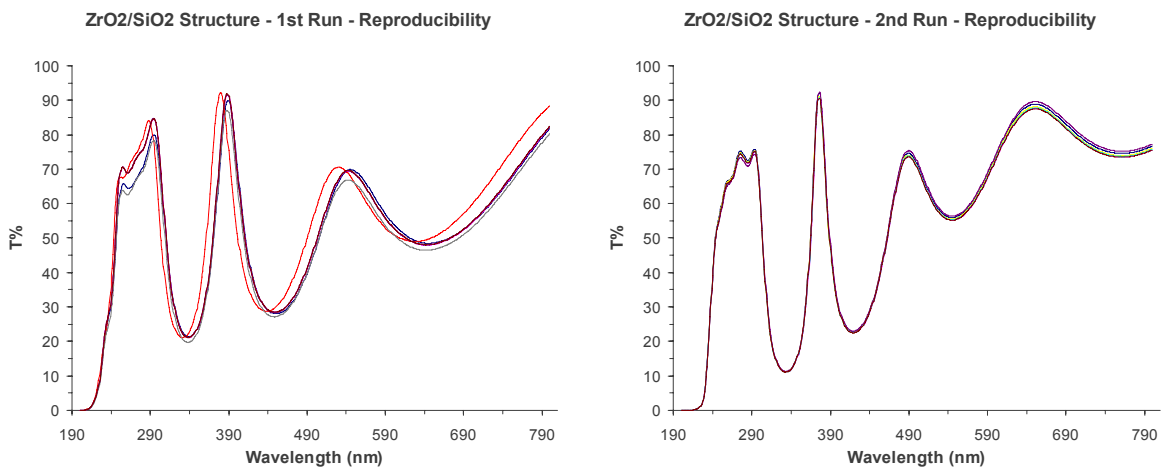


Figure 3.27. Transmittance measurements on Conjuntivities filters – Structure comprising ZrO_2/SiO_2 . Transmittance performances reproducibility between the different samples.

From the data results relative to $\text{ZrO}_2/\text{SiO}_2$ structure it's clear the improvement on the deposition process from the first run to the third. The peak values of transmittance result quite different from the target ones, but the requirements for this filter design was mainly related with the position of the slope around 300nm. Also from the transmittance reproducibility measurements is possible to observe how the performances of the filters improve from the first to the second run of preparation. Also in this case, the uniformity of the filter was tested by varying the size and position of the tested area.

In its planned fields of application these filters could be exposed to severe temperature and irradiance levels, for these reasons different thermal and photostability tests have been performed in order to demonstrate the durability of the films.

3.2.4. Stability tests

Interference filters are yet not used in long term monitoring of UV cause of their lack of long term stability. At LUXOR the thermal stability and the photostability of the interferential filters were taken into account. Several measurements were performed on multilayer structure as just-deposited and after long time period (up to 3 years). Both $\text{ZrO}_2/\text{MgF}_2$ and $\text{ZrO}_2/\text{SiO}_2$ structures were taken into account and tested. The details of these tests are reported in the next sessions.

3.2.4.1. Thermal stability tests

To verify the thermal stability of the filters two different procedures were followed. A first thermal cycling was performed at Delta Ohm on just-deposited filters. In the first cycle the temperature was increased from 25° to 80° in 1 hour. The filters were maintained at that temperature for another hour and then cooled down in 14 h. A second cycle was also performed at Delta Ohm by maintaining the samples at 80° for 2 days, and then cooling them down in 0.5 h. After these first thermal treatments, the characteristic of the filters were measured again, by using the Bentham double monochromator system at Delta Ohm, showing unchanged performance.

The next step was to verify the same filters 2 year after deposition and testing them in more hazardous conditions. By measuring the transmittance spectra of the filters after 1 or more years no significant variations were observed as illustrated in figure 3.x.

The thermal stability was then tested by using a furnace and maintaining the filters at the temperature reported in figure 3.28, i.e. warming up to 150°C in about 20 minutes and keep this temperature for 1 hour and then cooling down in another hour. This treatment was repeated three time for four different interferential filters: two $\text{ZrO}_2/\text{MgF}_2$ structures and two $\text{ZrO}_2/\text{SiO}_2$ structures. In both the cases the filters derive from different depositions. As can be easily observed in figure 3.x the $\text{ZrO}_2/\text{MgF}_2$ structure shows good stability in both the cases while the structure $\text{ZrO}_2/\text{SiO}_2$ shows a not perfect stability in one case.

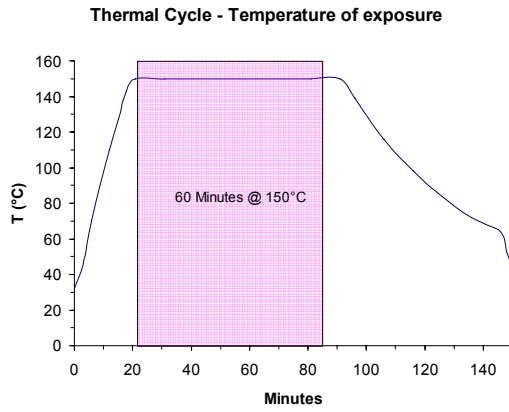


Figure 3.28. Temperature of Exposure for the multilayer structures tested.

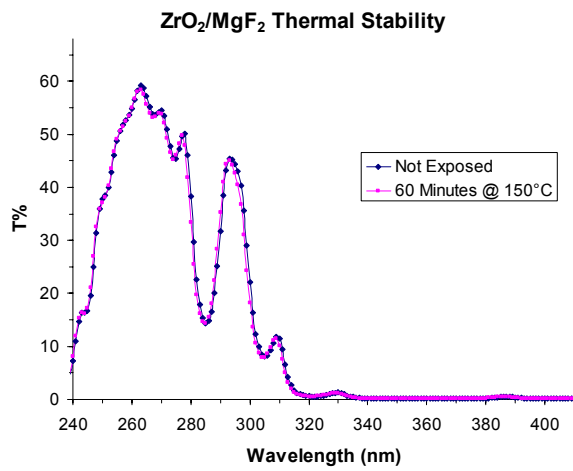


Figure 3.29. Thermal Stability Tests on ZrO₂/MgF₂ multilayer structures.

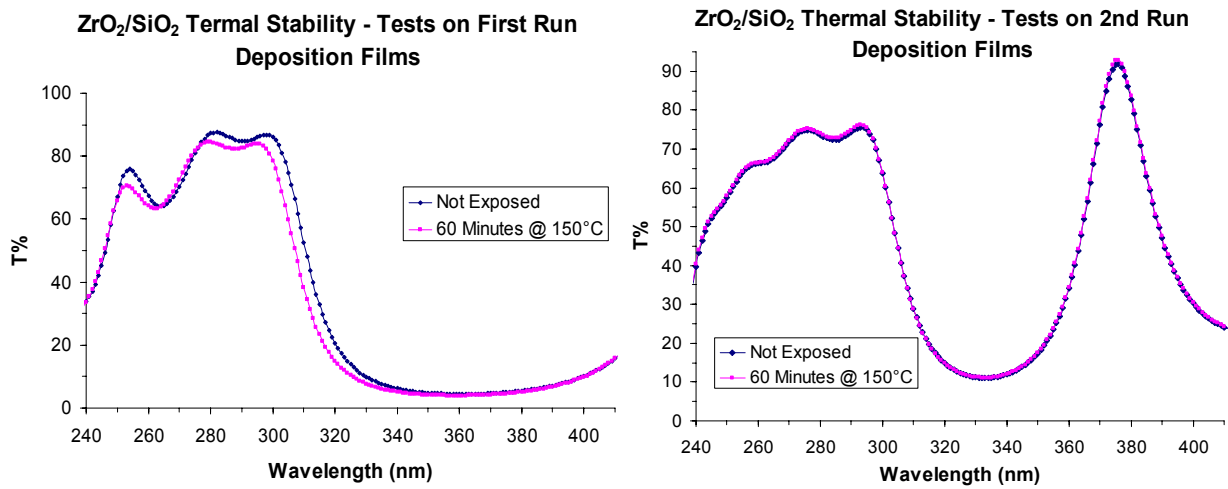


Figure 3.30. Thermal Stability Tests on ZrO₂/SiO₂ multilayer structures.

3.2.4.2. Photostability tests

In order to test the long time stability of the interferential filters under solar radiation a Lot Oriel solar simulator equipped with a 300 W xenon lamp was used to expose the multilayer structure under different dose of ultraviolet and full spectrum (290-2500nm) radiation [Ref Oriel]. Both ZrO_2/MgF_2 and ZrO_2/SiO_2 structures were tested some weeks after the deposition and after a long time period of 1 or more years. The irradiation sessions were organized always in many consecutive days (at least 10 days). During each session the filters were irradiated with a total UV dose of 200 SED (1 SED=100J/m²). This level of irradiation is very high and was chosen in order to test the filters in extreme conditions not possible with natural sources. After each session, the filter transmission was measured with the Varian Cary 5000 spectrophotometer. Also in this case four different interferential filters were tested: two ZrO_2/MgF_2 structures and two ZrO_2/SiO_2 structures. The filters derive from different depositions. The results of these measurements are reported in figure 3.31 for the measurements performed some weeks after the deposition and 1 years after the deposition.

As can be easily observed no systematic variation of the transmission curve with total accumulated dose was observed in the last ZrO_2/SiO_2 structure, while both ZrO_2/MgF_2 and the first ZrO_2/SiO_2 structures show a small but not negligible variation on the transmittance values.

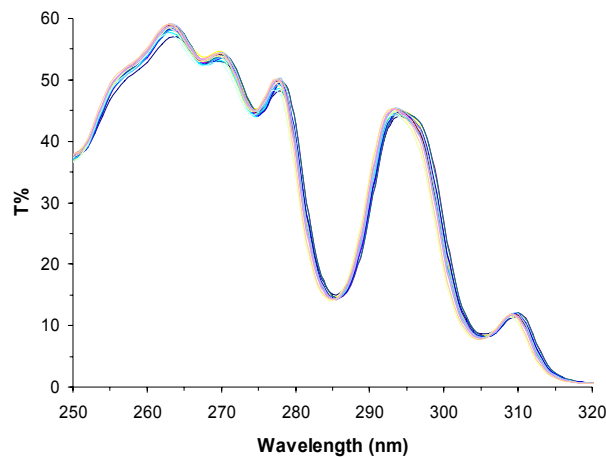


Figure 3.31. ZrO_2/MgF_2 Photostability Tests – 10 Days of Exposure (1h/day – 200SED/Day)

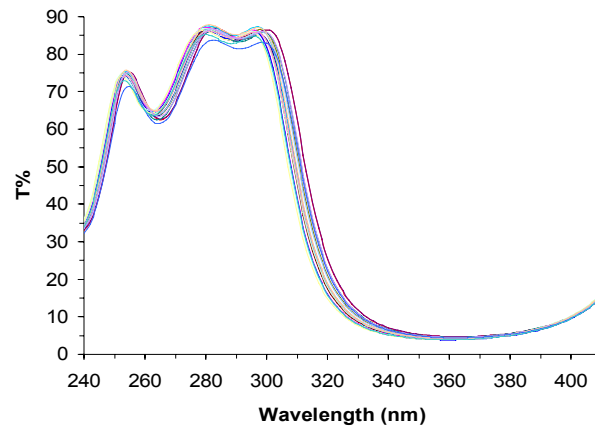


Figure 3.32. $\text{ZrO}_2/\text{SiO}_2$ Photostability – Tests on 1st Run Deposition Films – 10 Days of Exposure (1h/day – 200SED/Day)

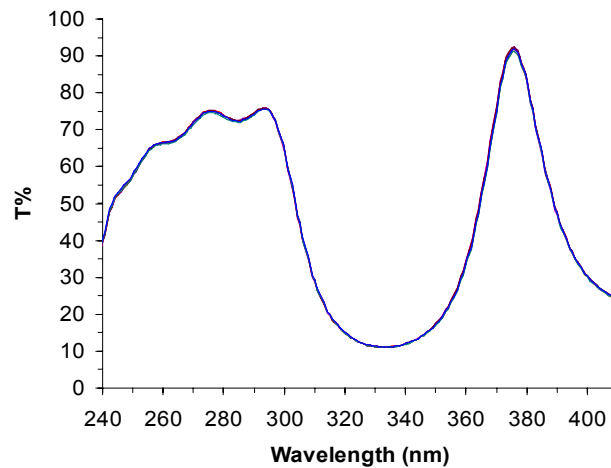


Figure 3.33. $\text{ZrO}_2/\text{SiO}_2$ Photostability – Tests on 2nd Run Deposition Films – 10 Days of Exposure (1h/day – 200SED/Day)

3.3. Laboratory activities: UV detector characterization and calibration

Broadband UV radiometers and spectroradiometers are the instruments used to determine the total irradiance or the spectral irradiance (i.e. irradiance as function of the wavelength) respectively. For any specific application of these instruments, the choice of the proper detector is fundamental. Some radiometers, for example, are designed in order to have a spectral response that matches an action spectrum which describes the relative effectiveness of UV radiation at a particular wavelength in producing a particular biological response [54]. As described above, this can be accomplished coupling a filter with a proper spectral transmission to a detector with a specific spectral response curve [55].

In the next sessions the characterization of commercial UV photodiodes types is presented. The samples considered are the following:

- SiC photodiodes of nominal active area of 0.22 mm^2 (six samples)
- p-i-n GaN photodiodes of nominal active area of 0.5 mm^2 (two samples)

- 3 different AlGaIn Schottky photodiodes, nominal active area of 0.5 mm²:
 - A: peak of response at 250 nm (2 samples)
 - B: peak of response at 300 nm (2 samples)
 - C: peak of response at 300 nm, built in UV glass window for low sensitivity above 400 nm, (2 samples)

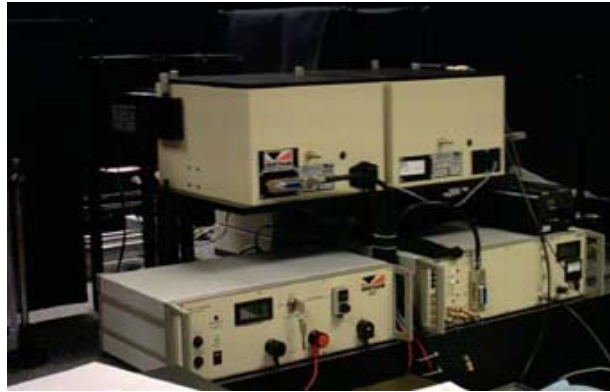


Figure 3.34. Bentham spectroradiometer at Deltaohm s.r.l.

3.3.1. Relative Spectral Response Measurements

Relative spectral response curve have been measured for all photodiodes. In this section the facility used, the methodology and the errors sources are presented.

3.3.1.1. Facility

Measurements have been performed at Deltaohm s.r.l. using a facility dedicated to radiometric measurements. It consists of Bentham f/4 double monochromator (focal length 250 mm), that can be equipped with two sets of gratings with different groove densities: 1200 l/mm or 1800 l/mm; in both cases, once the slits width is set, the spectral band-pass is defined. As a source, both a Halogen tungsten lamp and a Deuterium lamp can be used. The Deuterium lamp is mostly used at shorter wavelengths then 300 nm, where the Halogen lamp is unstable, while at longer wavelengths the Halogen lamp is preferred. A 15 cm diameter spherical mirror images the exit aperture of the monochromator on the detector. A Si calibrated detector with an active area of 1 cm² has been used in these measurements as the reference standard. The dynamic range of the whole system is 10⁶ and its spectral range of application is 200-900 nm.

3.3.1.2. Methodology

The measurements have been performed on all photodiodes comparing their output signals (photocurrents measured with a Keiltey 617 electrometer) with the calibrated Si photodiode one. Detectors have been mounted at the end of the monochromator on a (X,Y) translation stage which allows their displacement. The spherical mirror focuses the exit beam in a 2 mm diameter spot. Alignment of the detectors with respect to the incident beam have been performed visually setting the gratings position in order to have 550 nm radiation exiting the monochromator. Deuterium lamp has been used in

most measurements, even if some measurements have been carried on also with the Halogen one in order to double check the data. Slit widths have been set to have a spectral bandpass of 2 nm. A spectral scan was performed for both the photodiodes under test and the calibrated one in the same condition. The relative response R_λ of the photodiode under test has been recovered from the following expression:

$$R_\lambda = \frac{I_\lambda}{I'_\lambda} R'_\lambda \quad (3.2)$$

where I_λ and I'_λ are the photocurrents measured by the photodiode under test and the Si one respectively, and R'_λ is the spectral response of the Si photodiode, which is known by its calibration. Results are shown in figure 3.35: for each photodiode type, normalized data are reported as the average of the measurements performed for each sample, since quite similar responses have been observed. As told, in order to verify the independency of the data from the source used, some measurements have been performed with both lamps. In figure 3.36, both response curves for one of the SiC sample are reported; as shown, measurements are fully in agreement.

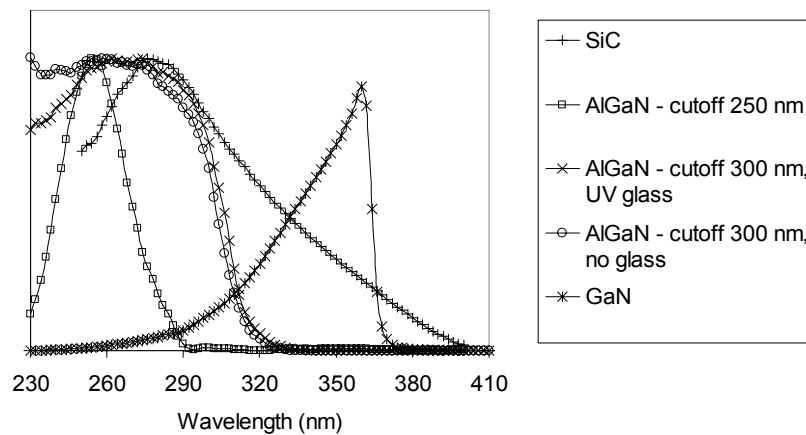


Figure 3.35. Relative spectral response curves for the different photodiodes.

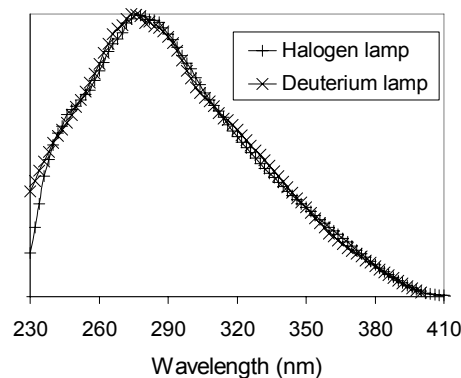


Figure 3.36 Relative spectral response curve for a SiC photodiode obtained from measurements with two different lamp sources.

3.3.1.3. Band-pass error

Measurements have been performed with a finite band-pass of 2 nm. This can be a source of error in the spectral ranges where the spectral response curve of the calibrated detector has a slope which is significantly different with respect to the one of the photodiode under test. The error amount can be evaluated using the following expression [56]:

$$u(R_{\lambda bw}) = \frac{b \cdot \beta^2}{6} \cdot \frac{dR_{\lambda}}{d\lambda}, \quad (3.3)$$

where $\beta = \frac{\Delta\lambda}{2}$ is half of the bandwidth and $b = \frac{d\Phi}{d\lambda} \cdot \frac{1}{\Phi - \lambda \cdot \frac{d\Phi}{d\lambda}}$; with Φ we have

indicated the flux incident on the detector.

Calculations have shown that the error amount due to finite band-pass is negligible if compared with other sources of error.

3.3.1.4. Percentage error

The percentage errors of the SiC, the GaN and the AlGaIn-type B photodiodes curves are reported in figure 3.37 (other AlGaIn photodiodes have quite similar error to AlGaIn type considered in the graph). The errors have been evaluated according the following propagation formula:

$$u_{rel}(R_{\lambda}) = \frac{u(R_{\lambda})}{R_{\lambda}} = \sqrt{\left(\frac{u(I)}{I}\right)^2 + \left(\frac{u(I')}{I'}\right)^2 + \left(\frac{u(R'_{\lambda})}{R'_{\lambda}}\right)^2} \quad (3.4)$$

where $u(I)$ and $u(I')$ are the errors associated to the photocurrent measurements; they have been evaluated from the S/N and taking into account also for the electronic noise; $u(R'_{\lambda})$ is the error on the calibration of the Si photodiode. Similar error amounts have been calculated for the other photodiodes.

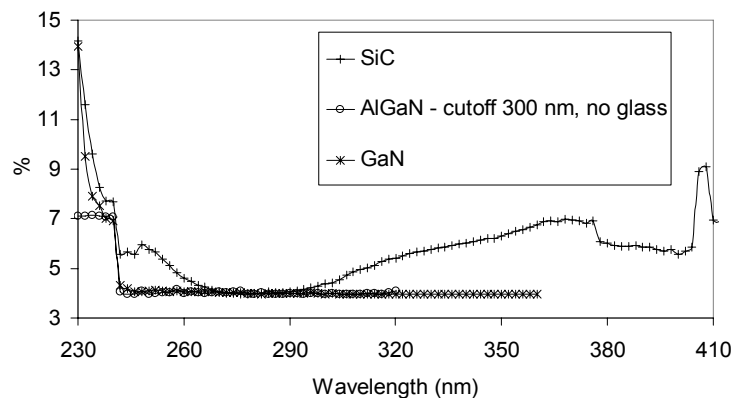


Figure 3.37. Percentage errors associated to the SiC, GaN and AlGaIn- type B photodiodes.

3.3.2. Absolute spectral response measurements

Absolute spectral measurements require that both the calibrated detector and the one under test collect the whole incidence beam; in this way formula (3.2) gives directly the absolute spectral response as function of the wavelength. As told before, in the Bentham spectroradiometer the exit beam is focused in a 2 mm diameter spot, much wider than the photodiodes effective area. A different set-up and methodology have been therefore used to perform these measurements.

3.3.2.1. Facility

Absolute spectral measurements have been carried out with an Optronic Laboratories double monochromator. Each monochromator is equipped with a 1200 l/mm grating. The effective aperture of the system is $f/4$ and the focal length of 250 mm. Band-pass can be varied using a set of interchangeable slits. During these measurements, a 300 W Xenon lamp has been used as a source. Differently from the Bentham instrument, beam exiting the monochromator is collimated. Again, the Si calibrated detector (active area of 1 cm^2) has been used as the reference standard. Photodiodes are mounted on a XYZ micrometric translation stage, which allows to properly position them.

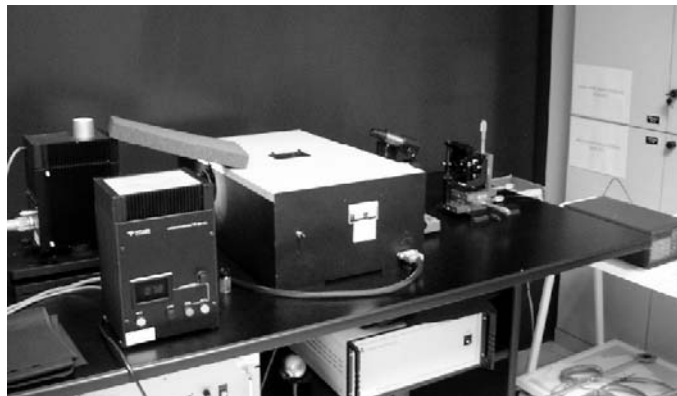


Figure 3.38. Optronic Laboratories spectroradiometer at Deltaohm.

3.3.2.2. Methodology

The gratings have been set in order to have 280 nm radiation wavelength exiting the monochromator. A SiC detector has been mounted on a the (X,Y,Z) translation stage. A (X=0,Y=0) position on the plane perpendicular to beam propagation direction has been determined moving the detector till finding the maximum output signal. A microscope have been focused to image this position (Figure 3.39). The collimated exit beam has been limited by an aperture of 2.5 mm diameter centred at (0,0). Inside this area we have verified that the beam is uniform. Acquisitions with the Si photodiodes, which has an active area of 1 cm^2 , have been performed with the aperture in place, while during measurements of the photodiodes under test the aperture was removed; in this case, in fact, the beam size is limited by the active area of the photodiodes itself. The microscope was helpful to align again the aperture, once removed, and each photodiode.

Assuming that the Si photodiode has a uniform response over the whole active area, the difference in the incident flux collected by the Si detector and the tested photodiodes

depends only on a geometric factor, which is the ratio between the 2.5 mm aperture area and the photodiode active area. The absolute spectral response at 280 nm has been therefore determined by the following formula:

$$R_{\lambda=280nm}^A = \frac{A_{ap}}{A_{ph}} \frac{I_{\lambda=280nm}}{I'_{\lambda=280nm}} R'_{\lambda=280nm}, \quad (3.5)$$

where A_{ap} and A_{ph} are the areas of the aperture and the photodiode under test respectively. The absolute spectral response curve (Figure 3.40) has been then obtained re-scaling the relative spectral measurements, given the absolute value at 280 nm:

$$R_{\lambda}^A = \frac{R_{\lambda=280nm}^A}{R_{\lambda=280nm}} R_{\lambda} \quad (3.6)$$

Photodiodes areas have been measured with an optical microscope.

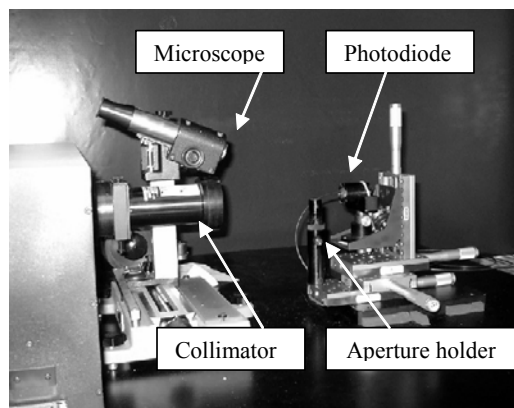


Figure 3.39. Set-up for the absolute spectral response measurements.

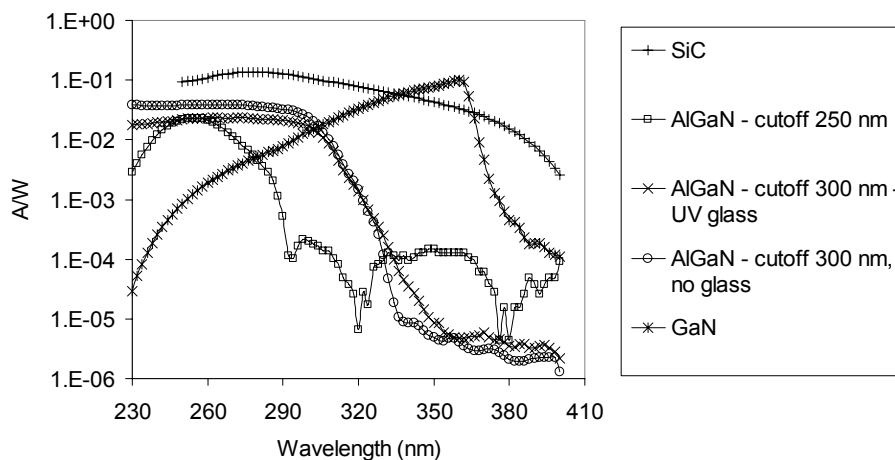


Figure 3.40 Absolute spectral response curves for the different photodiodes.

3.3.2.3. Lamp stability

Differently from halogen lamp, the Xenon lamp can be unstable over time. In order to quantify the error due to lamp instability, we have monitored the 280 nm output signal with a SiC photodiode over 15 minutes, which has been evaluated as the time necessary to complete a set of measurements associated to a photodiode. During this time the lamp has been varied of 2%, which is the maximum error that can be associated to a measurement (Figure 3.41).

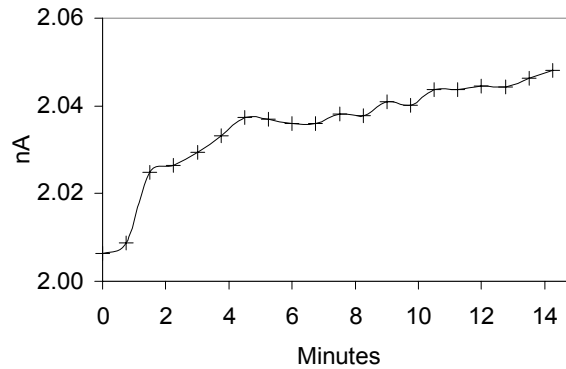


Figure 3.41. Stability of the XENON lamp over time.

3.3.2.4. Beam uniformity

The measurement procedure we have used is valid under the assumption that the incident beam is uniform. The uniformity of the beam has been evaluated on a 3×3 mm² area centered at the (0,0) position, after removing the aperture. A SiC photodiode has been translated in the X and Y direction at steps of 0.5 mm. For each position, a photocurrent acquisition has been performed. Results are reported in Figure 3.42. The beam has been evaluated uniform with a maximum deviation of 3%. In this percentage is included, again, the error due to lamp instability, even if we have tried to minimize the total time in which the data have been acquired.

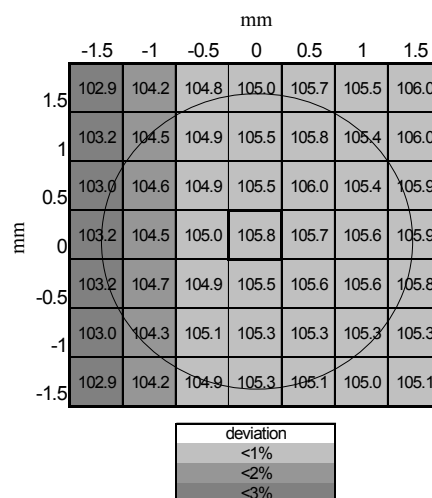


Figure 3.42. Photocurrent (pA) measurements to verify beam uniformity over a 3×3 mm² area.

3.3.2.5. Si photodiode active area uniformity

The measurement procedure we have used is valid under the assumption that the Si active area response is uniform over a reasonable area around its center. The uniformity of the detector has been evaluated on a 6×6 mm² area (Figure 3.43). In this measurements the Xenon lamp was replaced by the Deuterium one, to avoid the presence of errors due to lamp instability (Deuterium lamp is much more stable over time). The Si photodiode has been evaluated uniform with a maximum deviation of 2%.

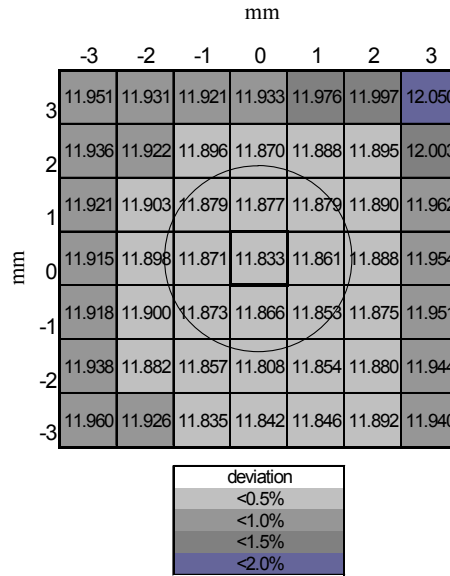


Figure 3.43. Si calibrated photodiode measurement (nA) to verify uniformity of response over an active area of 6×6 mm².

3.3.2.6. Percentage error

Errors associated to absolute response measurements at 280 nm have been calculated using the propagation formula associated to equation (3.5):

$$u_{rel}(R_{\lambda=280nm}^A) = \frac{u(R_{\lambda=280nm}^A)}{R_{\lambda=280nm}^A} = \sqrt{\left(\frac{u(A_{ap})}{A_{ap}}\right)^2 + \left(\frac{u(A_{ph})}{A_{ph}}\right)^2 + \left(\frac{u(I_{\lambda=280nm})}{I_{\lambda=280nm}}\right)^2 + \left(\frac{u(I'_{\lambda=280nm})}{I'_{\lambda=280nm}}\right)^2 + \left(\frac{u(R'_{\lambda=280nm})}{R'_{\lambda=280nm}}\right)^2} \quad (3.7)$$

Errors due to lamp instability and uniformity of the beam and Si detector have been then added quadratically to this error. The following total amounts have been founded:

$$u_{rel}(R_{\lambda=280nm}^A) = 6.0 \% \text{ for the SiC photodiode}$$

$$u_{rel}(R_{\lambda=280nm}^A) = 6.4 \% \text{ for the GaN photodiode}$$

$$u_{rel}(R_{\lambda=280nm}^A) = 6.2 \% \text{ fo the AlGaIn-type B photodiode.}$$

In order to evaluate the error associated to other wavelengths, the propagation formula associated to expression (3.6) must be considered:

$$u_{rel}(R_{\lambda}^A) = \frac{u(R_{\lambda}^A)}{R_{\lambda}^A} = \sqrt{\left(\frac{u(R_{\lambda=280nm}^A)}{R_{\lambda=280nm}^A}\right)^2 + \left(\frac{u(R_{\lambda=280nm})}{R_{\lambda=280nm}}\right)^2 + \left(\frac{u(R_{\lambda})}{R_{\lambda}}\right)^2} \quad (3.8)$$

The percentage error on the absolute measurements at a specific wavelength is therefore determined taking into account also the error on the relative measurement at the same wavelength and at 280 nm, as reported in Figure 3.37.

4. UV Source and Photoprotection

The sun is the main source of UV. The broad spectrum and intensity of UV from the sun are due to the high temperature at its surface and its size. The intensity of solar UV reaching the earth's atmosphere would probably be lethal to most living organisms on the earth's surface without the shielding afforded by the atmosphere. The ozone layer prevents almost all UV of wavelengths $\lambda < 290$ nm and a substantial fraction (in excess of 90% of the total energy) from 290 - 315 nm from reaching the earth's surface. Thus the terrestrial environment is exposed to UV between 290 nm and 400 nm. The spectrum, both before passage through the atmosphere and at sea level, is shown in figure 2.1 The solar radiation reaching the top of the earth's atmosphere is affected by the solar output and the earth-sun distance. Variations in solar output are much smaller than the variations caused by atmospheric attenuation factors.

4.1. Factors affecting solar UV levels

The total solar UV reaching the earth's surface, termed global UV can be divided into two components: direct and diffuse. Global UV reaching a horizontal surface is the quantity most often measured. For biological entities such as people and trees, UV hitting cylindrical or spherical surfaces may be more important. The amount and spectral distribution of solar UV irradiance reaching the earth's surface depends on a number of factors, including:

- wavelength of the UV
- solar zenith angle, which depends on latitude, date of the year and time of day
- ozone column thickness and vertical distribution
- molecular absorption and scattering (including localized gaseous pollutants)
- absorption, scattering and reflection by clouds
- reflectance characteristics (albedo) of the ground
- shadowing by surrounding objects
- altitude above sea level

The presence of cloud cover, air pollution, haze, or even scattered clouds, plays a significant role in attenuating UV. Clouds can block a significant portion of the UV which would have otherwise reached the surface. The transmission of UV radiation through clouds depends on cloud height, type and optical density. The resultant effect on UV transmission is difficult to assess particularly in the case of partial cloudiness. For complete cloud cover, the transmitted UV irradiance would decrease by 72% and for half cloud cover by 44%. In extreme cases cloud cover can decrease UV irradiance by over 90%.

4.1.1. Ozone depletion effects

Over 90% of the total atmospheric ozone resides in the stratosphere. The total ozone column is important for filtering solar UV. Only UVB is affected by changes in the ozone column. UVC is almost completely absorbed by ozone and oxygen in the atmosphere; even with severe ozone reduction UVC would still be effectively absorbed by the remaining oxygen. As stratospheric ozone levels decrease, the resulting higher levels of solar UVB could increase the production of reactive OH radical molecules, potentially increasing the chemical reactivity of the troposphere. In polluted areas with sufficient concentrations of oxides of nitrogen (NO_x) (above 0.5 ppb by volume) and hydrocarbon compounds this enhanced reactivity is calculated to result in greater levels of tropospheric ozone and other potentially harmful oxidized products, such as hydrogen peroxide and acids. The amount of ozone in the free troposphere is increasing for example over central Europe and other parts of the globe. The effect of these trends on UV radiation needs to be studied further [57]. For high sun angles, tropospheric ozone is a more effective absorber of UV radiation than stratospheric ozone because of the increased path length of scattered radiation in the lower atmosphere [58]. Changes in total column ozone were observed by both ground based and satellite based instruments from the WMO Global Ozone Observing System. The measurements show pronounced ozone depletion over Antarctica in months 9-12 (local early spring) [59]. Increases in biologically effective UVB were observed during this same time period [60]. Over representation of UVA in the common broad band meter action spectrum, relative to most biological action spectra, produces less pronounced relative and absolute changes in assessed UVB. Therefore under cloud free conditions common broad band meters are less sensitive in assessing the ground level UVB effects of ozone depletion than detectors with a steeper action spectrum response such as for DNA damage or for erythema.

4.2. Trends in UV

There have been no significant changes in ozone at the equator. Total column ozone over the Northern mid-latitudes has decreased by several percent over the past two decades. Efforts to detect changes in UV over long time periods have failed due to changes in column ozone. Besides the problems indicated in the interpretation and comparison of measurement data from different sites and sources, there are also insufficient direct solar terrestrial UVB measurements for constructing a global climatology or trend assessment due to some of the following [61]:

- problems in establishing appropriate instrumentation: either highly sophisticated and reliable spectral instruments or broad band instruments which fairly

represent the sensitivities of different biological and chemical targets (with different wavelength dependencies and sensitivity to different orientations),

- difficulty of maintaining accurate field instrument calibrations over many years
- practical limitations in establishing a global monitoring network especially with the potential for disturbance from locally polluted areas.

With insufficient spectral measurement data collected over long periods, data from the more extensively used broad-band measurement systems have been scrutinized. UV data from eight stations in the US showed decreases in UVB between 0.5% and 1.1% per year during a period of ten years [62]. However, this result does not agree with theoretical predictions and may be due to problems in the long-term calibration of meters or local pollution in mainly urban or semi-urban sites [63]. In Russia, a 12% decrease of UVB was observed in Moscow between 1968 and 1983 with a concurrent 15% increase in turbidity and a 13% increase in cloudiness. At the Jungfrauoch observing station in the Swiss alps (3.6 km above sea level), increases of $0.7 \pm 0.2\%$ per year in UVB were observed under clear sky conditions between 1981 and 1989. A comparison of summer spectral data weighted with the CIE erythral action spectrum using the same instrumentation at Lauder, New Zealand (45°S) and Neuherberg, Germany (48°N) showed weighted UV irradiances were 1.6 times larger in New Zealand due to decreased ozone column thickness.

4.3. UV monitoring

Recent public and scientific concern about ozone depletion and increased UV have led to the establishment of many UV monitoring centers in the last few years. Some years ago less than fifty UV monitoring stations were operating around the world. Today more than 250 monitoring centers are underway for a variety of reasons. Governmental agencies, scientific institutions, universities and private groups have begun to monitor UV. The World Meteorological Organization (WMO) has established a global network called Global Atmosphere Watch (GAW). The Global Environment Facility is supporting the creation of additional stations in developing countries. Various national and multi-national agencies are also operating and establishing UV monitoring networks.

The reasons for monitoring UV are generally divided into the following four areas:

- to provide information to the public on UV levels and variations,
- establishing a basic UV climatology,
- studying cause and effects of UV transmission, and
- detecting long term variability.

There are many difficulties in making accurate field measurements of ambient UV. Care must be taken that no part of the instrument is shaded from either direct or indirect sun; nearby surfaces must not change during the time period of monitoring; and routine maintenance such as snow and debris removal must be conducted systematically to avoid trend bias. The data must have spectral, temporal and angular resolution appropriate for validation of model calculations and for evaluation of biological effects. Frequent and reliable calibration of the instrumentation is necessary. UV monitoring for the detection of trends is difficult and failure to detect a trend may be due to lack of awareness of changes in instrument behavior and correction of it. Intercomparison of

different types of UV monitoring instruments have shown that individual instrument characteristics can cause substantial differences in measurements.

4.4. UV Artificial Sources

There are few artificial sources that result in human exposure to UV greater than that from the sun. However, exceptions are those used for medical therapy and diagnosis, cosmetic tanning. Industrial sources are generally effectively enclosed, but accidental exposure may occur. Any unfiltered optical source, whose emissions are due to the heating of a material e.g. a filament lamp, that emits significant quantities of UV will also emit visible and infrared radiations. In the case of high temperature tungsten halogen lamps biologically significant amounts of shorter wavelength UVB are also emitted. Some incandescent and discharge lamps have sufficient intrinsic filtration in the glass envelope of the lamp. Most man-made sources of UV can be grouped together in the categories shown below. The spectrum of the UV emitted varies from one source to another.

4.4.1. Incandescent sources

When a material is heated a large number of energy transitions occur within its molecules and optical photons are emitted. An ideally efficient emitter (radiator) is termed a black body radiator. The wavelength corresponding to the peak of the spectral emission of a black body radiator varies inversely as its temperature and as the temperature increases an increasing amount of UV is emitted. Incandescent sources whose temperatures are greater than about 2900 K emit significant amounts of UV with respect to possible effects on human health. The optical emission of the sun corresponds approximately to that of a black body radiator at a temperature of around 6000 K. In practice no material emits radiation with a black body spectrum. However, tungsten at high temperatures and molten metals approximate to theoretical black bodies. Such sources are termed grey bodies.

4.4.2. Gaseous discharge sources

The electrical excitation of a gas or vapour is a typical mechanism for generating optical radiation. An electric current is passed through a gas or a mixture of gases ionized to produce electrons and positive ions. Emissions are the result of electronic transitions in the atoms of a material from low to high energy states (absorption and excitation) followed by transitions from the high to low energy states (de-excitation and emission). This process is often combined with the process of luminescence, whereby the characteristic (line) photon emissions of the gas are absorbed by a luminescent material (luminophor or phosphor) which in turn emits optical radiation, typically as a continuum over a range of longer wavelengths. The 253.7 nm UV emission from a low pressure mercury vapour discharge is used as a source of excitation in low pressure fluorescent lamps. By raising the pressure of the discharge to a few atmospheres the emission lines increasingly broaden effectively forming a continuum. In some cases the 253.7 nm line emission will be self-absorbed by the vapour of the discharge.

4.4.2.1. Low pressure discharge lamps - Germicidal lamps

The low pressure mercury-discharge lamp is often used for the purpose of germicide and disinfection. Such lamps are very efficient emitters of UV. Approximately 50% of the electrical power is converted to UV of which up to 95% is emitted at a wavelength of 253.7 nm. An important example of germicidal lamps emission and monitoring are reported for experimental measurements performed with the erythema sensor developed [64].

4.4.2.2. Fluorescent lamps

The most common application of the low-pressure discharge is fluorescent lamps. These operate by means of a discharge between two electrodes through a mixture of mercury vapour and a rare gas, usually argon. Light is produced by conversion of 253.7 nm mercury emission to longer wavelength radiations by means of a phosphor coating on the inside of the glass envelope of the lamp. While the continuum emissions of fluorescent lamps are characteristic of the phosphors the narrow peak, spectral emissions are dominated by the characteristic line emission spectrum of the low-pressure mercury vapour discharge.

4.4.2.3. High pressure discharge lamps

The designation "high pressure discharge" lamps include the families of lamps often called high intensity discharge (HID), such as mercury vapour or metal halide lamps, where an electric arc is not created. At still higher pressures, arcs may be produced, e.g., the xenon or mercury short-arc lamps. The spectral emissions of the discharge are in the blue, green and yellow regions of the spectrum and a large amount of UV is also generated. The general construction of high-pressure mercury lamps is a fused silica (quartz) discharge tube containing the mercury/argon vapour discharge mounted inside an outer envelope of soda-lime or borosilicate glass. The outer glass envelope effectively absorbs most residual UV. Consequently the quantity of potentially harmful UV emitted by such lamps depends critically on the integrity of this envelope. Compared with ordinary high pressure mercury lamps the luminous efficacies of metal halide lamps are high. They are used for a range of industrial and commercial applications that include photochemical processing, graphic and photographic illumination, studio lighting, reprography and are also used for UVA cosmetic tanning equipment, for some medical applications and for solar radiation simulation.

4.4.2.4. Xenon, compact and linear arcs

Where an optical source of small size and of very high radiance is required a high pressure arc lamp may be used. These have a filling gas of mercury vapour, mercury vapour plus xenon gas or xenon gas. Metal halide types are also available. The spectral emission of xenon lamps, which at wavelengths shorter than infra-red, closely matches that of a black-body radiator at about 6000 K. This enables their use in photography and as solar radiation simulators. The spectral emission of xenon lamps, which at wavelengths shorter than infrared closely matches that of a black body radiator at about 6000 K, enables their use as solar radiation simulators. Their emission spectrum is continuous from the UV through to the IR regions. Large amounts of UVA, UVB and UVC are emitted by unfiltered lamps to the extent that they can present a

significant health hazard if incorrectly used. The luminance of compact xenon arcs may approach that of the sun and in some lamps with greater than 10 kW rating the luminance may exceed that of the sun. They therefore present a potentially severe retinal hazard if viewed. An example of the emission spectra of such a lamp are reported in figure for the 300 W Solar Simulator at LUXOR. The UVA, UVB, UVC and erythemally weighted emission are also reported in figure.

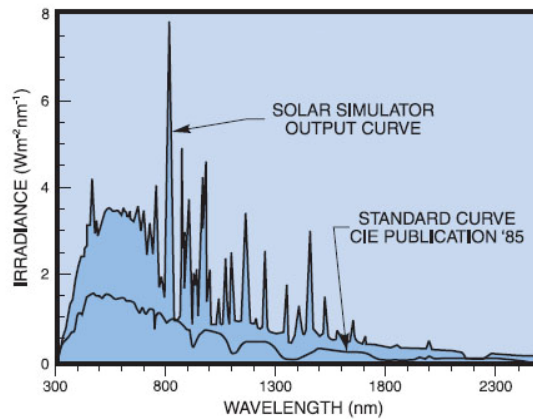


Figure 4.1. Irradiance spectrum of Lot-Oriel 300W Solar Simulator at LUXOR. Comparison with the standard solar emission on earth [65].

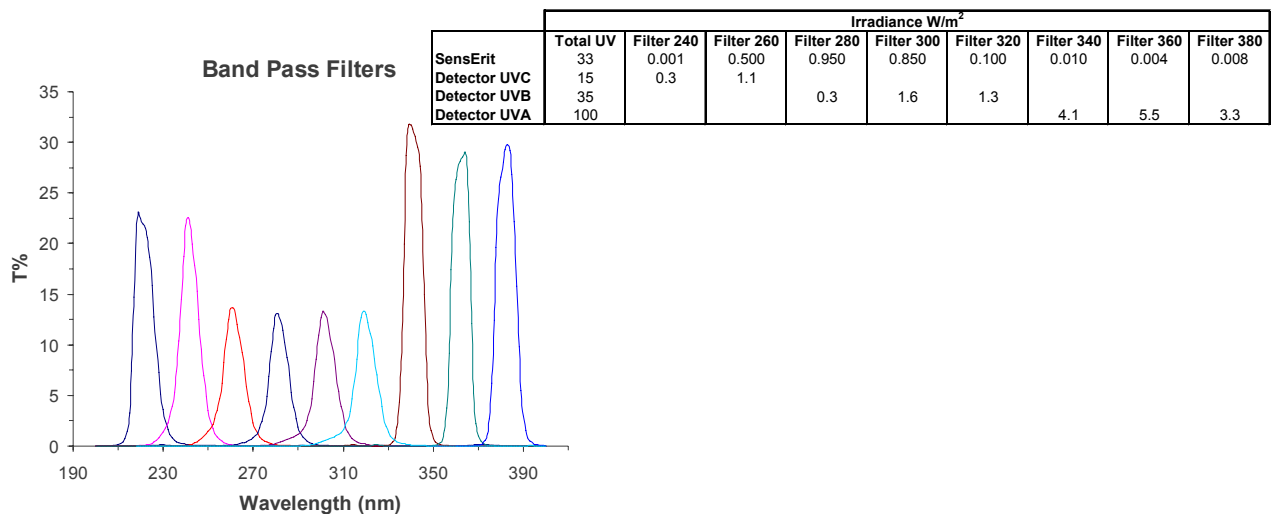


Figure 4.2. Irradiance measurements of a Xenon Source (Solar Simulator) performed with different radiometers and under different wavebands. The transmittance curves of the bandpass filters used for the measurements are also reported.

4.4.3. Arc welding

By comparison with gas flame processes, the emissions of UV from arc welding are very high and many data on the optical radiation emissions associated with a variety of electric arc welding processes have been published [66].

4.4.4. Sunbeds

Sunbeds are broadly used for cosmetic tanning purposes. There are four distinct types of lamps in use, each with different UV emission characteristics. Those are UVA, low-pressure fluorescent tubes; UVA, filtered high-intensity discharge lamps; UVB, low-pressure fluorescent tubes; UVB, filtered high-intensity discharge lamps. The emission characteristics and the health risks associated with the use of each type of lamp are different. The last two lamp types are associated with high levels of UVB and are now little used. They have been almost universally replaced by the predominantly UVA emitting lamp types. Some example sunbed of emission spectra are reported in figure 5.4. In table 4.1. some erythemally weighted irradiance measures performed with the developed instrument are reported demonstrating the possible hazardous deriving from periodical long exposures. As reported in table 4.1. is possible to observe how very high irradiance can be emitted from this kind of sources (measurements 23 and 24). In figure 4.3. the irradiance spectra of these two lamps are reported in comparison with a normal standard emission one.

Measurements	Effective Irradiance W/m ²
1	0.104
2	0.185
3	0.249
4	0.316
5	0.689
6	0.935
7	1.185
8	1.438
9	0.249
10	0.389
11	0.525
12	0.657
13	0.409
14	0.568
15	0.755
16	0.934
17	0.639
18	0.875
19	1.117
20	1.335
21	0.389
22	0.867
23	41.429
24	50.287
26	0.308
27	0.226
28	0.345

Table 4.1. Effective Irradiance measurements on different sunbed models.

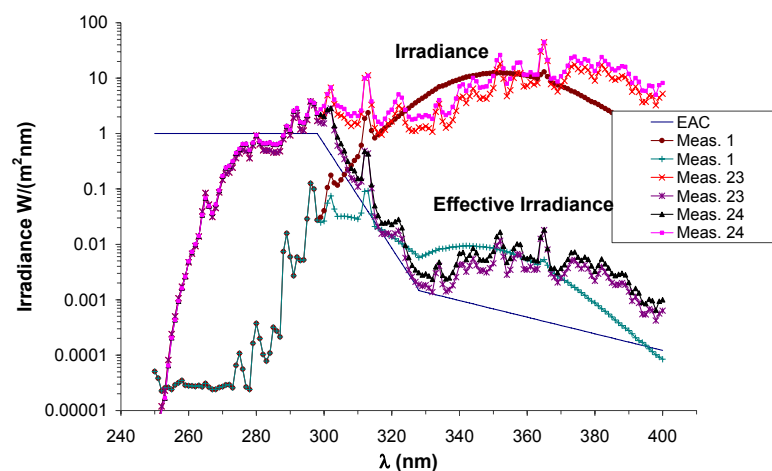


Figure 4.3. Irradiance (effective) values of sunbeds – Values correspondent to Measurements 1, 23 and 24

4.5. Protective measures - Photoprotection

It is widely accepted by scientific and medical authorities throughout the world that UV is potentially carcinogenic and capable of producing other undesirable health effects. It is sensible therefore to take steps to minimize UV exposure. Risks to health associated with exposure to UV from both natural and artificial sources can be substantially reduced by taking appropriate control measures. Since UV exposure occurs externally, simple measures can be taken to reduce the exposures received. A high degree of protection can be afforded by protective clothing, UV protective eyewear and by sunscreens for exposed skin.

4.5.1. Education

Concern about high incidences of skin cancer and eye damage have led to national educational campaigns in some countries to encourage people to protect themselves against excessive UV exposure from the sun and in the workplace. Educational programs directed at both the workforce and the public are intended to create an awareness of the adverse health effects that can result from overexposure to UV. Presently, in several different countries around the world, daily environmental UV levels are supplied to the general public in the form of UV indices. Their provision is intended to educate the public on the basic climatology of UV, increase awareness of the hazards of UV and provide information necessary to plan protection. Educational programs aim to produce a change in knowledge and attitudes, then a change in behavior and eventually a reduction in the incidence and mortality rates of skin cancer. A survey of sunscreen use on beaches in Brisbane, Australia found about 70% of females and males applied sunscreen. Half of the sunscreens provided the maximum protection (SPF 15+) and almost 90% used a waterproof formulation. However, the sunscreen was not applied over the entire body with over half neglecting ears and lower limbs [67]. Survey results show that sunburn is still occurring; in a randomly selected group of adults in Melbourne, Australia 16% reported sunburn over a summer weekend [68].

4.5.2. Protection Factors

The concept of a protection factor is useful when attempting to quantify the UV protection that items such as sunscreens, clothing and eyewear can provide [69]. To determine the protection factor, the following procedure is conducted. An effective dose (ED) of UV to the unprotected tissue is calculated by summing the incident solar spectral power over the wavelength range 290 to 400 nm. In order to determine the effective dose (ED_m) when the tissue is protected, the calculation is repeated with the spectral transmission of the protection item as an additional weighting. The protection factor (PF) is then defined as the ratio of ED to ED_m and is given by the following equation:

$$PF = \frac{ED}{ED_m} = \frac{\sum_{290}^{400} E(\lambda)S(\lambda)\Delta\lambda}{\sum_{290}^{400} E(\lambda)S(\lambda)T(\lambda)\Delta\lambda} \quad (4.1.)$$

Where $E(\lambda)$ is the spectral irradiance (W/m^2nm), $S(\lambda)$ is relative spectral effectiveness and $T(\lambda)$ is spectral transmission of protective item.

The inclusion of the spectral effectiveness function in the calculation ensures that sufficient weighting is given to the biologically effective wavelengths below 315 nm. A description of how the protection factors for fabrics, eyewear and sunscreens are determined is given in Roy and Gies [70] and CIE [71].

4.5.3. Clothing

Use of protective clothing provides one of the simplest means of reducing UV exposure. The degree of protection provided by clothing depends on the penetration of UV through materials and this can vary considerably. Fabrics which are visibly opaque tend to be more highly absorbent of UV, but the structure or weave of a material is the most important factor in determining its protective value. Color and thickness are a poor guide to UV protection. The transmission properties of some fabrics commonly used in the manufacture of clothing for everyday wear are given in table 4.2 (Welsh and Diffey 1981). Here the protection factor is an estimate of the protection afforded against biologically effective solar radiation. A high protection factor is associated with a tightly woven material. UV is transmitted and scattered through the interstices of the material itself rather than penetrating the fabric. Gies et al. (1992 – vedi sopra!!) have extended the concept of protection factor (PF) to fabrics and proposed the Ultraviolet Protection Factor (UPF). An example of fabrics transmittance curves measured at LUXOR within my Ph.D. activities is reported in figure 4.4.

Fabric	Structure	Colour	Thickness (mm)	% of T UV	Protection Factor
Nylon-tricel	Woven	Black	0.01	0.15	750
Nylon-viscose jacquard	Woven	Black	0.02	0.20	500
Nylon	Woven	White	0.01	1.07	55
Nylon-terylene mixture	Knitted	Blue	0.02	11	9
Nylon-acetate jersey	Knitted	Pink	0.02	24	4
Polyester-slub viscose	Woven	Pink	0.05	9	14
Polyester-printed lawn	Woven	Red	0.02	7	11
Polyester-jersey	Knitted	Fawn	0.03	7	14
Polyester-jersey	Knitted	Cream	0.04	5	19
Polyester-jersey	Knitted	Black	0.03	8	12
Polyester-jersey	Knitted	Orange	0.03	5	23
Polyester-jersey	Knitted	Turquoise	0.05	16	6
Polyester-jersey	Knitted	Brown	0.07	1.06	68
Polyester-jersey	Knitted	Black	0.05	4.04	23
Polyester-brushed jersey	Knitted	Blue	0.04	5.02	19
Polyester-brushed jersey	Knitted	Green	0.04	6.00	16
Polyester-bouclette	Knitted	Orange	0.04	3.00	33
Polyester-bouclette	Knitted	Purple	0.04	2.00	51
Cotton-needlecord	Woven	Brown	0.05	< 0.1	> 1000
Cotton-denim	Woven	Blue	0.05	< 0.1	> 1000
Cotton-printed	Woven	Brown	0.03	< 0.1	>1000
Cotton-printed	Woven	Cream	0.03	2.07	36
Wool-jersey	Knitted	Fawn	0.07	0.07	150

Table 4.2. UVB transmission properties of common fabrics [72].

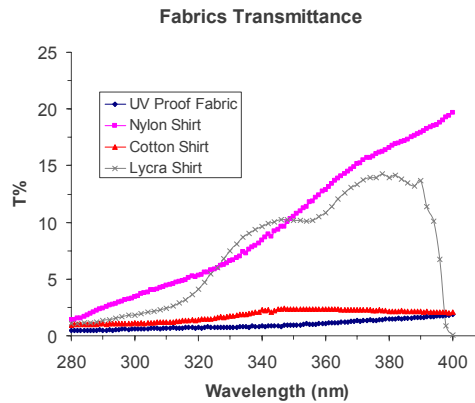


Figure 4.4. Example of Fabrics transmittance measured at LUXOR. Comparison between different materials.

4.5.4. Eye Protection

In industry there are many sources capable of causing acute eye injury within a short exposure time, while in the natural environment acute injury is likely to occur mostly in situations where solar UV is reflected onto the eye, such as from snow while skiing. A variety of eye protection is available with various degrees of protection appropriate to their intended use. Those intended for industrial use include, welding helmets, face shields, goggles and UV absorbing spectacles. For use in the outdoor environment, they include (ski) goggles for extreme exposure conditions and sunglasses. In industrial exposure situations the degree of ocular hazard can be assessed by measurement and comparison with recommended limits for exposure (IRPA/INIRC [73]). For outdoor workers and the general public, the most hazardous source of UV exposure is the sun. Adequately designed goggles afford protection against exposure to solar UV at high altitudes and on snow, but for most other exposure conditions, good UV absorbing sunglasses are an adequate means of eye protection. Transmission of UV through sunglasses varies considerably [69]. Gies et al. [74] have proposed a UV eye protection factor (EPF) for sunglasses similar to the one developed for fabrics and sunscreens. An example of eyeglass transmittance curves measured at LUXOR within my Ph.D. activities is reported in figure 4.5.

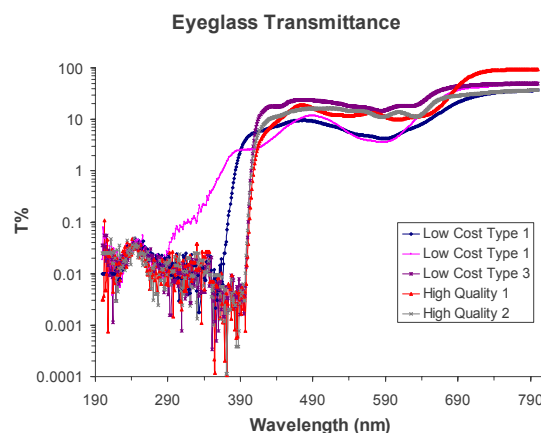


Figure 4.5. Example of Eyeglass transmittance measured at LUXOR. Comparison between high quality and low cost materials.

4.5.5. Sunscreens

Sunscreens are physical and chemical topical preparations which attenuate the transmission of solar UV into the skin by absorption, reflection or scattering. Physical sunscreens, for example zinc oxide and titanium dioxide, function by reflecting and scattering and provide protection against a broad spectrum of UV and visible wavelengths. They are normally nontoxic and have few known adverse effects. Sunscreens based on chemical absorbers contain one or more UV-absorbing ingredients which generally absorb UVB radiation more strongly than UVA. Para-aminobenzoic acid (PABA) and its derivatives, salicylates, cinnamates and camphor derivatives primarily absorb UVB and transmit UVA; benzophenones essentially absorb UV of wavelengths of less than 360 nm. The generally accepted parameter for evaluating the efficacy of sunscreen preparations is the sun protection factor (SPF), which is defined as the ratio of the least amount of UV required to produce minimal erythema after application of a standard quantity of the sunscreen to the skin to that required to produce the same erythema without sunscreen application. Hence, at present the protection efficacy of a sunscreen is evaluated by using erythema as the main end point. Therefore, until very recently, most sunscreens were designed to absorb UVB wavelengths with little or no absorption in the UVA. Sunscreens also protect against the induction of skin cancer (Diffey, 2005 [75]), mainly by reducing UV-induced DNA damage but the relationship between erythema and skin cancer is still unknown. Determining the relative role of UV wavelengths in immune suppression and skin cancer development may have broad implications in sunscreen design (Ullrich et al. 2002 [76]). Results by Ananthaswamy et al. (2002) demonstrate that the mutation of the p53 tumour suppressor gene may serve as an end point of skin cancer development while sunscreens can inhibit this gene mutation. Nghiem et al. (2001) [77] demonstrated that UVA may be playing a dual role in melanoma development, namely both induction and promotion by suppressing the immune response. This may explain previous findings indicating that UVB-absorbing sunscreens were incapable of interfering with UV-induced enhancement of melanoma growth in mice (Wolf et al, 1994)

Within my Ph.D. I've been involved in a scientific project related to the development of a standard method to assess sunscreens protection by in-vitro test in the UVA spectral region. Increasing awareness of the need for UVA protection led to the formulation of chemical products with several active ingredients to give overlapping absorption in the entire wavelength range of 290 400 nm. Physical sunscreen as titanium dioxide and zinc oxide block already a wider spectrum of the UVA rays with respect to chemical sunscreen. The UVA protection therefore change with formulas and amount of chemical added. Due to the absence of a standardized test to assess UVA protection, product labelling is very confusing, mainly because there is no a final consensus on both method and labelling criteria. The research has been funded by the University of Padova (Ateneo Project 2005, "Development of a new in-vitro approach for the evaluation of sunscreens efficacy and validation of labelling", PI: Prof. Mauro Alaibac). A laboratory for this purposes was created during 2006 (Figure 4.6) at LUXOR. The laboratory comprises all facilities necessary for in-vitro tests of sunscreens, which are based on measurements of transmission and reflection (regular and diffused) of sunscreens applied to skin equivalent models. To perform those measurements, a UV/VIS/IR Varian Cary 5000 double grating monochromator with an integrating sphere

is used. An Oriel simulator, 300 Watt is used to test photo-stabilities of sunscreens, which is verifying changing of optical properties before and after irradiation.

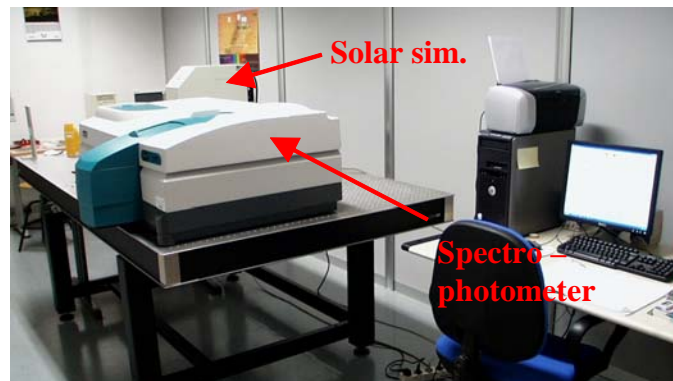


Figure 4.6. Laboratory for sunscreens tests

During the first months of activity in this field I've study the optical and morphological properties (Figure 4.7) of different in-vitro support, as Vitro-Skin®, Transpore®, rough quartz and teflon, on which sunscreens have to be applied. With respect of each support fully optical characterization have been performed, evaluating for example photo-stability of the support itself, properties of diffuse scattering of the support alone ecc.

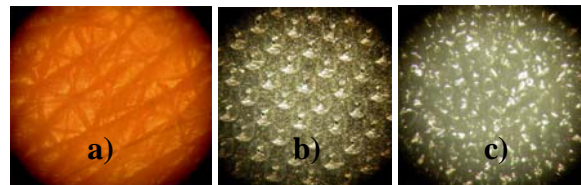


Figure 4.7. a) In vivo microscopic image of skin (50x Optical Zoom). b) Microscopic image of Transpore 3M (20x Optical Zoom). c) Microscopic image of hydrated Vitro Skin (20x Optical Zoom).

A method to applied different sunscreen formulation (chemical, physical or mixed) to each type of support according with COLIPA recommendation have been developed. Reproducibility of results for different application on same support of the same sunscreen formula have been verified. Measurements of regular and diffuse transmission of different products have been performed. I'm now evaluating the correlation between in vivo SPF as declared on labelling, chemical/physical filter composition and test results; for example, it is very interesting that products distributed by different companies, while providing similar SPF values on label, have very different total transmission spectra (Figure 4.8) (and therefore different protection in different spectral ranges); this have been verified to be true independently from the support used. Moreover, I've tested some commercial formulation for photo-stability (Figure 4.9). Results demonstrate very different behaviour for different sunscreen formula, demonstrating that physical and chemical filters have very different stability property.

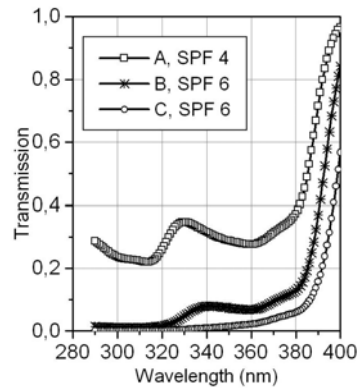


Figure 4.8. Transmission spectra of three different commercial products, applied on Transpore, with similar SPF.

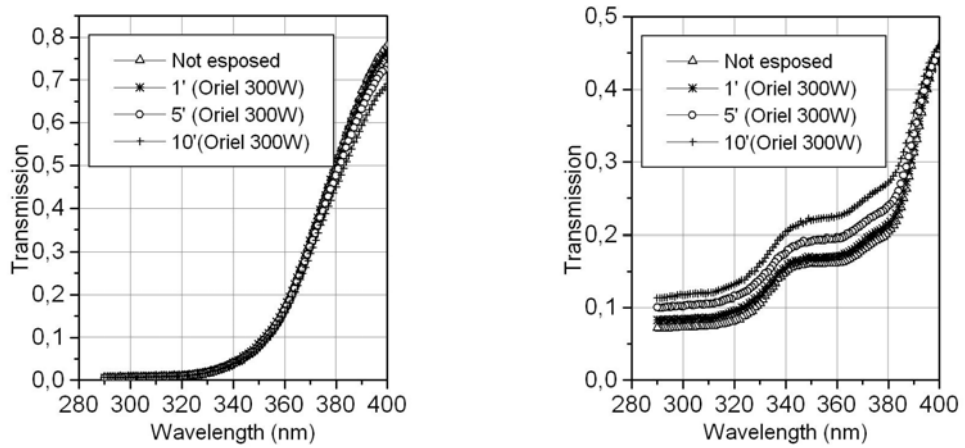


Figure 4.9. Photostability of two different commercial products

5. Instruments realization and application

Several prototype instrumentation have been developed. Sensors with erythema like response curve have been realized and patent, moreover this instrument won the prize “Veneto Innovazione 2005” for the collaboration between University and Industry. Other sensors with particular response curves have been designed, such as Vitamin D like response, DNA damage, Eye Cataract, etc.

All these instrumentation could be used in several application on earth and space environment. The ground UV level monitoring have just been discussed above, while possible application in extraterrestrial environments will be discussed in the next pages.

An overview of the Senserit (SENsor ERITema) is shown in figure with its nominal response curve, perfectly correspondent with Erythema Action Curve. Moreover the response curves obtained with the very first prototypes are shown. With this instruments we have measured effective irradiance from natural and artificial source with an error below 10%.



Figure 5.1. LUXOR Broad-band Radiometers.

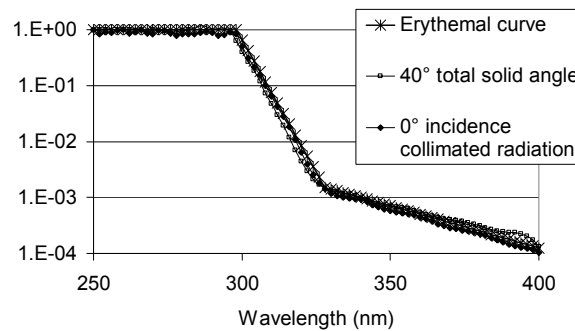


Figure 5.2. Senserit® Radiometer. Image and Attended Performance.

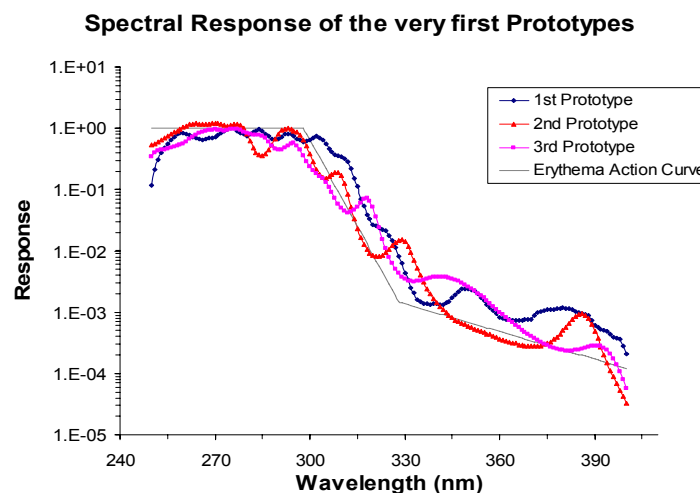


Figure 5.3. Senserit® Prototypes performance.

5.1. Prototype realization

All sensor components were assembled in a black plastic case, with a diffuser as the input optics. The radiometers consist of the detector designed for outdoor operation, and the recorder that performs all control and data storage functions.

The relative spectral response of all the systems were measured by the use of the f/4 Bentham double spectral monochromator equipped with 1800 lines/mm gratings and halogen–tungsten (for $\lambda > 300$ nm) and deuterium lamp (for $\lambda < 300$ nm) sources. Measurements were performed at 2 nm steps with 2 nm spectral bandwidth. The results were compared with the ones expected according to the measured characteristics of each single component. The output photodiode current was amplified by a current voltage amplifier mounted on a proximity circuit inside the radiometer head. Besides the amplifying function, the circuit allowed the measurement of the photocurrent in four different scales automatically selected to avoid saturation. The radiometer head was connected to an indicator by a cable (figure 5.1). Inside the indicator there was also another amplifier. Two trimmers allowed the setting of the instrument zero and sensibility. On the display the total effective irradiance value (W_{eff}/m^2) is displayed.

5.1.2. Calibration

To determine the absolute spectral response of the radiometric heads calibrations were performed at a particular wavelength. The absolute response at other wavelengths was recovered by rescaling the previously obtained relative spectral response curves. The Bentham instrument collected the radiation emitted by a set of low pressure mercury lamps and filtered by an interferential filter centered at the chosen wavelength. In this way very high spectral purity was obtained. A lens system was placed after the exit slit to collimate the beam. A silicon photodiode calibrated at National Physics Laboratory (NPL, UK) was used as the standard reference. Absolute calibration was obtained by a comparison between measurements performed with the two detectors, i.e., the reference photodiode and prototype radiometric head. Calibration errors were estimated to be, in all the cases, lower than 10%.

5.1.3. Cosine response

Traditionally instruments for solar radiation measurements have an angular response close to that of the cosine law, therefore measuring the energy flux through a horizontal surface. It is very difficult to make an instrument with perfect cosine response and usually only some of the most expensive instruments, like spectroradiometers, have the complicated entrance optics that assures good angular response for incident zenith angles over 75 degrees. In the case of Solar UV radiation measurements some compromise is justifiable. First, even when the sun is low, most of the UV energy comes from the sky (scattered UV) and therefore the effect of an imperfect angular response is greatly reduced. Secondly, when the daily dose is measured the biggest contribution is integrated for small solar zenith angles. Lastly, for long term UV trend analysis the shape of the angular response is not as critical as its repeatability across the network and stability with time.

Due to the poor quality of the diffuser choose for the prototypes realization, measurements with the prototypes were only accurate for collimated spectral radiation. Nevertheless, much better performance could be obtained if the quartz was replaced by Teflon.

5.2. Characterizing the performances of the radiometers

According to the document "UVNET WG1: Guidance for UV power meter classification for particular applications" [78], wherein a standard method to fully characterize a UV meter by the use of 12 parameters was proposed, in the next pages the definition and evaluation of these parameters are reported for the Senserit Radiometer. Analogous procedures have been followed with the other radiometers.

The following characteristics of integral measuring radiometers influence the uncertainty of measurements, and are used for a characterization of the performance. The name for the characteristic has been taken from the physical effect influencing its quantity for easy memorizing the meaning.

5.2.1. Calibration uncertainty u_{cal}

The calibration uncertainty u_{cal} describes the uncertainty provided by the calibration of the radiometer.

The calibration uncertainty results from the uncertainty of measurement and from the uncertainty of the calibration standard. The value of the latter has to be taken from the calibration certificate of the standard and has to be stated with the characteristics of the radiometer. Other uncertainties can result from:

- 🕒 aging of the standard
- 🕒 uncertainty of the working standard, if used
- 🕒 uncertainty of the measurement of the electrical quantities of the standard and its geometrical adjustment
- 🕒 uncertainty due to the calibration conditions
- 🕒 stray radiation
- 🕒 temperature changing of the radiometer by heating caused by the radiation of the standard
- 🕒 other influence on the radiometer for ambient conditions, which have not been mentioned so far, but existed during calibration

Taking into consideration all the conditions the total uncertainty was, in all the cases, under 10%.

5.2.2. Short wavelength range response characteristic u

The short wavelength range response characteristic u describes the responsivity of the radiometer head in respect of the short wavelength range beyond the respective weighting function.

The short wavelength range response u of a radiometer head is the ratio of the signal Y_s when the head is irradiated by a defined UV source combined with a specified UV filter, to the signal Y when it is irradiated by the same source without the filter, according to equation (5.1)

$$u = \left| \frac{Y_s}{Y} - u_0 \right| \quad (5.1)$$

where u_0 is according to equation (5.2)

$$u_0 = \frac{\int_0^{\infty} S_{\lambda,s} \cdot \tau(\lambda) \cdot s(\lambda)_{eff,rel} \cdot d\lambda}{\int_0^{\infty} S_{\lambda,s} \cdot s(\lambda)_{eff,rel} \cdot d\lambda} \quad (5.2)$$

Where:

$\tau(\lambda)$ - spectral transmittance of the filter for determining the short wavelength range response

$S_{\lambda,s}$ - spectral distribution of the lamp used for determining the short wavelength range response

$s(\lambda)_{eff,rel}$ - relative spectral weighting function

The short wavelength range response is to be determined by irradiating the radiometer by a UV source and appropriate filter, suitable for the weighting function under consideration. In our case, we use a UVC lamp and a short wavelengths cut-off filter (in order to block all the radiation above 250nm). A value of $2 \cdot 10^{-4}$ has been obtained for u .

5.2.3. Long wavelength range response characteristic r

The long wavelength range response characteristic r describes the responsivity of the radiometer head in respect of the long wavelength range beyond the respective weighting function.

The long wavelength range response of a radiometer head is according to equation (5.3) the ratio of the signal Y_l , when the head is irradiated by a defined source, combined with a specified long wavelength range cutting filter, to the signal Y when it is irradiated by the same source without the filter.

$$r = \left| \frac{Y_l}{Y} - r_0 \right| \quad (5.3)$$

where r_0 is according to equation (5.4)

$$r_0 = \frac{\int_0^{\infty} S_{\lambda,A} \cdot \tau(\lambda) \cdot s(\lambda)_{eff,rel} \cdot d\lambda}{\int_0^{\infty} S_{\lambda,A} \cdot s(\lambda)_{eff,rel} \cdot d\lambda} \quad (5.4)$$

Where:

$\tau(\lambda)$ - spectral transmittance of the filter for determining the long wavelength range response

$S_{\lambda,A}$ - spectral distribution of the lamp used for determining the long wavelength range response

The long wavelength range response has been measured by irradiating the radiometer head with a source, emitting an sufficient radiation level in the long wavelength range of the considered weighting function. The combined filter blocks the long wavelength range of the considered weighting function (>400nm). The value obtained for y was $4 \cdot 10^{-4}$.

5.2.4. Directional response characteristic f_2

The directional response characteristic f_2 describes the responsivity of the radiometer head to radiation incidence other than perpendicular (cosine law).

For the measurement of directional response, a point radiation source shall be placed in front of the radiometer head. The distance in-between must be greater than the radiometric limiting distance. Special precautions should be taken to exclude stray radiation from the acceptance area of the radiometer head. The radiometer head has to be adjusted with its optical axis towards the source. Rotation of the radiometer head around a horizontal or vertical axis varies the angle of incidence referred to the center of the acceptance area of the radiometer head. The center of revolution should be coincident with the center of the acceptance area. Measurements of the signal as a function of the angle of incidence shall be carried out in at least two mutually perpendicular planes. For a radiometer the systematic deviation in directional response to the incident radiation is given according to equation (5.5)

$$f_2^*(\varepsilon, \varphi) = \left| \frac{Y(\varepsilon, \varphi)}{Y(\varepsilon = 0^\circ, \varphi) \cdot \cos \varepsilon} - 1 \right| \quad (5.5)$$

where

$Y(\varepsilon, \varphi)$ - output signal as a function of the angle of incidence

ε, φ - according to figure.

For characterizing the directional response, the characteristic f_2 according to equation (5.6) is used:

$$f_2 = \int_0^{\frac{85^\circ \cdot \pi}{180^\circ}} |f_2^*(\varepsilon, \varphi = 0)| \cdot \sin 2\varepsilon d\varepsilon \quad (5.6)$$

For the radiometers designed a f_2 value of $f_2 = 0.65$ in the case of a quartz diffuser, and $f_2 = 0.065$ in the case of a Teflon diffuser have been evaluated experimentally following the procedure described above.

5.2.5. Linearity characteristic f_3

The linearity characteristic f_3 describes the deviation of the radiometer response for different levels of radiation.

The input - output characteristic of a radiometer describes the relation between the output quantity (reading) and the input quantity. The linearity of a radiometer is the property whereby the output quantity of the detector is proportional to the input quantity. In general, perfect linearity of a radiometer can not be assured. For the measurement of the input - output characteristic and determining the deviation in linearity, the radiometer head has to be irradiated continuously or in steps with defined levels of irradiance. With each level of input quantity, the output quantity (reading) shall

be recorded. For performing such measurements, certain setups for stepwise varying the irradiance on the radiometer head (in general with a step ratio of 1:2) are mentioned in the literature. The measurements for high levels of irradiance may also be determined by testing the linearity of the radiometers components (radiometer head, amplifier) separately.

The function of systematical deviation $f_3^*(Y)$ in linear response of radiometers is given in equation (5.7)

$$f_3^*(Y) = \frac{Y}{Y_{\max}} \cdot \frac{X_{\max}}{X} - 1 \quad (5.7)$$

where

Y - output signal due to irradiance on the radiometer head with an input quantity X

X_{\max} - input value corresponding to the maximum output signal Y_{\max} (largest value of the measurement range)

Y_{\max} - output signal due to irradiation on the radiometer head with the input X_{\max} .

To characterize the deviation in linearity within the different ranges, the characteristic f_3 according to equation (5.8) is used. It equals the maximum value of the function of systematical deviation $f_3^*(Y)$ in equation (5.7).

$$f_3 = f_3^*(Y)_{\max} \quad (5.8)$$

The response linearity of the sensor can be derived through the characterization performed on photodiodes [79] since the other components do not affect this property. The linearity of the detectors was evaluated by using different setups. For the linearity at high intensity two lamps 300 W Xe and a 1000 W Xe–Hg were used. The intensity of the Xe–Hg lamp was varied; moreover, the photodiode was exposed to only one or both sources by using a shutter system. Detector output signals were registered, and it was verified that photocurrent values in the case of simultaneous exposure to both lamps correspond to the sum of the values acquired with each source. The maximum deviation from the linearity was found to be 3.5% for an output total signal of some μA . The same approach was used to verify the linearity for a low intensity signal; in this case two halogen lamps were used and the maximum deviation was found to be 3.2% for an output total signal of 90 pA. The operating range of the sensor was between a few mW/m^2 and $100 \text{ W}/\text{m}^2$.

5.2.6. Display unit characteristic f_4

The display unit characteristic f_4 describes the influence of the analog or digital display unit of radiometers.

The measurement accuracy of radiometers analog display is determined by the class of the analog apparatus. The deviation of a radiometer due to the class of analog display is characterized by the parameter f_4 according to equation (5.9)

$$f_4 = k \cdot [\text{class}] \quad (5.9)$$

where

k - factor due to changing output range (e.g. $k = 10$ when the switching of the measurement range is at the ratio of 1:10). and is according to equation (5.10)

$$k = y_{B,\max} / y_{A,\max} \quad (5.10)$$

where

$Y_{A,\max}$ full scale reading in the more sensitive range A

$Y_{B,\max}$ full scale reading in the less sensitive range B

The accuracy of digital display radiometers is influenced by the relative accuracy error of reading and the quantization error (in general ± 1 digit). Accordingly, the parameter f_4 is given by equation (5.11).

$$f_4 = |f_{\text{display}}| + \frac{k}{P_{\max}} \cdot |d| \quad (5.11)$$

where

f_{display} - relative accuracy error of reading, in %

k - factor for range changing according to equation (5.10)

P_{\max} - the number of different output codes possible (e.g. for a 3 1/2 digit display, $P_{\max} = 1.999$)

d - quantization error

5.2.7. Fatigue characteristic f_5

The fatigue characteristic f_5 describes the stability of the radiometer responsivity for constant irradiation for longer periods.

Fatigue is the reversible temporal change in the responsivity, under constant operating conditions, caused by incident irradiance. Fatigue should be measured with temporary stable irradiation at a level close to the highest measurable one. The used source and the related radiometric quantity shall be stated. The operating conditions (ambient temperature, supply voltage, etc.) should be held constant. The output signal should be measured as a function of the irradiation period. Before performing the test, the radiometer head should not be exposed to radiation for at least 24 hours.

For showing the fatigue, the function of systematical deviation $f_5(t)$ is given according to equation (5.12)

$$f_5(t) = \frac{Y(t)}{Y(t_0)} - 1 \quad (5.12)$$

Where:

t - elapsed time since the beginning of illuminating the radiometer head with the constant irradiance

$Y(t)$ - output signal at time t

t_0 - reference time, e.g. 10 s

For characterizing, the characteristic f_5 according to equation (5.13) and the level of irradiance or luminance used for the test are to be stated:

$$f_5 = \frac{Y(30 \text{ min})}{Y(10 \text{ s})} - 1 \quad (5.13)$$

Where:

$Y(30 \text{ min})$ - output signal 30 minutes after the beginning of the irradiation

$Y(10 \text{ s})$ - output signal 10 seconds after the beginning of the irradiation

A Lot-Oriel 300Wfull spectrum solar simulator that ensures a well stabilized irradiation was used to irradiate the radiometer. The instrument was previously kept unexposed to radiation for 1 week. The fatigue parameter f_5 was evaluated to be 0.035 after 30 min of exposure.

5.2.8. Temperature dependence characteristic f_6

The temperature dependence characteristic f_6 describes the influence of ambient temperature different from calibration temperature.

Temperature dependence characterizes the influence of the ambient temperature on the absolute responsivity and the relative spectral responsivity of the radiometer. If the radiometer is operated within an ambient temperature different from that used during calibration, measurement errors can occur. In order to measure a temperature dependence, the entire radiometer must be exposed to the desired temperature. The instrument must attain thermal equilibrium before starting the measurement.

In case there is a fatigue effect, the radiometer head should be irradiated only during the measurement. The measurement should be performed at least for ambient temperatures of 25°C (reference temperature) and 40°C. Radiometers which are used in the field should also be measured at an ambient temperature of 0°C. The measurement should be performed at an irradiation level on the radiometer head that

approaches the largest value of an arbitrary measurement range. Within the range of ambient temperature between T_1 and T_2 the temperature coefficient is in linear approach according to equation (5.14):

$$\alpha(T_1, T_2) = \frac{Y(T_2) - Y(T_1)}{T_2 - T_1} \quad (5.14)$$

where

T_1, T_2 - range limits of ambient temperature

$Y(T_1), Y(T_2)$ - reading at the respective ambient temperature

The change of the output signal referred to the signal received at the ambient temperature of 25 °C prescribed for calibration is used for characterizing. For evaluating the characteristic f_6 , a prescribed temperature difference ΔT is used according to equation (5.15) in conjunction with an upper temperature level of 40 °C and a lower temperature level T , applicable for the measurement task

$$f_6(T, \Delta T) = \left| \alpha(T, 40^\circ\text{C}) \cdot \frac{\Delta T}{Y(25^\circ\text{C})} \right| \quad (5.15)$$

where:

T - ambient temperature level of 25 °C with radiometers used for interior measurements or 0 °C with radiometers also used for outdoor field measurements

ΔT - temperature difference, prescribed for different measurement tasks. For laboratory used radiometers a value of 2 °C, otherwise a value of 10 °C shall be used.

Although dedicated measurements were been performed, we concluded that the detector head response was not critically dependent on temperature variations. This conclusion was based on the characteristic of its components: diffuser, filter, and detector, with only some possible limitation about Teflon stability. This behavior was different from detectors based on phosphor conversion since their efficiency was temperature dependent.

5.2.9. Modulated radiation characteristic f7

The modulated radiation characteristic f7 describes the influence of modulated radiation at various frequencies, different than that of DC-operated lamps.

When measuring modulated radiation, the reading of a radiometer can deviate from the arithmetic mean value if the frequency of the modulated radiation is below the lower frequency limit, and if the peak overload capability is exceeded or if the settling time is not completed.

The range between the lower frequency limit f_{lo} and the upper frequency f_{up} of sinusoidal modulated radiation (modulation degree 1, see figure 2) is determined for a

radiometer. Within this range the meter reading shall not differ more than 5 % from the reading for unmodulated radiation of the same arithmetic mean value. The lower frequency limit f_{lo} of sinusoidal modulated radiation is the minimum frequency where the meter reading does not differ more than 5 % from the reading for unmodulated radiation of the same arithmetic mean. The upper frequency limit f_{up} of sinusoidal modulated radiation is the maximum frequency where the meter reading does not differ more than 5 % from the reading for unmodulated radiation of the same arithmetic mean.

The measurement of the upper and lower frequency limits can be performed by means of a DC operated source and a rotating sector disc. A homogeneously irradiated acceptance area is not required. The signal level for the measurement of modulated radiation must lead to a reading near the full scale of the used measuring range. In order to show the function of systematical deviation $f_7(f)$ for modulated radiation versus the frequency, equation (5.16) is given:

$$f_7(f) = \left(\frac{Y(f)}{Y(f=0 \text{ Hz})} - 1 \right) \quad (5.16)$$

Where:

$Y(f=0\text{Hz})$ - output signal for irradiation with unmodulated radiation

$Y(f)$ - output signal for irradiation, modulated with frequency f , with the same arithmetic mean value as for steady-state irradiation.

To characterize the effect of modulated radiation, the characteristics f_7 (100 Hz) for 100 Hz, $f_7(f_{lo})$ for the lower frequency limit and $f_7(f_{up})$ for the upper frequency limit are used.

5.2.10. Polarization response characteristic f_8

The polarization response characteristic f_8 describes the influence of polarized radiation to the responsivity of the radiometer.

The output signal of a radiometer can depend on the polarization condition of the measured radiation. In this case, the output signal Y changes when the linearly polarized quasiparallel incident radiation is rotated around the direction of incidence.

In order to measure the polarization dependence, unpolarized radiation from a point source is required.

To achieve complete depolarization of the radiation (including the tilted glass plate), a polarizer (e.g. two sheet polarizers placed back to back with their axes in parallel) is placed in front of the radiation source. The polarizer can be rotated around the direction of incidence in order to change the position of the plane of polarization.

The maximum Y_{max} and minimum Y_{min} output signals of the radiometer are then measured while rotating the first polarizer. The measurements are to be carried out for at least two angles α , which differ in 90° .

To characterize the polarization dependence, the characteristic $f_8(\theta)$ is given according to equation (5.17)

$$f_8(\theta) = \frac{Y_{\max}(\theta) - Y_{\min}(\theta)}{Y_{\max}(\theta) + Y_{\min}(\theta)} \quad (5.17)$$

To characterize the polarization dependence, the characteristic f_8 is stated for an angle of incidence $\theta=30^\circ$, $\theta=0^\circ$.

The f_8 measurement has been performed by using a MgF_2 UV polarized and the value obtained was $1 \cdot 10^{-5}$.

5.2.11. Spatial response characteristic f_9

The spatial response characteristic f_9 describes the influence of non-uniform irradiation of radiometers.

The construction of some radiometer heads can lead to a significant non-uniform spatial responsivity over the acceptance area, including the relative spectral responsivity. With a uniform irradiation on the acceptance area, a non-uniform responsivity is without influence. For the measurement, a radiation source is arranged. A circular aperture with an inner diameter of 1/10, and an outer diameter of double the size of the acceptance area is placed in front of the radiometer head's acceptance area. Stray radiation should be avoided on the radiometer head. The circular aperture has to be placed at five positions in front of the radiometer head's acceptance area as follows:

Position 1: clear opening of the circular aperture centered in the middle.

Positions 2 to 5: center of clear opening of the circular aperture are placed at a point, which is located 2/3 along the radius from the center of the acceptance area. The four positions (2 to 5) are at 90° intervals around the center of the entrance aperture.

The output quantities Y_1 to Y_5 are to be measured at those five positions.

For characterizing the influence of non uniform irradiation on the acceptance area, the characteristic f_9 according to equation (5.18) is used:

$$f_9 = \frac{\sum_{i=1}^5 |Y_i - \bar{Y}|}{5\bar{Y}} \quad (5.18)$$

where according to equation (5.19)

$$\bar{Y} = \frac{1}{5} \cdot \sum_{i=1}^5 Y_i \quad (5.19)$$

where

Y_i - output signal at one of the five positions on the acceptance area of the radiometer head with the input quantity X .

Our radiometers have always small active area ($<1\text{mm}^2$) and spatial response characteristics were in every case negligible.

5.2.12. Range change characteristic f_{11}

The range change characteristic f_{11} describes the influence of range settings of display units or amplifiers.

When changing the range of a radiometer to the adjacent, a systematical deviation may occur. For the measurement of the error arising from a range change, the irradiation on the radiometer head is to be adjusted to produce a reading of 90 % of full scale in the more sensitive range A. The irradiation is then increased by a factor k . When increasing the irradiation, the range is changed to the less sensitive range B.

The error due to range change must be determined for each range. In order to characterize it, the characteristic f_{11} according to equation (5.20) is used.

$$f_{11} = \frac{Y_B}{k \cdot Y_A} - 1 \quad (5.20)$$

Where:

Y_B - reading in the less sensitive range B with the input quantity X_B being k times as large as X_A

Y_A - reading range in the more sensitive range A with the input quantity X_A at about 90 % of full scale

k - factor according to equation (5.10)

X_A - input quantity creating the reading Y_A

Following this procedure a f_{11} value of $3 \cdot 10^{-4}$ has been measured.

5.3. Application in artificial source monitoring

Long exposition to artificial UV radiation cause burns, skin aging, erythema and even melanoma cancer. In the European regulation EN60335-2-27 the toxicity of UV radiation emitting machines for domestic use is discussed and upper-limit exposition effective dose are established. As well as other artificial sources, sun tanning units must be monitored and certified according with the law. There is the necessity to develop a clear

measurement procedure to verify sunbed irradiance in metrological laboratories, and to develop portable instrumentation for the irradiance verification in situ. Senserit® Radiometer was initially developed and patented [80] for sun tanning units monitoring. In this session, the performances of the instrument applied to this task are presented.

As illustrated above, the radiometer spectral response theoretically matched the EAC very closely. Due to the difficulties on thin film deposition, the prototypes curve deviated from the target owing to the fact that the filter transmission was not the nominal one. In order to evaluate prototypes performance, the application to sunbed lamps irradiance measurement was considered. The spectra of 10 different lamps measured by the use of the Bentham double spectral monochromator have been taken into account (some are reported in figure 5.4). To perform these measurements, an integrating sphere (10 mm circular aperture) was used as the entrance optics of the system and placed in different positions inside the sunbeds. The detector was a photomultiplier tube with a bialkali photocathode. Measurements were performed by using the 1800 line/mm grating, at step of 1 nm, with a spectral bandwidth of 1.8 nm. The sunbed irradiance values were obtained by a comparison to a deuterium lamp calibrated at NPL and used as the reference source. The total effective irradiance of all the lamps was derived by using both the EAC and the absolute spectral response of the prototypes. The mean value of all W_{eff}/m^2 values calculated in the two cases was derived, and a correction factor C to be applied to the radiometer output was found according to the following relation:

$$\text{Average}[(W_{\text{eff}} / m^2)_{\text{CIE}}] = C \times \text{Average}[(W_{\text{eff}} / m^2)_{\text{PROTOTYPE}}] \quad (5.21)$$

The W_{eff}/m^2 values related to the spectra of the lamps in figure were calculated by using both the EAC and the absolute spectral response corrected by the C factor. The results are reported in table 5.1 with the percentage difference (error), which was used to represent the error of the prototypes for each single measure. As can be seen in table 5.1 the mismatch of the data derived by using the CIE nominal EAC and those provided by the instrument were on the order of a few percent. Several tests in real sun tanning units were also performed (see cap.4), allowing the determination of the total effective irradiance received by a subject on different body parts.

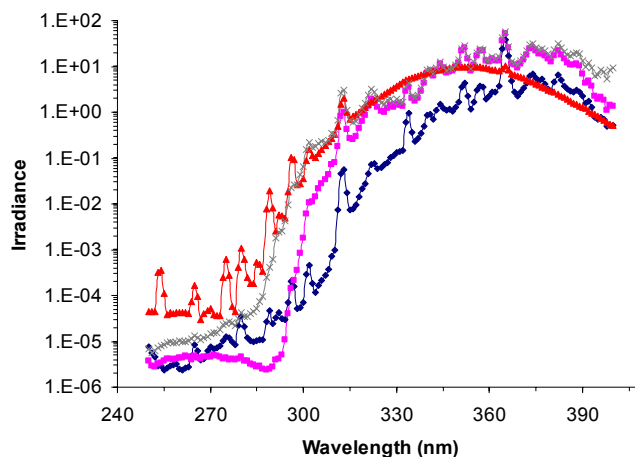


Figure 5.4. Example of Irradiance values of commercial sunbeds.

	Nominal	1st Prototype	2nd Prototype	3rd Prototype
Total Irradiance W/m ²	0.104	0.285	0.136	0.206
	1.175	3.135	1.624	1.830
	0.469	1.507	0.701	1.014
	0.484	1.480	0.722	0.996
	0.369	1.101	0.502	0.739
	0.657	1.904	0.944	1.301
	0.365	1.102	0.521	0.711
	0.228	0.655	0.309	0.524
	1.340	4.326	1.729	2.054
	0.409	1.535	0.535	0.518
Correction Factor C		2.745	1.313	1.986
		2.668	1.382	1.557
		3.217	1.496	2.164
		3.058	1.491	2.058
		2.986	1.361	2.005
		2.896	1.437	1.980
		3.022	1.428	1.950
		2.881	1.357	2.303
		3.228	1.290	1.533
		3.752	1.309	1.266
	Mean Value	3.045	1.386	1.880
Total Irradiance W/m ² With Correction Factor C	0.104	0.094	0.098	0.110
	1.175	1.030	1.171	0.973
	0.469	0.495	0.506	0.539
	0.484	0.486	0.521	0.530
	0.369	0.361	0.362	0.393
	0.657	0.625	0.681	0.692
	0.365	0.362	0.376	0.378
	0.228	0.215	0.223	0.279
	1.340	1.421	1.247	1.092
	0.409	0.504	0.386	0.276
Irradiance Error %		-9.853	-5.319	5.648
		-12.404	-0.329	-17.174
		5.630	7.912	15.079
		0.411	7.570	9.469
		-1.940	-1.804	6.609
		-4.893	3.639	5.302
		-0.766	3.031	3.716
		-5.394	-2.140	22.492
		6.008	-6.943	-18.492
		23.202	-5.618	-32.650

Table 5.1. Effective Irradiance computed with EAC and prototypes response curves.

5.4. Application in extraterrestrial environments

The acquaintance of the level of radiation in terrestrial and extraterrestrial lands is therefore indispensable for the validation of life hypothesis on other planets (example survival of bacteria, fungi etc), in order to plan and prevent activities that consider the presence of man in environments with high UV radiation, for the verification of the damage on constituent materials and structures of satellites, vehicles etc, for the correlation of all the effects listed with the solar cycles and emission.

We have evaluated the possibility to realize some experimental prototypes that can carry out radiometry in the ultraviolet spectral range in various space environments.

This activity is framed in a series of plans already started in this field, for which there are a series of consolidated collaborations, others in starting phase, with scientific (Clinica Dermatologica Università di Padova, Istituto Superiore di Sanità) and industrial (Galileo Avionica, DeltaOhm s.r.l) Italian partner working in the field of the ultraviolet radiation. Prototypes of ultraviolet instrumentation for earth applications with artificial sources have been already realized and patented (Italian patent [ref] –international patent pending).

The prototype instrumentation that can be realized can find an application in various fields and future missions, which comprise:

- ① satellites in terrestrial orbit, for the study and the verification of phenomena associated to solar cycles, space weather and geomagnetic storms: as an example, some phenomena have been verified, such as the degradation of satellites coverings in equatorial orbit due to the solar ultraviolet radiation.
- ② planetary environments: in atmosphere absence elevate levels of radiation must be attended on planetary grounds, as on the Moon and on Mars. The acquaintance of the level of UV solar irradiation in these environments allows for example to formulate hypothesis on the possibility of life and biological evolution of bacteria and elementary species.
- ③ study of the circumterrestrial and lunar environments. In forecasting of the takeover of stable space human colonies it must be planned the exploitation of the external solar radiation for the creation of an environment with "similar-solar" irradiance into the colonies favoring the normal biological processes related with the light. The acquaintance of the level of radiation in the environment is therefore necessary.
- ④ Space vehicles: the acquaintance of UV levels inside the space cabins (example ISS), allows to characterize possible risk zones (for example close to the windows) in which the UV level turns out elevated (as an example that structures in quartz, highly shielding for ionizing radiations, are highly transparent to UV). In addition the acquaintance of UV level inside the space vehicles is useful to verify if the levels of UV radiation are sufficient to prime some biological processes in the astronaut, as an example the vitamin D production, that contributes to fight the phenomenon of osteoporosis.
- ⑤ Astronaut helmet: UV dosimetry at the level of the astronaut helmet allows to verify if the protecting shielding in the case of a " space walk" is sufficient to avoid development of problems at the eyes related to excessive UV exposure

- ② sounding balloons: may be taken into consideration the possibility of mounting some radiometers on sounding balloons for modelize the solar radiation profile with the height

5.4.1. Activity Description

The objective is the study and the realization of some prototypes of radiometer, some dedicates to solar UV observation at various spectral bands, other dedicates to the detection of total effective radiation following several biological action curves.

The first preview the connection of a detector system, an interferential filter pass-band type and a diffuser, the second ones preview the study of particular filters that guarantee that the total spectral response of the instrument is equivalent to a specific biological action curve. It has to be reminded that the action curves attribute a weightening factor to the wavelengths of the incident radiation proportional to the damage that it brings. Some action curves taken into consideration are erythema, fotocheratite, fotoconguntivite, DNA, Bacillus Subtilis etc.

The planned activities can be summarized:

- ② Study of the level of radiation attended in several environments based on the existing literature. This activity is useful in order to plan, related with the applications, the choice of the compounds for the prototypes, in particular the detectors, whose thresholds of detection must vary in relation with the attended signal
- ② Chosen of the useful detectors for the measurements of such levels. In fact it's possible to adopt various systems of detection, with various spectral sensibility and curves, in relation with the purpose of the object. As an example, the prototype already developed has been realized with a SiC photodiode, but other solid state devices [81] and photomultiplier have been analyzed.
- ② Design of the single components (filters, diffusers etc). The response curve of every radiometer depends on the curve of transmission of the filters, that will have opportunely designed. The diffusive response of the system depends on the entrance optic, in particular from its geometric shape and the material that constitutes it.
- ② Design of the electronic chains. For every prototype an oportune amplification electronic will be designed and will be equipped with data logger for the data recording and visualization.
- ② Upgrade of the existing laboratory. The existing laboratory is currently equipped with a solar simulator, a Xenon lamp, a UV spectrograph (single monochromator) and a spectrophotometer for the measurements of filters transmission. In order to realize this plan in efficient and continuous way is necessary to purchase a double monochromator system and a calibrated detector useful for the spectral characterization of the detectors and the prototypes, for such activities we are collaborating from external partners so far. Moreover the purchase of some accessory to completion of the already existing instrumentation is necessary.

- ② Realization of the single components. The detectors will be purchased among those commercially available. Filters and diffusers will be realized according custom specifics.
- ② Test of the single components. Measurements of spectral sensibility and response will be carried out on the detectors. Measurements of transmission and diffusive properties on the diffusers, measurements of transmission on the filters
- ② Prototypes assemblage. A mechanical system for the assembly of the components will be designed and realized, the reading electronics will be connected with the components.
- ② Prototypes characterization. The relative spectral response curve of the prototypes will be measured. Moreover these will be calibrated using reference sources.
- ② Test of prototypes in operating conditions. Some experiments will be chosen for the validation of the prototypes (with artificial sources or taking advantage of the solar emission)
- ② Study of the impact of several environments on the developed instruments and on their lifetime (for example bombarding particle to the single components, the detectors, the assembled instruments). These tests will be carried out in a particles accelerator like the one presents at INFN LNL Legnaro.
- ② Study of the effects of UV irradiation with solar simulator (present in our laboratories) on the materials and components (for example time stability of the response)
- ② Thermal cycles on the components for the validation of the stability

5.5. Astronautical applications

As remarked above UV radiation is related with several photobiological reactions. The effects of solar UV radiation can interest individual organisms as well as whole ecosystems. The dangerous effects of excessive UV irradiation could be serious, but, however, UV radiation has also beneficial effects. One of these is the cutaneous synthesis of vitamin D. The fat-soluble vitamin D's most important role is maintaining blood levels of calcium, which is accomplished by increasing absorption of calcium from food and reducing urinary calcium loss. In fact, in adults, vitamin D deficiency may result in a softening of the bones known as osteomalacia. This condition is treated with vitamin D, sometimes in combination with calcium supplements. In people of any age, vitamin D deficiency causes abnormal bone formation. It occurs more commonly following winter, owing to restricted sunlight exposure during that season. Living in an area with a lot of atmospheric pollution, which can block the sun's ultraviolet rays, also appears to increase the risk of vitamin D deficiency.

The well known strong dependence of vitamin D synthesis from UVB exposure leads to consider the possible problems subsequent from a permanence in space environments such as of a space station or a futuristic lunar permanent station. In fact natural UVB from sunlight is normally absent in the closed environment of a space station like ISS. Therefore it's necessary to investigate the UV radiation climate inside the station

resulting from different lamps as well as from occasional solar irradiation behind a UV-transparent quartz window.

This kind of measurements could be performed using an UV dosimeter such as a Biofilm or a radiometer with a specific response curve.

Such instrumentations were just applied on Earth in several studies in which monitoring of the UV irradiation were performed in different geographical areas.

5.5.1. Bone Loss in Space Flight

Astronauts can be exploring the surface of Mars as early as 10 years from now. During the 6 to 12 month journey the astronauts can experience an environment that will produce important modifications in the body. One of the most important problem could be the bone loss that would put them at serious risk of fracture upon return to a gravitational environment, either on Earth or on Mars. Several parameters have been found to be related with bone loss and one of these is connected with the vitamin D sub-production. The studies on this problem had given some important results: during space flights lasting longer than one month, astronauts undergo significant losses of bone mass and bone mineral density in the weight bearing areas of the skeleton, particularly the spine and lower limbs, as a result of the unloading produced by weightlessness in the microgravity .

Several studies have been published on this subject [82-87]. The findings of these spaceflight and immobilization studies, conducted over the past 35 years, may be summarized as follows:

- Significant bone loss occurs in humans and animals exposed to weightlessness during spaceflight
- Urine and fecal calcium excretion is increased resulting in a negative calcium balance
- Calcium resorption from bone is increased and absorption from gut is decreased
- Bone mineral density decreases
- Critical weight-bearing areas lose density most rapidly and the rate of loss is approximately 1-2% per month
- Non-weight-bearing areas are affected in the long term
- Osteoblast proliferation and activity are reduced while osteoclast activity either remains the same or increases slightly
- Bone growth is slowed
- Fracture repair is impaired
- Bone strength is reduced

Several conclusions may be drawn regarding the significance of these skeletal changes in terms of human spaceflight.

Astronauts and cosmonauts spending a significant period in weightlessness (> 1 month) will experience a loss of bone strength and a subsequent increase in fracture risk during:

- ② Activities on Earth (walking / running, falls)
- ② Intravehicular / extravehicular activity (IVA / EVA) on Mars or in weightlessness

A fracture occurring on Mars (3/8 G) has serious consequences to the individual and crew due to:

- ② remoteness (limited medical resources)
- ② possible inhibition of fracture repair and immune responses associated with weightlessness
- ② loss of functionality in terms of the crew member's skills and duties (increased workload on remaining crew members)

5.5.2. The role of Vitamin D

Vitamin D and its active metabolites have many different functions in the human body. The most important one is the regulation of mineral homeostasis in target tissues intestine, bone and kidney, and especially the control of the calcium and phosphorus serum levels. Changes in calcium metabolism have a strong influence on bone metabolism which is changed in microgravity during spaceflights. A significant loss of bone mass can be observed even after short-term space missions (Oganov et *al.*, 1992 [88]). The influence of vitamin D and of possible changes in its level on bone metabolism during prolonged spaceflights are largely unknown.

During the German-Russian MIR'97 mission the UV radiation climate inside the Russian space station Mir was investigated in the UVE Experiment to determine whether UV radiation onboard Mir is sufficient for a cutaneous synthesis of vitamin D. The sources of UV radiation onboard may be the sun shining through a UV-transparent quartz window or artificial UV lamps. The biological UV dosimetry with the DLR-biofilm was done at different locations in the space station and performed as personal UV dosimetry (Rettberg et al., 1998 [89]) for one of the cosmonauts. In addition the serum levels of 25(OH)D of the same cosmonaut were determined before, during, and after the mission and compared to the controlled dietary intake of vitamin D. The conclusions of the study give some preliminary results (the measurements on human body were performed on a single cosmonaut):

- ② Inflight serum levels of vitamin D and its metabolites are not the cause of changes in calcium and bone metabolism observed in microgravity.
- ② Vitamin D supplementation is not necessary in short-term space missions.
- ② For long-term missions a sufficient vitamin D level should be maintained either by controlled nutrient intake of vitamin D and/or by the regular exposure to special UV lamps like those in sun-beds.

5.5.3. Proposed experimental study and procedure

An extension of the several Earth studies is possible applying similar instrumentations and methods. Using biologically weighting UV dosimeters will be possible to determine

the biological effectiveness of the UV radiation present at different locations in a space environment such as the International Space Station. Such dosimeters could be applied on the human body (suit) to determine the personal UV dose of an individual cosmonaut (for different biological effects, such as Erythema, Vitamin D synthesis, Eye Cataract, DNA Damage, etc).

Focusing the experiment on the Vitamin D production and interaction with bone loss, this study could show if the UV radiation climate inside the International Space Station is sufficient for an adequate supply of vitamin D and if particular conditions (such as exposure to UV Lamp) could interact with bone formation. The collected data could be correlated with cosmonaut's serum real time analysis with possible distinction of different individual irradiation.

Measuring the natural solar UV radiation reaching the inside of the ISS through the windows will be possible to evaluate the dangerousness of such radiation and eventually conjecture a possible application of filters that can modify the space solar spectrum to a Earth like shape.

A design for a UV "sun-bed" cabin will be a possible result of the study.

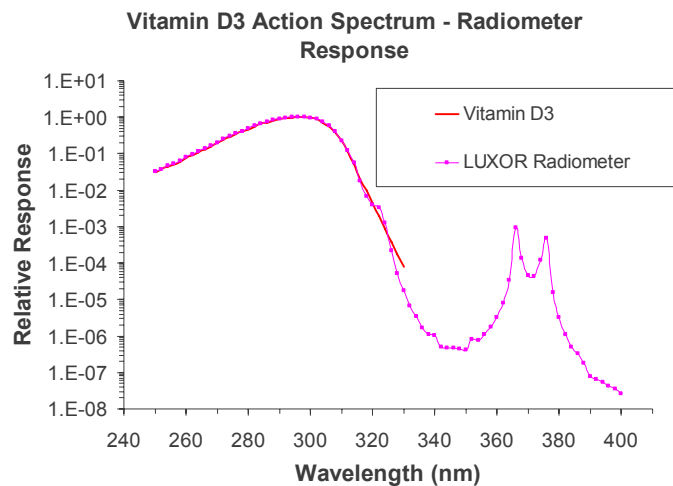


Figure 5.5. Vitamin D synthesis like radiometer

A compact and integrated radiometer could be applied at the cosmonaut body (suit) for several days of flight to monitor the received dose. Several other radiometers could be applied at different locations in the ISS (some of these behind the quartz windows) for some days of flight. An integrated electronic system could store the measured data at fixed time during the flight (for example during the daylight time of the flight).

In addition, some operations have to be performed to determine the serum level of vitamin D of the cosmonaut. Available data indicate that the principal function of Vitamin D, i.e. optimizing intestinal calcium absorption, is expressed by serum 25-hydroxyvitamin D 25(OH)D concentration (R.P. Heaney 2005 [90]).

For determination of 25-hydroxyvitamin D metabolites (25(OH)D₂ and 25(OH)D₃), serum samples have to be prepared by adding one volume of acetonitrile, followed by an

extraction and a purification step with C₁₈ cartridges (Reinhardt et al., 1984 [91]). The 25(OH)D₂ and 25(OH)D₃ metabolites have then to be separated by high performance liquid chromatography using a silica column with hexan/isopropanol (98/2) as solvent. All samples have to be measured in duplicate during the same assay sequence. Standard solutions of 25(OH)D₂ and 25(OH)D₃ have to be handled in the same way. The vitamin D metabolites will be quantified using a tritium labeled protein binding assay with rat serum as receptor (Hollis, 1984 [92]).

Serum samples of the cosmonaut could be analyzed during a preflight period. Other samples of cosmonaut's serum could be obtained and analyzed during the mission.

After reentry, several other controls have to be done for a fixed period to evaluate the variation of the serum level of vitamin D.

To evaluate the correlation between the Vitamin D and the bone loss, serum analysis has to be performed in order to evaluate the phenomenon of bone formation. This could be evaluated by various serum assays (A. Caillot-Augussea 1998 [93]). Osteocalcin (or BGP for bone gla protein) is a noncollagenous protein synthesized by mature osteoblasts. Low concentrations are found in platelets and megakaryocytes. One fraction of BGP (about 15%) is released into the systemic circulation in either intact or fragmented forms that can be measured separately. Bone alkaline phosphatase (BAP), a tetrameric glycoprotein, is an enzyme involved in bone mineralization. It is released into the circulation as a dimer after cleavage by a phospholipase. The carboxyl-terminal propeptide of human type 1 procollagen (PICP) splits off from the procollagen in a 1:1 molar ratio and reflects osteoblastic differentiation.

Bone resorption can be evaluated by measuring the urinary excretion of free and total pyridinoline (Pyr) cross-links and type I collagen C-telopeptide (CTX) (Crosslaps(TM)), which contains Pyr cross-links. Pyr and deoxypyridinoline (D-Pyr) cross-links are trivalent molecules that stabilize the mature collagen molecule. These molecules are degraded by the lysosomal enzymes of osteoclasts during bone resorption. After circulating in the blood, they are excreted in urine in a free form or bound to peptidic fragments (60%). CTX is an eight-amino-acid small peptide of known sequence. It is released when bone collagen is degraded and then excreted in the urine.

Apart from mechanical forces, bone remodeling is regulated by systemic hormones, including parathyroid hormone (PTH) and 1,25-dihydroxycholecalciferol (calcitriol). To date, only slight and transient changes in these hormones have been observed in humans after spaceflight. Other factors are therefore thought to be involved in the changes observed in bone remodeling: variations in stress-related hormones [cortisol, somatotropin (GH), somatomedin (IGF-1), or prolactin] or a direct effect of weightlessness on bone cells.

6. Conclusions

In this work several activities related with the UV radiation monitoring and dosimetry have been presented. During my Ph.D. I've hardly worked on all the different aspects of radiometric instruments development. Starting from the design of the very first instrument concept I've analyzed the various components such as the diffuser element, the interferential filter and the detector. Different UV transparent materials have been tested for diffusive properties. From my measurements it's possible to conclude that few materials have good Lambertian behavior. Long and detailed analyses have been carried on innovative designed filters. Aspects as thin film grown and stability have been seriously taken into consideration giving very interesting results. Both $\text{MgF}_2/\text{ZrO}_2$ and $\text{SiO}_2/\text{ZrO}_2$ multilayer structures have shown to be very stable in time and under severe conditions. Several photodiode UV detectors have been fully characterized and a new method for absolute spectral response measurement has been developed.

Finally, different prototypes have been realized and applied in scientific applications demonstrating the good performances of the radiometers.

To conclude:

- Several prototype instrumentations have been developed. Sensors with erythema like response has been improved and Patented;
- Very innovative optical filters have been designed and tested;
- Several brand new radiometers with different response curves have been developed;
- The new instrumentation has been applied in radiometric measurements of various type of sources (Natural and Artificial);
- The techniques of deposition of the materials for the filters realization have been improved and different methods for optical constants derivation have been analyzed;
- Within an interfaculty project a new laboratory (@ Luxor – DEI) for UV/Vis/NIR spectrophotometric measurements has been implemented;
- Photo-protection and photo-stability tests on different materials have been performed in the new laboratory;
- Interfaculty collaborations with Dermatologic Clinic and Department of Biology for various application of the developed technologies have been established.

References

1. Hausser, KW, Vahle, W: Die Abhängigkeit des Lichterythems und der Pigmentbildung von der Schwingungszahl (Wellenlänge) der erregenden Strahlung. *Strahlentherapie* 1921 13: 41,
2. Coblenz, W.W. (1932). *The Copenhagen meeting of the Second International Congress on Light*. *Science* 76, 412-415.
3. De Fabo EC & Noonan FP (1983) Mechanism of immune suppression by ultraviolet irradiation in vivo. *J Exp Med*, 157: 84-98.
4. Gibbs NK (1993) Is ultraviolet immunosuppression initiated by photosensitization of urocanic acid. In: de Grujil FR ed. *The dark side of sunlight*. Utrecht, The Netherlands, Utrecht University.
5. Sutherland JC & Griffin K (1981) Absorption spectrum of DNA for wavelengths greater than 300nm. *Radiat Res*, 86: 399-410.
6. Menzies, SW, Greenoak, GE, Reeve, VE, & Gallagher, CH (1991) Ultraviolet radiation-induced murine tumors produced in the absence of ultraviolet radiation-induced systemic tumor immunosuppression. *Cancer Res*, 51: 2773-2779.
7. Setlow RB, Woodhead AD, & Grist E (1989) Animal model for ultraviolet radiation-induced melanoma: platyfish-swordtail hybrid. *Proc Natl Acad Sci (USA)*, 86: 8922-8926.
8. Rapp LM & Smith SC (1992) Morphological comparisons between rhodopsin-mediated and short wavelength classes of retinal light damage. *Invest Ophthalmol Vis Sci*, 33: 3367-3377.
9. Kataoka H & Fujiwara Y (1991) UV damage specific protein in xeroderma pigmentosum complementation group E. *Biochem Biophys Res Commun*, 175: 1139-1143.
10. Stephenson TJ, Royds J, Silcocks PB, & Bleehen SS (1992) Mutant p53 oncogene expression in keratoacanthoma and squamous cell carcinoma. *Br J Dermatol*, 127: 566-570.
11. G. B. Ivry, C. A. Ogle, and E. K. Shim, "Role of sun exposure in melanoma," *Dermatol Surg*. **32**, 481–492 (2006).
12. P. Autier, "Perspective in melanoma prevention: the case of sunbeds," *Eur. J. Cancer* **40**, 2367–2376 (2004).
13. Vermeer M, Schmieder GJ, Yoshikawa T, Van den Berg J-W, Metzman MS, Taylor JR, & Streilein JW (1991) Effects of ultraviolet B light on cutaneous immune responses of humans with deeply pigmented skin. *J Invest Dermatol*, 97: 729-734.
14. Jose JG & Pitts DG (1985) Wavelength dependency of cataracts in albino mice following chronic exposure. *Exp Eye Res*, 41: 545-563.
15. Bochow TW, West SK, Azar A, Munoz B, Sommer A, & Taylor HR (1989) Ultraviolet light exposure and risk of posterior subcapsular cataracts. *Arch Ophthalmol*, 107: 369-372.
16. Bidigare RR (1989) Potential effects of UVB radiation on marine organisms of the Southern Ocean: distributions of phytoplankton and krill during Austral spring. *Photochem Photobiol*, 50: 469-477.
17. Boyd, R.W., *Radiometry and the Detection of Optical Radiation*, New York, John Wiley & Sons, 1983, ch. 6, pp. 95-97.
18. CIE (1987) *International lighting vocabulary published jointly by the International Electrotechnical Commission (IEC) and the International Commission on Illumination (CIE)*. Geneva, International Electrotechnical Commission (ISBN 2-8273-0006-0).
19. Parrish JA, Jaenicke KF, & Anderson RR (1982) Erythema and melanogenesis action spectra of normal human skin. *Photochem Photobiol*, 36: 187-191.
20. McKinlay AF & Diffey BL (1987) A reference action spectrum for ultra-violet induced erythema in human skin. *CIE J*, 6: 17-22

21. M.J. Peak, J.G. Peak and B.A. Carnes, "Introduction of direct and indirect single-strand breaks in human cell DNA by far- and near-ultraviolet radiations: Action spectrum and mechanisms." *Photochem. Photobiol.*, 45, pp.381-387, 1987
22. M.M. Caldwell, L.B. Camp, C.W. Warner and S.D. Flint, "Action spectra and their key role in assessing biological consequences of solar UV-B radiation", In *Stratospheric Ozone Reduction, Solar Ultraviolet Radiation and Plant Life*, Worrest Caldwell (eds.), pp.87-111, Springer, Heidelberg, 1986
23. Mitchell, B.G., "Action Spectra for ultraviolet photoinhibition of Antarctic phytoplankton and a model of spectral diffuse attenuation coefficients", In *Response of Marine Phytoplankton to Natural Variations in UV-B Flux*, (Edited by G. Mitchell, I. Sobolev and O. Holm-Hansen), *Proc. of Workshop*, Scripps Institution of Oceanography, La Jolla, CA, April 5, 1990
24. Quintern LE, Horneck G, Eischweiler V, & B ker H (1992) A biofilm used as ultraviolet dosimeter. *Photochem Photobiol*, 55: 389-395.
25. IRPA/INIRC (1991b) International Radiation Protection Association/International Non-Ionizing Radiation Committee. In: Duch ne AS, Lakey JRA, & Repacholi MH ed. *IRPA guidelines on protection against non-ionizing radiation.*, New York, McGraw-Hill.
26. European regulation EN 60335-2-27, 1997-03; IEC 60335-2-27,1995-05.2, "Specification for safety of household and similar electrical appliances. Particular requirements. Skin exposure to ultraviolet and infrared radiation (International Electrotechnical Commission, 1995).
27. MacLaughlin JA, Anderson RR, Holick MF. Spectral character of sunlight modulates the photosynthesis of previtamin D3 and its photoisomers in human skin. *Science*. 1982; 1001-1003
28. Cogan D.G. and Kinsley V.E.: Action Spectrum of keratitis produced by ultraviolet radiation, *Arch.Ophth*. 36: 670-677, 1946
29. Flint, S. D. and M. M. Caldwell (2003) A biological spectral weighting function for ozone depletion research with higher plants. *Physiologia Plantarum* 117, 137-144.
30. Rundel RD (1983) Action spectra and estimation of biologically effective UV radiation. *Physiol Plant* 58: 360-366
31. Caldwell MM, Camp LB, Warner CW, Flint SD (1986) Action spectra and their key role in assessing biological consequences of solar UV-B radiation change. In: Worrest RC, Caldwell MM (eds) *Stratospheric Ozone Reduction, Solar Ultraviolet Radiation and Plant Life*. Springer, Berlin, pp 87-111, ISBN 3-540-13875-7
32. Clancy, J. L.; Bukhari, Z.; Hargy, T. M.; Bolton, J. R.; Dussert, B. W.; Marshall, M. M. Using UV to inactivate *Cryptosporidium*. *J. Am. Water Works. Assoc.* 2000, 92 (9), 97-104
33. Hadas Mamane-Gravetz, Karl G. Linden, Alexander Cabaj, and Regina Sommer, "Spectral Sensitivity of *Bacillus subtilis* Spores and MS2 Coliphage for Validation Testing of Ultraviolet Reactors for Water Disinfection ", *Environ. Sci. Technol.*, 39 (20), 7845 -7852, 2005
34. G. Seckmeyer and G. Bernhard, "Cosine error correction of spectral UV irradiances," in *Atmospheric Radiation*, K. H. Stamnes, ed., *Proc. SPIE* **2049**, 140–151 ~1993!.
35. U. Feister, R. Grewe, and K. Gericke, "A method for correction of cosine errors in measurements of spectral UV irradiance," *Solar Energy* **60**, 313–332 ~1997!.
36. F. Bais, "Spectrometers: operational errors and uncertainties," in *Solar Ultraviolet Radiation Modeling, Measurements and Effects*, C. S. Zerefos and A. F. Bais, eds., Vol. 52 of NATO ASI Series I, *Global Environmental Change* ~Springer-Verlag, Berlin, 1997!, pp. 163–173.
37. M. Blumthaler and A. F. Bais, "Cosine corrections of global sky measurements," in *The Nordic Intercomparison of Ultraviolet and Total Ozone Instruments at Izana October 1996. Final Report*, B. Kjeldstad, B. Johnsen, and T. Koskela, eds. ~Finnish Meteorological Institute, Helsinki, 1997!, pp. 161–172.

38. Bias, A.F., Kazadzis, S., Balis, D., Zerefos, C.S. and Blumthaler, M. "Correcting global ultraviolet spectra recorded by a Brewer spectroradiometer for its angular response error", *Applied Optics*, 37, 6339-6344 (1998)
39. **D.Garoli**, P.Nicolosi, F.Frassetto, F.Rigato, V.Rigato, S.Nannarone, A.Giglia, "Reflectance measurements and optical constants in the EUV-VUV region for SiC with different C/Si ratio", *Applied Optics*, Vol. 45, Issue 22, pp.5642-5650 (August 2006)
40. **D. Garoli**, G. Monaco, F. Frassetto, M.G. Pelizzo, P. Nicolosi, L. Armelao, V. Matterello, V. Rigato, "Thin film and multilayer coating development for the extreme ultraviolet spectral region", *Radiation Physics and Chemistry*, Volume 75, Issue 11, November 2006, Pages 1966-1971
41. J. A. Woollam, "Ellipsometry, Variable Angle Spectroscopic," in *Wiley Encyclopedia of Electrical and Electronics Engineering*, New York: Wiley, (2000) 109-117.
42. H. G. Tompkins and W. A. McGahan, *Spectroscopic Ellipsometry and Reflectometry*, New York: Wiley, 1999.
43. H. G. Tompkins and E. A. Irene (eds.), *Handbook of Ellipsometry*, New York: William Andrew, 2005.
44. C. M. Herzinger, B. Johs, W. A. McGahan, J. A. Woollam, and W. Paulson, "Ellipsometric Determination of Optical Constants for Silicon and Thermally Grown Silicon Dioxide via a Multi-sample, Multi-wavelength, Multi-angle Investigation", *J. Appl. Phys.*, **83** (1998) 3323-3336.
45. F. Wooten, *Optical Properties of Solids* (Academic Press, NY, 1972)
46. 46 P. I. Rovira, A. S. Ferlauto, J. Koh, C. R. Wronsky, and R. W. Collins, *J. of Non-Cryst. Solids*, **266-269**, 279 (2000).
47. 47 J.C. Manificier, J. Gassiot, and J.P. Fillard, *J. Phys. E* **9**, 1002 (1976).
48. 48 R. Swanepoel, *J. Phys. E* **16**, 1214 (1983).
49. 49 R. Swanepoel, *J. Phys. E* **17**, 896 (1984)
50. 50 I. Chambouleyron, J.M. Martínez, A.C. Moretti, and M. Mulato, *Appl. Optics* **36**, 8238 (1997).
51. E.G. Birgin, I. Chambouleyron, and J.M. Martínez, *J. Comput. Physics* **151**, 862 (1999). [E.G. Birgin would happily provide copies of the software to the interested public. See address in authors' section].
52. M. Raydan, *SIAM J. Optim* **7**, 26 (1997).
53. Maria-Guglielmina Pelizzo, **Denis Garoli**, Piergiorgio Nicolosi, "Realization of a radiometric head for measurements of ultraviolet total erythemal effective irradiance", *Applied Optics*, Vol. 46, Issue 22, pp.4977-4984 (August 2007)
54. CIE (International Commission on Illumination) Research Note 1987, "A reference action spectrum for the ultraviolet induced erythema in human skin, CIE J.6, 17-22.
55. D. L. Richardsa, R. E. Daviesb and J. L. Boonea, "A selective Pt-CdS photodiode to monitor erythemal flux", *Journal of Photochemistry and Photobiology B: Biology*, Vol. **47**, Issue 1, pg. 22-30, 1998.
56. C. Green, B. L. Diffey, and J. L. M. Hawk, "Ultraviolet radiation in the treatment of skin disease," *Phys. Med. Biol.* **37**, 1-20 (1992)
57. WMO (1993) World Meteorological Organization Report of the second meeting of the ozone research managers of the parties to the Vienna Convention for the protection of the ozone layer. Geneva 10-12 March.
58. Brühl C & Crutzen PJ (1989) On the disproportionate role of tropospheric ozone as a filter against solar UV radiation. *Geophys Res Lett*, 16: 703-706.
59. UNEP-WMO (1989) Scientific assessment of stratospheric ozone: 1989 WMO Global ozone research and monitoring project, United Nations Environment Programme, World Meteorological Organization, Geneva (Report No 29).
60. NSF (1993) National Science Foundation, Div Polar Programs, Report to P Penhale (NSF) & CR Booth (Biospherical Instruments), Antarctic Support Assoc US.
61. Driscoll CMH (1992) Solar UV trends and distributions. *Natl Radiat Prot Board Bull*, 137: 7-13.

62. Scotto J, Cotton G, Urbach F, Berger D, & Fears T (1988) Biologically effective ultraviolet radiation: surface measurements in the US 1974-1985. *Science*, 235: 762-764.
63. Munkata N (1993) Biological effective dose of solar ultraviolet radiation estimated by spore dosimetry in Tokyo since 1989. *Photochem Photobiol*, 58(3): 386-392.
64. Trevisan, S. Piovesan, A. Leonardi, M. Bertocco, P. Nicolosi, M. G. Pelizzo, and A. Angelini, "Unusual high exposure to ultraviolet-C radiation," *Photochem. Photobiol.* **82**, 1077-1079 (2006).
65. *Spatial Distribution of Daylight—CIE Standard Overcast Sky and Clear Sky*, CIE Standard S 003_E-1996 (Commission Internationale de l'Eclairage, Vienna, 1996), p. 3.
66. Sliney DH & Wolbarsht ML (1980) *Safety with lasers and other optical sources -A comprehensive handbook*. New York, London, Plenum Press.
67. Pincus MW, Rollings PK, Craft AB, & Green A (1991) Sunscreen use on Queensland beaches, Australia. *J Dermatol*, 32: 21.
68. Hill D, White V, Marks R, Theobald T, Borland R, & Roy C (1992) Melanoma prevention: behavioural and nonbehavioural factors in sunburn among an Australian urban population. *Prev Med*, 21: 654-669.
69. Gies HP, Roy CR, & Elliott G (1992) Ultraviolet radiation protection factors for personal protection in both occupational and recreational situations. *Radiat Prot Aust*, 10(3): 59-66.
70. Roy CR & Gies HP (1993) Personal protection against solar ultraviolet radiation. In: *Proceedings of the International Symposium on UV, Munich 4-6 May 1993*. German Ministry of the Environment, Munich, Germany, pp 47-52.
71. CIE (1991) Sunscreen testing (UVB). Vienna, Commission on Illumination (CIE Technical report - Publication No. CIE 90).
72. Welsh D & Diffey B (1981) Protection against solar actinic radiation afforded by common clothing fabrics. *Clinical and Experimental Dermatology* 6: 577-582.
73. IRPA/INIRC (1991b) International Radiation Protection Association/International Non-ionizing Radiation Committee. In: Duchêne AS, Lakey JRA, & Repacholi MH ed. *IRPA guidelines on protection against non-ionizing radiation.*, New York, McGraw-Hill.
74. Gies HP, Roy CR, & Elliot G (1990) A proposed UVR protection factor for sunglasses. *Clin Exp Optom*, 73: 183-189.
75. B.L. Diffey, "Sunscreens and melanoma: the future looks bright", *British Journal of Dermatology* 153, pp378-381, 2005
76. Ullrich SE, Kripke ML, Ananthaswamy H. N. "Mechanisms underlying UV-induced immune suppression: implications for sunscreen design", *Experimental Dermatology* 11 (s1), 13-16, 2002.
77. Nghiem DX, Kazimi N, Clydesdale G, Ananthaswamy HN, Kripke ML, and Ullrich SE, "Ultraviolet A Radiation Suppresses an Established Immune Response: Implications for Sunscreen Design", *Journal of Investigative Dermatology* 117, pp. 1193-1199, 2001
78. UVNET WG1: Guidance for UV power meter classification for particular applications Thematic Network for Ultraviolet Measurements - EU Contract No SMT4-CT97-7510 (DG 12 - EGAA), First Annual Report March 1999
79. M. G. Pelizzo, P. Ceccherini, D. Garoli, P. Masut, and P. Nicolosi, "Taratura della sensibilità spettrale e caratterizzazione di fotodiodi per le regioni spettrali dell'UVA, UVB e UVC," presented at *Metrologia & Qualità*, 23-24 February 2005, Torino, Italy.
80. M. G. Pelizzo, P. Nicolosi, P. Ceccherini and D. Garoli, Italian patent, TO2005A000249, 14 April 2005; International Application PCT_IB2006_000848, 11 April 2006.
81. M. G. Pelizzo, P. Ceccherini, D. Garoli, P. Masut, and P. Nicolosi, "Absolute spectral response measurements of different photodiodes useful for applications in the UV spectral region," *Nonimaging Optics and Efficient Illumination Systems*, R. Winston and R. J. Koschel, eds., *Proc. SPIE* **5529**, 285-293.

82. Asling, C.W., *Histological studies on tibial bone of rats in the 1975 Cosmos 782 flight, in Final reports of U.S experiments flown on the Soviet satellite Cosmos 782, S.N. Rosenzweig and K.A. Souza, Editors. 1978, NASA TM-78525. p. 276-307.*
83. Birykov, N. and Krasnykh, I.G., [Changes in optical density of bone tissue and calcium metabolism in the cosmonauts]. *Kosm Biol Med*, 1970. 4: p. 42-45.
84. Globus, R.K., Bikle, D.D., and Morey-Holton, E., *Effects of simulated weightlessness on bone mineral metabolism. Endocrinology*, 1984. 114(6): p. 2264-2270.
85. Grigoriev, A.I., Bugrov, S.A., Bogomolov, V.V., Egorov, A.D., Kozlovskaya, I.B., Pestov I.D., Polyakov, V.V., Tarasov, I.K., *Medical results of the Mir year-long mission. Physiologist*, 1991. 34(Suppl): p. S44-S48.
86. Holick, M.F., *Perspective on the impact of weightlessness on calcium and bone metabolism. Bone*, 1998. 22(5 Suppl): p. 105S-111S.
87. Hughes-Fulford, M., *Altered cell function in microgravity. Exp Gerontol*, 1991. 26(2-3): p. 247-256.
88. Oganov, V.S., Grigor'ev, A.I., Voronin, L.I., Rakhmanov, A.S., Bakulin, A.V., Schneider, V.S. and LeBlanc, A.D., [Bone mineral density in cosmonauts after flights lasting 4.5-6 months on the Mir orbital station]. *Aviakosm Ekolog Med*, 1992. 26(5-6): p. 20-24.
89. P.Rettberg, G.Norneck, A.Zittermann, M.Heer, *Biological dosimetry to determine the UV radiation climate inside the MIR station and its role in Vitamin-D biosynthesis, Adv. Space Res. Vol.22. No.12 (1998), pp.1643-1652*
90. Robert P.Heaney, *The Vitamin D requirement in health and disease, The Journal of Steroid Biochemistry & Molecular Biology (2005)*
91. Anne Caillot-Augusseau¹, Marie-Hélène Lafage-Prousta, Claude Soler¹, Josiane Pernod², Francis Dubois¹, and Christian Alexandria, *Bone formation and resorption biological markers in cosmonauts during and after a 180-day space flight (Euromir 95), Clinical Chemistry 44: 578-585, 1998*
92. Hollis B. W., *Comparison of equilibrium and disequilibrium assay conditions for ergocalciferol, cholecalciferol and their major metabolites, Steroid B&hem. 21, 8 1-86 (1984)*
93. Reinhardt, T. A., R. L. Horst, J. W. Orf , B. W. Hollis, *A microassay for 1,25-dihydroxyvitamin D not requiring high performance liquid chromatography: application to clinical studies, J. Clin. Endocrinol.Metab. 58, 91-98 (1984)*

Attached

STRUTTURA DEL WORK-BREAKDOWN (WBS)

Livello			Descrizione attività (titolo WP)	Ore	I anno					II anno				III anno			
1	0	0	Radiazione UV: principi teorici e tecnologie per la misura	1000	50	150	150	150	150	150	100	100	50	50	50		
	1	0	Studio aspetti teorici radiazione UV ed interazione radiazioni - materia	250	25	25	25	25	25	25	25	25	25	25	25		
		1	Interazione radiazione UV - uomo							25	25	25	25	25			
	2	0	Sensori per la radiazione UV	150		50	25	25	25		25						
	3	0	Tecnologie ottiche per l'ultravioletto	600	25	75	100	100	100	75	50	25	25	25			
		1	Progettazione e sviluppo di ottiche Multistrato	485	25	50	80	80	50	75	50	25	25	25			
		2	Design ed analisi di sistemi ottici	115		25	20	20	50								
2	0	0	Attività di laboratorio: caratterizzazioni e misure	1200	150	150	150	150	150	150	100	100	50	50	50		
	1	0	Caratterizzazione sorgenti UV naturali ed artificiali	600	75	75	75	75	75	75	50	50	25	25			
		1	Studio e misura irradiazione solare naturale in diverse località										5	5			
		2	Simulazione in laboratorio della radiazione solare – Strumenti e misure										20	20			
	2	0	Misure di caratterizzazione su ottiche multistrato	600	75	75	75	75	75	75	25	25	25	25	25		
		1	Tecniche spettrofotometriche per la caratterizzazione di materiali per l'UV								25	25	25	25	25		
	3	0	Studio e caratterizzazione sostanze UV assorbenti								25	25	25	25	25		
		1	Sviluppo di tecniche di misura per la caratterizzazione di schermi solari								25	25	25	25	25		
3	0	0	Realizzazione e applicazione strumenti	850	80					50	80	120	150	150	170	50	
	1	0	Studio possibili applicabilità degli strumenti	100	10					5	10	10	25	25	35		
	2	0	Messa a punto prototipi e strumenti finali	650	70					40	60	100	100	100	100	25	
	3	0	Valutazione di possibili estensioni	100						5	10	10	25	25	35	25	
4	0	0	Scrittura Tesi e rapporti	700	20	10	30	40	50	30	35	35	75	50	75	250	
	1	0	Programma di dottorato	50	20				15				15				
		1	I anno – preparazione	20	20												
		2	II anno - revisione	15					15								
		3	III anno - revisione	15									15				
	2	0	Rapporti e articoli	150		20	40	40	10	10	10	10	10				
	3	0	Tesi di dottorato	500					15	20	25	25	40	50	75	250	




DESCRIZIONE DEL WORK-BREAKDOWN

WP	Descrizione tecnica
100	Verrà approfondita a livello teorico e progettuale la conoscenza sulle tematiche legate alla radiazione UV: aspetti fisici, tecniche di misura, tecnologie ottiche e di rilevazione e principi di progettazione delle tecnologie stesse
200	Attività di laboratorio che comprenderanno misure per la caratterizzazione di sorgenti e di rivelatori, ma anche misure su ottiche per questa regione spettrale
300	La parte del lavoro di realizzazione ed applicazione degli strumenti sviluppati verterà sulla messa a punto dei progetti ideati e sulla valutazione delle possibili applicazioni per misure in ambito ambientale e non.

GANNT BAR-CHART (B.-C) DEL PROGRAMMA

Livello	Descrizione attività (titolo WP) ed eventi	I anno	II anno	III anno
Evento	Presentazione per l'approvazione	▼		
1 0 0	Radiazione UV: principi teorici e tecnologie per la misura			
1 0	Studio aspetti teorici radiazione UV ed interazione radiazioni – materia			
1	Interazione radiazione UV – uomo			
2 0	Sensori per la radiazione UV			
3 0	Tecnologie ottiche per l'ultravioletto			
1	Progettazione e sviluppo di ottiche Multistrato			
2	Design ed analisi di sistemi ottici			
Evento	Accertamento formazione generale e Ammissione al II anno		▼	
Evento	I accertamento della formazione spec.		▼	
2 0 0	Attività di laboratorio: caratterizzazioni e misure			
1 0	Caratterizzazione sorgenti UV naturali ed artificiali			
1	Studio e misura irradiazione solare naturale in diverse località			
2	Simulazione in laboratorio della radiazione solare – Strumenti e misure			
2 0	Misure di caratterizzazione su ottiche multistrato			
1	Tecniche spettrofotometriche per la caratterizzazione di materiali per l'UV			
3 0	Studio e caratterizzazione sostanze UV assorbenti			
1	Sviluppo di tecniche di misura per la caratterizzazione di schermi solari			
Evento	Ammissione al III anno			▼
Evento	II accertamento della formazione spec.			▼
3 0 0	Realizzazione ed applicazione strumenti			
1 0	Studio possibili applicabilità degli strumenti			
2 0	Messa a punto prototipi e strumenti finali			
3 0	Valutazione di possibili estensioni			
Evento	S/W Review			▼
Evento	Ammissione all'esame finale			▼
4 0 0	Scrittura Tesi e rapporti			
1 0	Programma di dottorato			
1	I anno – preparazione			

	2	II anno – revisione																		
	3	III anno – revisione																		
	2	0	Rapporti e articoli																	
	3	0	Tesi di dottorato																	
Evento			Esame finale (entro Febbraio anno dopo)																	↑

	Primo livello
	Secondo livello
	Terzo livello

QUADRO CREDITI

	Evento/attività	Data	ore	CFU	ECTS
0	The ORESTE project (Thebault)	11/01/05	2	0,25	
1	Collegio SMTS + PREPARAZ. E PRESENTAZIONE	10/2/05			0,8
2	Metrologia & Qualità (IV Congresso – TO) + Presentazione	22-24/2/05	24+12		1,5
3	Fisica Spaziale (Bernacca)	4-8/4/05	8	1	
4	Epistemologia della misura (Angrilli)	4-8/4/05	12	1,5	
5	Elementi di Ottica (Naletto)	4-8/4/05	12	1,5	
6	Triangolazione ottica per l'acquisizione di modelli 3D	16/05/05	2	0,25	
7	The Challenger of evolving a manned mission to Mars	18/05/05	2	0,25	
8	Verifica di prestazioni per sistemi di misura senza contatto	23/05/05	1,5	0,2	
9	Utilizzo dello Unified Modelling Language per l'analisi e la documentazione del software	23/05/05	2	0,25	
10	Studio del laser tissue welding per l'aerostasi polmonare	9/06/05	2	0,25	
11	Specchi multistrato aperiodici per impulsi ultra brevi	30/06/05	2	0,25	
12	Experimental challenges for seeded FELs (William Graves)	1/07/05	2	0,25	
13	Sonno e modificazioni in microgravita' (Stegagno)	7/7/05	2	0,25	
14	Sonno e modificazioni (Angrilli)	8/07/05	2	0,25	
15	Alterazioni fisiologiche cerebrali e cognitive in microgravita' (Angrilli)	8/07/05	8	1	
16	Fisica Spaziale (Bernacca)	4-8/7/05	10	1,25	
17	Rivelatori (Poletto)	4-8/7/05	12	1,5	
18	Misure di temperatura in ambiente ostile (Debei)	4-8/7/05	8	1	
19	Fisica Spaziale (Bernacca)	09/05	4	0,5	
20	Elaborazione Dati (Debei)	09/05	8	1	
21	Analisi Numerica (Zilli)	09/05	12	1,5	
22	Elementi di Astronomia (Barbieri)	??	40	5	
23	Newrad 2005 (Davos – CH)	17-19/10/05	24		1
24	UVNet 2005 (Davos – CH) + Poster	20-21/10/05	16+12		1,2
25	Carrier-envelope phase of laser pulses: direct measurement, frequency combs and time-domain applications (P, Dombi – Villorosi)	26/10/05	2	0,25	
26	Strumentazione Aerospaziale (Lorenzini)	Gen/Mar-06	50	6	
27	Ferri, ESA applicazioni industriali	1/2/06	2	0,25	
28	Fiera Milano – Capitale Umano (Stand CNR) + Presentazione	16-17-18/03/06	24+24		2
29	"Deposizione di film sottili tramite laser", (R,Frison)	21/3/06	2	0,25	
30	Giornata Majorana	28/3/06	4	0,5	
31	More than Moore (Munari)	30/3/06	2	0,25	
32	Fisica delle superfici (Berti)	Apr/Giu-06	50	6	

33	Exploring Titan (Owen)	11/4/06	2	0.25	
34	Comunicazioni quantistiche e comunicazioni caotiche - dalla fisica moderna alla sicurezza dell'informazione	4/5/06	4	0,5	
35	Tecnologia piezo per NANO posizionamento (Micos)	17/5/06	4	0,5	
36	A tethered spacecraft mission allowing insertion into low Io orbit (J,Sammartin)	26/5/06	2	0,25	
37	Quantum seminar (accademia galileiana)	4/5/06	4	0,5	
38	Modelli di reazione diffusione e formazione di configurazioni spaziali in ecologia (Gallo, Marchesini)	5/06/06	2	0.25	
39	Computational mass spectrometry for protein identification" (Dr. C. Garutti, DEI)	8/06/06	2	0.25	
40	Flexible Slow and Fast Light in Optical Fibres (Thevenaz / DEI)	15/06/06	2	0.25	
41	Metrology, Modeling, and Control in Photolithography (Kameshwar Poolla / Poletto)	3/7/06	2	0.25	
42	Seminario su "peer review" (Ghezzi /DEI)	13/9/06	2	0.25	
43	Rivelazione di forme 3D con proiezione di luce strutturata (Braga / Poletto)	30/10/06	2	0.25	
44	Elettronica quantistica (Tondello)+esame	31/10/06	58	21.75	
45	Preparazione presentazione per ammissione III anno	10/11/06	4	0.5	
46	METODI PER LA RIVELAZIONE DI OSSIGENO TRAMITE TDLAS (Tuneable Diode Laser Absorption Spectroscopy)	2/12/06	2	0,25	
47	C.I. di Metodologie Biologiche (Mod. A) Francesca Dalla Vecchia (Mod. B) Luisa Dalla Valle	19/2/07-5/4/07	32+32	8	
48	Scuola Nazionale "Rivelatori ed Elettronica per Fisica delle Alte Energie, Astrofisica ed Applicazioni Spaziali" INFN Laboratori Nazionali di Legnaro,	26-30/3/2007	40	5	
49	Tecniche per il vuoto e film sottili (V.Palmieri)+esame	Gen/07 – Apr/07	40	45	
50	Scuola Nazionale "ARS2" – Applicazione della radiazione di sincrotrone allo studio di materiali nanostrutturati e dei film sottili	22-26 Aprile 2007	36	4.5	
51	Convegno "Generare Classe Dirigente"	11/05/07	4	0.5	
52	Scuola Internazionale "Summer School on Adaptive Optics" – Santa Cruz (California)	4-10/8/07	40	5	
53	"Thin Film/Multilayer Design and Characterization for VUV Spectral Regions" – Meeting at Lawrence Livermore National Laboratories (LLNL) + preparazione talk	21/8/07	40		1.6
54	12th ESP (European Society of Photobiology) Congress + preparazione talk + preparazione n.2 poster – Bath UK	1-6/09/07	40+40		3.2
	Totale parziale			126.7	11.3
	Totale (ECTS)				51.8